

# **RCA REVIEW**

***a technical journal***

**RADIO AND ELECTRONICS  
RESEARCH • ENGINEERING**

**VOLUME XV**

**JUNE 1954**

**NO. 2**

RADIO CORPORATION OF AMERICA

DAVID SARNOFF, *Chairman of the Board*

FRANK M. FOLSOM, *President*

CHARLES B. JOLLIFFE, *Vice President and Technical Director*

JOHN Q. CANNON, *Secretary*

ERNEST B. GORIN, *Vice President and Treasurer*

---

RCA LABORATORIES

E. W. ENGSTROM, *Executive Vice President*

---

RCA REVIEW

C. C. FOSTER, *Manager*

THOMAS R. ROGERS, *Business Manager*

---

*Copyright, 1954, by RCA Laboratories, Radio Corporation of America*

---

PRINTED IN U.S.A.

RCA REVIEW, published quarterly in March, June, September, and December by RCA Laboratories, Radio Corporation of America, Princeton, New Jersey. Entered as second class matter July 3, 1950 at the Post Office at Princeton, New Jersey, under the act of March 3, 1879. Subscription price in the United States and Canada; one year \$2.00, two years \$3.50, three years \$4.50; in other countries: one year \$2.40, two years \$4.30, three years \$5.70. Single copies in the United States, \$.75; in other countries, \$.85.

# RCA REVIEW

*a technical journal*

RADIO AND ELECTRONICS  
RESEARCH • ENGINEERING

---

*Published quarterly by*

RCA LABORATORIES

*in cooperation with all subsidiaries and divisions of*

RADIO CORPORATION OF AMERICA

---

---

VOLUME XV

JUNE, 1954

NUMBER 2

---

## CONTENTS

	PAGE
The Metrechon—A Halftone-Picture Storage Tube .....	145
L. PENSAC	
Synthesis of Constant-Time-Delay Networks .....	163
M. S. CORRINGTON AND R. W. SONNENFELDT	
Synthetic-Pattern Generator for the Solution of Certain Instrumentation Problems in Television .....	187
R. C. WEBB	
Broadbanding of Resonant-Type Microwave Output Windows .....	204
T. S. CHEN	
Design Considerations for Frequency-Shift-Keyed Circuits .....	230
W. LYONS	
Application of Brewster's Angle to the Design of Coaxial-Line Components for Microwaves .....	238
B. A. DAHLMAN	
A Minimum Noise Figure for the Traveling-Wave Tube .....	252
S. BLOOM AND R. W. PETER	
RCA TECHNICAL PAPERS .....	268
AUTHORS .....	271

---

**RCA REVIEW** is regularly abstracted and indexed by *Industrial Arts Index*, *Science Abstracts* (I.E.E.-Brit.), *Electronic Engineering Master Index*, *Chemical Abstracts*, *Proc. I.R.E.*, and *Wireless Engineer*.

# RCA REVIEW

## BOARD OF EDITORS

*Chairman*

D. H. EWING  
*RCA Laboratories*

G. M. K. BAKER  
*RCA Laboratories*

M. C. BATSEL  
*Engineering Products Division*

G. L. BEEDS  
*Radio Corporation of America*

H. H. BEVERAGE  
*RCA Laboratories*

G. H. BROWN  
*RCA Laboratories*

I. F. BYRNES  
*Radiomarine Corporation of America*

D. D. COLE  
*RCA Victor Home Instrument Division*

O. E. DUNLAP, JR.  
*Radio Corporation of America*

E. W. ENGSTROM  
*RCA Laboratories*

A. N. GOLDSMITH  
*Consulting Engineer, RCA*

O. B. HANSON  
*National Broadcasting Company, Inc.*

E. W. HEROLD  
*RCA Laboratories*

R. S. HOLMES  
*RCA Laboratories*

C. B. JOLLIFFE  
*Radio Corporation of America*

M. E. KARNS  
*Radio Corporation of America*

E. A. LAPORT  
*RCA International Division*

C. W. LATIMER  
*RCA Communications, Inc.*

G. F. MAEDEL  
*RCA Institutes, Inc.*

H. B. MARTIN  
*Radiomarine Corporation of America*

H. F. OLSON  
*RCA Laboratories*

D. S. RAU  
*RCA Communications, Inc.*

D. F. SCHMIT  
*Radio Corporation of America*

S. W. SEELEY  
*RCA Laboratories*

G. R. SHAW  
*Tube Division*

R. E. SHELBY  
*National Broadcasting Company, Inc.*

A. F. VAN DYCK  
*Radio Corporation of America*

I. WOLFF  
*RCA Laboratories*

V. K. ZWORYKIN  
*RCA Laboratories*

*Secretary*

C. C. FOSTER  
*RCA Laboratories*

---

## REPUBLICATION AND TRANSLATION

Original papers published herein may be referenced or abstracted without further authorization provided proper notation concerning authors and source is included. All rights of republication, including translation into foreign languages, are reserved by RCA Review. Requests for republication and translation privileges should be addressed to *The Manager*.

# THE METRECHON—A HALFTONE-PICTURE STORAGE TUBE\*

BY

L. PENSAK

Research Department, RCA Laboratories,  
Princeton, N. J.

*Summary*—The Metrechon is an experimental two-beam cathode-ray tube with a new type of storage target which allows pictures with varying amplitudes (halftones) to be stored, and produces output signals for viewing on a kinescope. Thousands of copies of the output can be obtained with little deterioration of the halftone values. The target is a composite structure of fine metal mesh in contact with a thin sheet of insulator. The portions of the insulator covering the holes are the storage elements. These can be charged by bombardment with a "writing" electron beam. The signal is "read" by scanning the target with a low-velocity beam which is modulated by the stored charges. Reading can go on at the same time as writing or erasing.

## INTRODUCTION

ALL known storage tubes depend on the storage of electric charges on insulators.<sup>1</sup> The differences among the various tubes come about from the manner in which (a) the charges are put onto the insulator (the writing operation), (b) the charges produce an output signal (the reading operation) and (c) the charges are removed (the erasing operation) to clear the insulator for further writing. Writing is accomplished by bombardment, the charge pattern resulting either from secondary emission effects<sup>2</sup> or from bombardment-induced conductivity.<sup>3</sup> Reading and erasure are commonly combined so that removal of the charges also produces an output signal.<sup>2</sup> More than one copy of the stored signal can be obtained when the reading beam is made small enough to remove only part of the stored charge on each scan.<sup>3</sup> However, any change of stored charge changes the output signal level of the succeeding copies. This deterioration of the output signal can be prevented by separating the reading and erasing operations.

\* Decimal Classification: R138.31.

<sup>1</sup> M. Knoll and B. Kazan, *Storage Tubes*, John Wiley and Sons, New York, N. Y., 1952.

<sup>2</sup> A. S. Jensen, J. P. Smith, M. H. Mesner, and L. E. Flory, "Barrier Grid Storage Tube and its Operation," *RCA Review*, Vol. 9, p. 112, March, 1948.

<sup>3</sup> L. Pensak, "The Graphechon — A Picture Storage Tube," *RCA Review*, Vol. 10, p. 59, March, 1949.

Such separation can occur when the reading beam is unable to land on the stored charges and yet can be modulated by them in a kind of grid control action. Erasure can be accomplished by the writing beam or by the use of a third beam. A tube which operates in this manner can produce signals from its stored charges without disturbing them and, therefore, produces multiple identical copies. This is the basic principle of the Metrechon.

### TUBE CONSTRUCTION

A schematic diagram of the tube is shown in Figure 1 and a photograph is shown in Figure 9. It consists of low-velocity gun

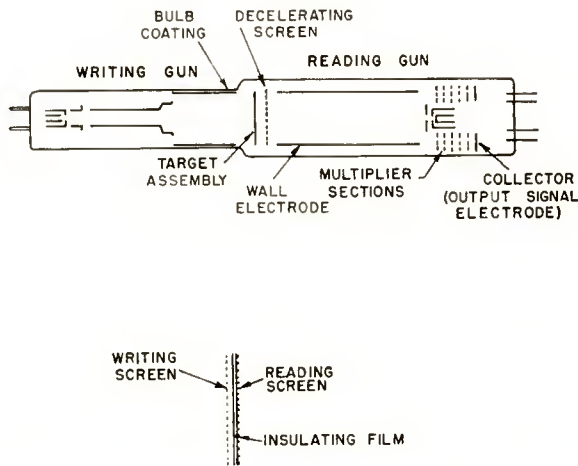


Fig. 1—Schematic outline of the Metrechon and an expanded cross section of the target assembly.

similar in principle to the type used in the image orthicon,<sup>4</sup> a storage target, and conventional cathode-ray gun. The low-velocity reading-gun cathode can be grounded, and all other voltages referred to hereafter are with respect to it. The writing cathode-ray gun is operated with its cathode at 1000 to 2000 volts negative. The target is shown enlarged below the tube outline. It consists of a thin sheet of insulator with a metal mesh on one surface. There are several ways of building such a target. One way is to metallize a mesh on a thin sheet of mica. Another is to seal a thin film of high-resistivity glass to a sheet of

<sup>4</sup> A. Rose, P. K. Weimer, and H. B. Law, "The Image Orthicon, A Sensitive Television Pickup Tube," *Proc. I.R.E.*, Vol. 34, p. 424, July, 1946.

electrolytic mesh. Because the fineness of the mesh determines the maximum number of storage elements on a target of limited diameter, over 700 meshes per inch are used. The metal side of the target faces the reading gun and is called the front surface. Within a few thousandths of an inch from the back, a second fine-mesh screen of metal is located. This is called the "writing" screen. The bulb wall back of the writing screen is coated with an electrical conductor. This serves to collect secondary electrons that might emerge through the

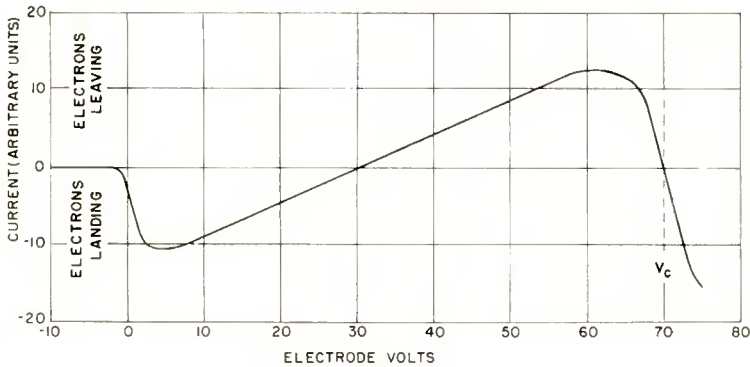


Fig. 2—A typical curve of secondary emission effects when the landing voltage of electrons is varied.

screen and acts as an anode to the writing cathode-ray gun. The remaining electrodes are similar to those described in the references. The external magnetic focusing and deflecting fields are also conventional and so will not be described.

#### PRINCIPLES OF THE READING OPERATION

The several modes of operation are described below.

##### *Landing-Current Theory*

Figure 2 shows a typical curve of current to an electrode (metal or insulator) as a function of its potential with respect to a grounded cathode. Because of the range of energies in electrons from a hot cathode, it may take a small negative bias to prevent any landing. As the electrode becomes more positive, landing occurs and goes to a maximum value. Because secondary electron emission starts at comparatively low landing voltages, the current begins to decrease, and somewhere between 15 and 150 volts, depending on the material, the secondary emission ratio reaches unity and the electrode current is zero. This is called the first crossover point. At higher voltages, the

current reverses and more electrons leave than arrive. If the electrode is not conducting but insulated or made of insulator, its potential cannot be held by conduction and must drift to some equilibrium value at which the current is zero. If landing starts at below the first crossover potential, the surface is driven in the negative direction until no further landing occurs, i.e., approximately zero volts. If landing starts at above the first crossover, the surface tends to go positive and is generally limited by the collector potential ( $V_c$ ).<sup>\*</sup> A second limit that occurs on composite targets will be described below.

#### Current Curve and Potential Diagram

Given a composite target of metal mesh and insulator in the holes as shown in Figure 1, it is possible to explain the target current versus mesh potential curves of Figure 3 using the potential diagram of Figure 4. As a starting condition with the mesh at zero volts with

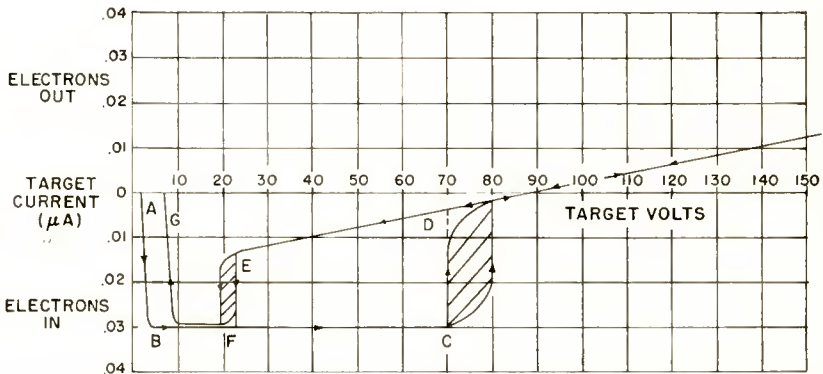


Fig. 3—Variation of target current when the target voltage is slowly raised from zero to over 100 volts and then slowly lowered to zero.

respect to the cathode, the insulator potential also goes to zero as its equilibrium condition. Contact potential difference between cathode and mesh prevents any landing of current until the mesh is above +2 volts.<sup>5</sup>

As the mesh is made more positive, electron landing starts and quickly rises to a maximum value (line AB, Figure 3). At the same time, the insulator tends to go positive by capacity coupling to the mesh. This allows electrons to land on it as well, but, because it is

<sup>\*</sup> See Reference (1), p. 11.

<sup>5</sup> J. Millman and S. Seely, *Electronics*, McGraw-Hill Book Company, Inc., New York, N. Y., 1941, p. 157.

below first crossover, its potential is reduced to zero and no further landing can occur. In Figure 4 the straight line at  $45^\circ$  is merely a reference line to show mesh potential on the same scale as insulator potential. Line AC on the axis shows the insulator staying at zero volts as the mesh goes positive.

Line BC in Figure 3 shows that the current landing on the mesh is essentially unchanged over the potential range from 10 to 70 volts. This means that any secondary electrons that might have escaped from the metal are suppressed by the coplanar grid action of the zero

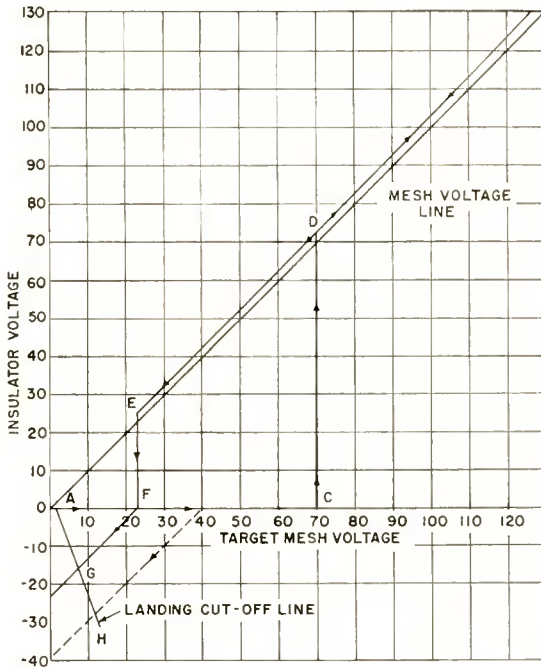


Fig. 4—The insulator voltage cycle when the target mesh voltage is slowly cycled once from zero to 100 volts and back to zero.

potential of the insulator in the holes of the mesh. Therefore, all electrons that land are trapped and the current is constant. However, as the mesh is made more positive, the difference in potential between it and the insulator increases, causing some surface conduction on the insulator. As long as this leakage current is less than the electron landing on the insulator, the insulator potential can be held near ground. At approximately 70 volts difference, this is no longer possible. The insulator potential starts to rise and the higher landing

velocity of electrons causes increasing secondary emission which speeds up the rise. The insulator then quickly "jumps" positive to point D. This jump occurs at slightly different values for the different elements due to small differences in insulation and other second order effects. It is, therefore, possible to make part or all of the target jump by choosing the appropriate mesh potential. The shaded area of Figure 3 shows this spread of jumping points as a range of currents which vary with the waiting period for each measurement. The maximum potential of the insulator is now set by the target mesh which, in turn, acts as a coplanar grid to bias off secondary emission if the insulator goes too positive. Measurements show that the insulator does not go more than three volts above the mesh. The sudden decrease in landing current at about 70 volts as shown in Figure 3 is now due to the insulator being near the mesh potential so that secondaries from the mesh can escape. At 90 volts, the current is zero. This is a true measure of the mesh crossover potential because the insulator cannot contribute current as long as it stays insulating. For all potentials above this, the insulator is held near the mesh potential by secondary emission.

As the mesh potential is reduced, the insulator is forced down with it (line DE) by the grid action of the mesh in suppressing secondary emission until the insulator is no more than several volts positive with respect to the mesh. However, when the insulator potential is lowered in this manner to just below its first crossover potential, the excess electron landing causes it to jump to ground potential (point F) where no further landing of the beam is possible. A similar range of irregularities is found here due primarily to variations in secondary emission ratio among the elements. From this point, as the mesh goes more negative, the insulator goes below ground by capacitive coupling with the mesh and the target current cuts off earlier (point G). The insulator voltage follows line FG (Figure 4) to end up at -24 volts instead of the zero where it started. A repeat cycle will now follow along the line GFCD. Any positive excursion of the target will show this effect. If the mesh is raised to +40 volts, where the jump does not occur and then lowered again, the insulator will go negative as shown by the dashed line in Figure 4 and end up at 40 volts negative. A good way of restoring the insulator to a zero potential value with the mesh at zero is to bring the insulator surface to above the first crossover, turn on the beam to make the elements more positive, turn off the beam and bring the mesh back to zero. The elements are now positive and, on turning the beam on again, they go to zero. With fast switching, the beam current need not be turned off and on as its effect during switching time is small.

### Modes of Operation

From the potential plot of Figure 4, it can be seen that several modes of operation are possible.

1. Mesh at 2-5 volts. The insulator can be driven negative to bias off landing. This allows reading as long as the charges can stay unchanged. This is discussed later.

2. Mesh at 30-70 volts. The insulator can be driven positive or negative and be held stable in either position at the maximum or minimum potential by the secondary emission effects of the reading beam. This gives a black and white picture that will last indefinitely. Although this principle has been used in other storage tubes,<sup>6,7</sup> the voltage range between cathode and maximum potential is reduced over that used in other tubes. This makes the tube more sensitive to writing and, in addition, needs no separate holding beam.

3. Mesh at 20-25 volts. The insulator can be driven negative to modulate the secondary emission from the mesh if it starts above the crossover potential. In this case, the stored charge is slowly erased due to landing of the reading beam but the erasure rate can be varied by operating near or above the crossover potential. It can also be driven positive to enhance the secondary collection from the mesh but will also erase with reading.

4. Mesh at 5-20 volts. The insulator can be driven negative to bias off the secondary emission from the mesh. This pattern should hold, but rather large changes of insulator potential may be required to produce appreciable modulation of the reading output.

In general, given a reading equilibrium, the writing beam can always produce a disturbance which will be read out, and its duration will depend on the several factors that determine how the disturbance is erased. These factors are:

1. Landing of the reading beam, if any.
2. Leakage of electrical charge due to the finite resistivity of the dielectric.
3. Landing of positive ions generated in the residual gas of the tube by the reading beam. This effect causes the ulti-

---

<sup>6</sup>J. A. Rajchman, "The Selective Electrostatic Storage Tube," *RCA Review*, Vol. 12, p. 53, March, 1951.

<sup>7</sup>A. V. Haeff, "A Memory Tube," *Electronics*, Vol. 20, p. 80, September, 1947.

mate limit to duration of a stored charge when a mode of operation is chosen that does not allow beam landing, and an insulator is used with a very good resistivity. Insulators have been found that have a decay constant of as long as several days. This is discussed below.

### Landing Control

This section deals with mode (1) operation and with the amount of negative potential on the insulator elements required to control landing of the beam on the mesh. Obviously, this potential will vary with the potential of the mesh. Figure 5 is one set of measurements that shows the way in which the target current varies as a function of insulator potential for several values of mesh potential. When the insulator is driven negative by the action of the writing beam, the retarding potential in the holes restricts and eventually cuts off landing of the low-voltage beam on the mesh. These curves are very much like the grid-control curves of triodes, consisting of a linear portion

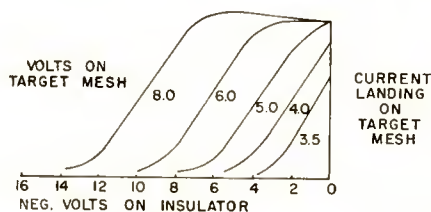


Fig. 5—A typical set of target-current curves as the insulator is driven negative by the writing action.

which will be used for the halftone range of output signals and a small curved section near cutoff where the beam is unable to land and is, therefore, totally reflected. The portion of the beam that does land is subtracted from the incident beam and the remainder is reflected into the multiplier section whose output is, therefore, a function of the insulator potential at the point being scanned.

At low mesh potentials, the target current decreases directly from zero insulator potential, but at higher mesh potential there is a flat portion of the curve, and at still higher potentials the current actually still increases before decreasing. This is due to lens action in the individual holes of the target. The target mesh normally intercepts about half of the incident beam when the lenses are weak due to low mesh potential. However, as the mesh is made positive, the lenses become stronger and when the insulator is made negative, the lenses become strong enough to change the direction of the beam to force more

electrons towards the mesh surrounding each hole. Therefore, the initial effect is to increase the landing current. As the insulator becomes still more negative, its field begins to extend enough in front of the mesh to reduce the number of electrons that can get through and landing is reduced. Eventually all landing is cut off. The negative potential required for this condition increases linearly with positive mesh potential. This is shown in Figure 4 (line AH) which shows the cutoff potential of the insulator as a function of mesh potential.

#### WRITING AND ERASING OPERATION

##### *Writing by Collector Modulation*

It is necessary to discuss writing and erasing before going into more detail on the reading process and its bearing on storage. Writing has been investigated in some detail primarily with mode (1) reading as both the most sensitive and stable for an ultimate radar application. This mode requires that the insulator be driven negative by the writing beam for purposes of laying down a charge pattern and, because the reading beam does no erasing, the writing beam must be made to do this too. If the writing beam is to erase, it must be able to remove electrons as well as put them down. In general, it is not desirable to change the beam voltage to obtain the two operations. Therefore, the beam voltage is chosen so as to produce a secondary emission ratio of about two. This is in the range of 1000 to 2000 volts, and is obtained by operating the writing gun cathode below ground. Writing can now be accomplished by putting negative potentials on the writing screen (see Figure 1). From Figure 2, it is seen that an insulator under bombardment tends to shift towards collector potential due to collection or suppression of secondary electrons. In this case the writing screen, by virtue of its close spacing to the back of the target and fine mesh, becomes the only effective collector seen by the back of the target. It is therefore possible to set the potential of the insulator surface the same as that of the writing screen when the writing beam is turned on. Any change of potential of the back of the target insulator causes the front of the insulator in the holes to go to almost the same potential due to the capacitive coupling between the front and back of the target. This capacitive effect is quite high due to the thinness of the target. There is some loss by capacity division to the adjacent metal of the mesh, but this is small if the insulator film is thin compared to the spacing between wires of the mesh. By this means the insulator can be driven below ground potential.

*Writing by Beam-Current Modulation*

A variation of the above principle is used in actual practice. The writing screen is set negative to approximately 100 volts, and the writing beam current is turned on during scanning to an amount only sufficient to drive the insulator less than 10 volts negative. Figure 5 shows that no more than 3 volts may be necessary. The reason for this method of operation is that wherever the writing beam strikes, secondary electrons are generated. When the writing screen is only a few volts negative, the secondaries are first driven back into the bombarded spot, driving it negative to the screen potential. The areas just outside the spot are then the nearest positive surfaces and so collect the subsequent secondaries to be driven negative in turn. This results in broadening of the spot and shows up as a loss in resolution. However, if the writing screen potential is sufficiently negative, it drives the secondaries back to the target before they can spread very far and so minimizes the loss of resolution.

One practical limit to the amount of negative potential that can be applied to the writing screen is the effect of the electrostatic forces between it and the target. At much over 100 volts, the force can be sufficient to stretch the writing screen or even tear parts of it loose from its supporting ring. These parts may then touch the back of the target and spark through the insulator or show lack of mechanical support in other ways.

Erasure of the negative charges can be obtained by setting the writing screen potential back to ground and bombarding part or all of the target. There is now a collecting field between the negative areas and the writing screen and the secondary emission causes them to go positive to ground. The "unwritten" areas are left unchanged.

#### TUBE CHARACTERISTICS IN MODE 1 OPERATION

*Test Procedure*

Mode (1) was chosen for more detailed study because it seemed to have fewer problems than other modes in the application of radar to television scan conversion. Many of the characteristics have been described above. More specific data and the methods of obtaining them will be described in this section.

Because it was considered impractical to set up a simulated radar system in the early stages of tube development, all testing has been with a television-type writing signal. The video signals obtained from sources such as a monoscope (type 2F21), were passed through a gated video amplifier. This unit shorted out the video signal except

for periods of  $1/30$  second when it was opened by a gate signal triggered by one of the vertical synchronizing signals. The repetition rate of this gate signal could be set at predetermined values down to once in two seconds, and a manual switch provided arbitrarily longer intervals between writing flashes. This manual switch also had a position in which blank raster signals could be applied to the writing gun grid for erasure purposes. The voltage for the writing screen was also generated by the same signal that operated the gate. The writing screen was, therefore, grounded at all times except during a writing period.

### Writing Speed

In the sample tubes made, the writing guns were designed for a maximum beam current of 5 microamperes at 2000-volt operation in

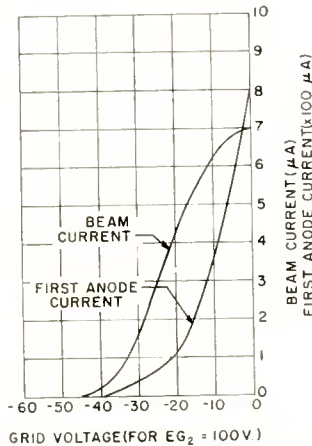


Fig. 6—Typical characteristics for the writing gun used in the experimental tube when operated at 200 volts.

order to get the smallest spot size possible. Such currents are adequate for the writing speeds contemplated in radar or television applications. A typical set of values for beam current and first anode current are shown in Figure 6. If other properties such as higher beam currents for still higher writing speeds, or other types of deflection are desired, these features would be incorporated into new tubes.

By measuring the peak video signal amplitude and the bias, it is possible to measure the peak beam current during writing. It was found that a monoscope pattern could be written onto the target in one pass with a peak current of 2 microamperes and with saturation modulation of the reading signals in the highlights when the target

potential is set at +3 volts. Because the pattern could be considered as consisting of 120,000 beam spots and was written in 1/30 second, it can be said that the writing speed was better than .3 microsecond per spot. The maximum writing speed is approximately .1 microsecond per spot because three times more beam current was available than was used.

### *Resolution*

First, it must be recognized that resolution is not adequately defined by a single number. In common television practice, the number of lines resolution means limiting resolution of the test wedge on a 4 or 3 aspect rectangular pattern. Where scans other than television are to be used, it is more useful to define resolution in terms of percentage modulation of the output as a function of the number of alternate black and white signals across a target diameter. For coarse patterns, the ratio of maximum to minimum reading output signal can be called 100 per cent modulation. As the pattern becomes finer, this ratio falls off to zero (i.e., no distinguishability).

The limiting factor in the resolution of the Metrechon is the fineness of the mesh of the target. Both reading and writing beams are good enough to resolve the 720 mesh of the existing tubes. The mesh limits the resolution due to noise effects arising from interaction of the charge pattern with the writing screen and the imperfect registry of the writing screen with the reading screen. In other words, wires can shadow the landing of beam in the control areas of the storage surface if not properly located. This causes a reduction in resolution to approximately one half the theoretical limit of 900 lines as set by the storage target mesh alone.

Resolution can be measured by applying to the writing gun sine waves from an oscillator which is synchronized with respect to the horizontal synchronizing pulses. The gun is biased beyond cutoff so that current flows only during the positive peaks of the sine waves. These signals can be written onto the target in a single pass, and provide a stored pattern of a series of vertical bars. They should be written just hard enough to produce full reflection in reading. The oscillator can be adjusted in frequency to vary the number of lines on the target from 25 to 300. This corresponds to a frequency range of .5 to 5.5 megacycles. Because horizontal deflection amplitude must be adjusted so that the target diameter is just covered with the lines, the procedure of putting down on the target a burst at approximately 500 kilocycles and counting the lines in the reading output can be used to check the alignment. The alignment holds constant when higher frequencies are used. The reading output was measured on a line

selector oscilloscope. This procedure was used in obtaining the data for Figure 7. It is seen that the half-amplitude value occurs at about 430 lines (4.25 megacycles) per target diameter. The limiting resolutions (5 per cent modulation) occurs near 550 lines per target diameter. If this figure is taken to be the horizontal resolution of a 4 x 3 television raster, then the vertical resolution is limited to 412 lines. However, because a television raster is an inscribed rectangle in the circle of the target, only 80 per cent of the full target diameter is available for the horizontal width. Thus the limiting vertical resolution in television use would be approximately 330 lines. This value could be improved by making new tubes with finer target mesh, 1000 to 1500 mesh having been made. Such mesh has not yet been available in sufficient quantity for development purposes, and therefore was not tried.

### Erasing

Erasing occurs when the writing screen is at ground and the beam

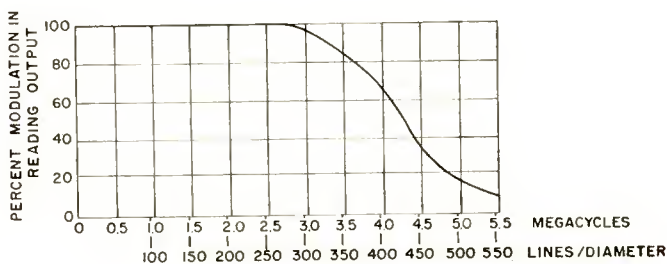


Fig. 7—A typical resolution curve.

strikes a negative area. Secondaries are collected until the area reaches ground. However, the collection efficiency decreases as the potential difference decreases due to the space charge of the emerging secondaries. Therefore, the rate of erasure decreases asymptotically as equilibrium is approached. Thus, the erasing is higher for strong written signals than for weak ones and complete erasure on a single scan is not possible unless the scanning speed is very low.

Measurements on erasing speed were made by writing a full signal bar pattern and "flash" erasing by a blank raster signal of known current. The amount of remaining signal was read by a line selector oscilloscope as in resolution measurements. It was found that the output signal amplitude dropped to about 35 per cent on a single erasure with a beam current of 4.5 microamperes for 1/30 second. The second flash dropped it to below 10 per cent. Thus, over 90 per

cent erasure could be obtained by two passes. After four passes, the remaining signal was down in the noise on the oscilloscope and barely discernible on the display kinescope. Lower erasing beam currents, of course, lower the erasing rate to arbitrarily low values.

A suggestion for operating equipment, especially for developmental or test purposes, is to include a means for switching the target and writing screen together up to +80 or +100 volts. This brings the target above the first crossover and allows the reading beam to completely erase all stored charge by secondary emission. The writing beam should also be turned on to erase all charges on the back of the target at the same time. Switching back to operating potentials now provides a target free of all residues of old signals.

### *Halftone Response*

Good halftone response means that the output signal is proportional to the input signal amplitude. The input signal is effective in terms of charge "written" on the insulator and, for a given scanning speed, is proportional to the writing-beam current. However, the latter varies with the square (or higher power) of the shift of grid voltage from cutoff bias, as is true for most cathode-ray guns. Therefore, the writing signal should be put through a nonlinear circuit which compresses the positive values of signal to the square root (or less) of the initial amplitude.<sup>8</sup> Unless such a device is used and properly adjusted, the input-output curve of the tube will be distorted by the nonlinearity of the writing gun.

In order to bypass such circuit problems for test purposes, the input signal was simulated by setting the writing screen to some negative direct-current value and turning on the writing beam as a blank raster to bring the insulator to screen potential by secondary emission. An output signal can now be obtained as a function of the insulator potential. Such curves are shown in Figure 8 for small changes in target mesh potential. The output signal scale was adjusted to provide equal saturation values in order to compare curve shapes. These curves also show the constant slope and shift of horizontal position that was found in Figure 5 described above.

In general, the control curve is linear in 70 to 80 per cent of the operating range. The choice of operating curve depends on whether one wishes to use it to show all input signals or to clip off (with respect to output) the weak signals. Also, the erasure can be faster and more nearly the same for both small and large signals if the curve

---

<sup>8</sup> B. M. Oliver, "A Rooter for Video Signals," *Proc. I.R.E.*, Vol. 38, p. 1301, November, 1950.

is chosen that does not start to rise at the zero point but later as in the 2.9-volt curve of Figure 8.

The control characteristic may also vary with location on the target area due primarily to imperfect adjustment of landing uniformity. The test samples built to date have not been designed to reduce this error to a minimum. The result is that the operation has been uniform to better than 10 per cent in the area of four-fifths of the target diameter. Flaws of various kinds may also contribute errors, but there is reason to expect less than 5 per cent errors with well made tubes.

The uniformity of response over small areas is better than over the whole target. In other words, it is possible to detect small differences in input with respect to the surrounding area even though the whole target may show a shading effect many times larger. Although this small area uniformity has not been measured, it may be close to

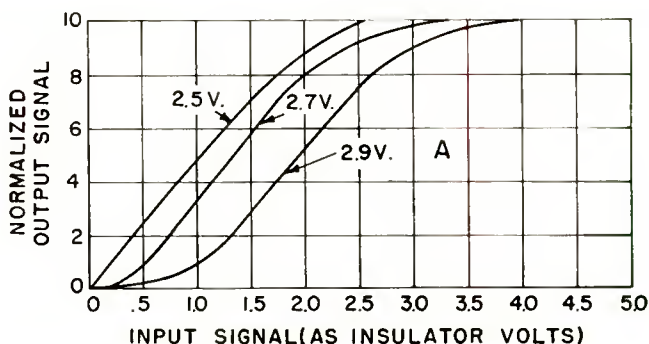


Fig. 8—Typical input-output transfer characteristics for different target mesh potentials.

1 per cent. For some applications, such as search radar, it may be of considerable use to a trained operator.

It should be noted that reading decay will also be affected by the control curve. A stored signal is reduced at a constant rate during continuous reading. Therefore, the input signal ordinate of Figure 8 can be regarded as a time axis read backward, and the output signal falls off along the chosen control curve. It is apparent that for some of the curves there may be a residue of stored signal, due either to incomplete decay or incomplete erasure, and yet no output signal is present. This residue may affect the halftone value of subsequent writing.

#### *Storage Properties*

The storage of signals in the tube may be considered from several

points of view depending on the application. If a signal is written in and the tube turned off, the signal will decay at some rate determined in the limit by the resistivity of the insulator. This might be called "retention time" and is exponential in time with a time constant (decay to  $1/e$  of the initial value) of several days or more. If a signal is written in and the reading process is by mode (2), the signal is held indefinitely in either of the two stable values, and there is no loss with time. If a signal is written in and reading is by mode (1) operation, then the decay varies with reading beam current, reading duty cycle, gas pressure, position on the target, and choice of control characteristic. This can be called "reading decay," and the term "reading duration" can refer to the time for a signal to decay to half its initial value. Reading duration is of the order of 10 minutes with continuous scanning at standard television rates. The signal can also be written in and some partial erasure by the writing beam be allowed to shorten the reading duration if so desired. Storage can thus be decreased to the limit set by erasing speed and scanning rates.

Since mode (1) reading is of major interest, its decay can be described as follows: Assume that a charge pattern has been written on the target and then all writing has been stopped. Reading is then started by scanning at standard television rates. The output signal slowly begins to fall off primarily due to the landing of positive ions on the target. These are generated by the reading beam colliding with the residual gas molecules in the tube which are present because normal tube processing causes the ultimate vacuum to fall in the range of  $10^{-8}$  to  $10^{-7}$  millimeter of mercury. By setting the potential of the decelerating screen 5 to 10 volts positive with respect to the wall electrode, it is possible to repel all of the ions generated in the wall space. Some ions are generated in the space between the decelerating screen and the target, but these are less than 10 per cent of the total number generated and so cause little loss of signal in even a half hour of continuous reading. The major effect is due to ions generated in the higher potential region of the first dynode and possibly in the multipliers. Because the ions are not deflected, their landing is concentrated as a large defocused area near the center of the target. In general, the rate of decay of signal output is linear with reading time.

#### *Mechanical Resonance*

The target and writing screen are both thin membranes under tension on a support ring and, therefore, have mechanical resonance frequencies in the same sense as a drum head. Also, in many types of operation, it is necessary to switch the voltage between them at some cyclic rate and, therefore, the screens will be periodically mechanically

driven by the electrostatic forces. If the switching rate of the writing screen happens to be at the resonant frequency of either of the screens, the amplitude of resonance will give rise to audible sounds from the tube and, in the extreme, may cause damage by tearing of the screen from its support. There is very little damping because the tube is evacuated. Therefore, care should be taken to avoid exciting such resonance. However, because there is little damping, the resonant frequency is quite sharp and slight detuning is generally sufficient to avoid trouble.

#### POSSIBLE APPLICATIONS

The application for which the tube was developed is the storage of radar PPI (plan position indicator) patterns and their conversion

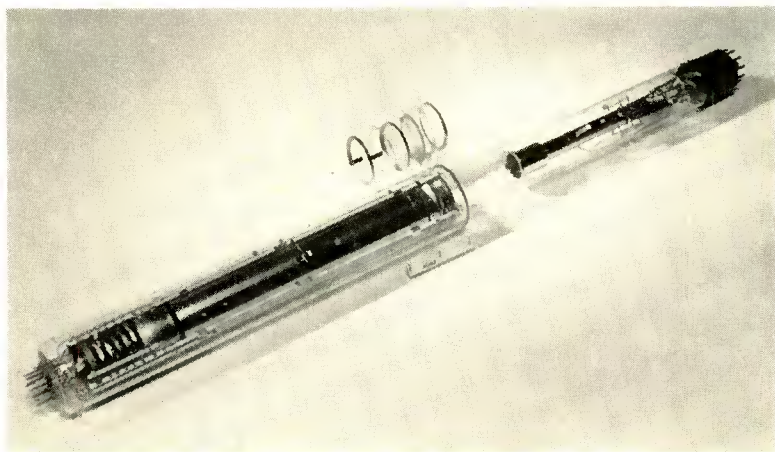


Fig. 9—The Metrechon tube.

to television-type scan for viewing on a kinescope or relaying by television techniques to a remote point. This was the purpose of the Graphechon,<sup>3</sup> but its lack of halftone response was a limitation. Although no tests have as yet been made with radar systems, it is expected that the halftone operation of the Metrechon will provide increased detectability of signal in the presence of noise over the Graphechon and over the direct viewing of radar in a P7 phosphor cathode-ray tube. It is expected that the stable storage of the initial signal values will give an operator more time to search for small differences as compared to his having to follow the strobe with his eyes in order to catch them before they decay. Because the tube integrates

input signals, it could take full advantage of integration to improve signal-to-noise ratio for final display. The erasure can be set to partial or full as desired and controllable with respect to area if the system so requires. A number of such possibilities have been considered and more may be found.

With some modification, including the use of electrostatic deflection plates, the tube may prove useful for storage of fast single transients. The performance of the Graphechon in such applications<sup>9</sup> may be equalled or exceeded by the Metrechon. The tube may also have use in nuclear physics for storing pulses occurring at too great a rate for conventional equipment to handle, and then counting and analyzing the reading output at more practical rates. The pulses can be applied to the grid of the writing gun to produce up to 10 million pulses per second or more if necessary. The writing beam can be scanned in a rectangular raster to spread the spots of charge over the target for the duration of one "frame" which can be chosen to allow 10,000 or more spots to be stored. A reading system can then be designed to count and measure the magnitude of the stored charges at slower rates. There are undoubtedly problems that must be solved before such a system can be practical, but it looks like it might be a valuable tool for research work.

Another application might be the storage of one frame of a television picture created, for example, by an industrial television system and used to catch an event that occurs only intermittently. The tube has been tested for this purpose and, while it necessarily causes some deterioration of the picture quality, it does work fairly well.

Many other applications for the tube will be considered and tried as its properties become known to people with special problems.

#### ACKNOWLEDGMENT

The writer wishes to acknowledge with gratitude the contribution of many people in the Laboratories to this project and particularly to L. E. Flory for his supervision and guidance of the work, P. K. Weimer for having suggested the basic principle of the tube, H. B. Law for the technique of making the targets, and W. H. Bleacher for the successful fabrication of the targets.

---

<sup>9</sup> L. E. Flory, W. S. Pike, J. E. Dille, and R. W. Smith, "A Storage Oscilloscope," *RCA Review*, Vol. 12, p. 220, June, 1951.

# SYNTHESIS OF CONSTANT-TIME-DELAY NETWORKS\*†

BY

MURLAN S. CORRINGTON AND RICHARD W. SONNENFELDT

Consumer Products Division, Radio Corporation of America,  
Camden, N. J.

*Summary*—When a low-pass filter has a constant time delay, the response to a unit-step function will be symmetrical about the fifty per cent rise point. Such a transient response is very desirable in television receivers since it increases the apparent detail contrast and the sharpness of transitions from black to white, resulting in a high-quality picture.

The desired frequency response can be analyzed as a Fourier series in frequency. The terms of the series can be synthesized easily by pieces of delay lines, the responses of which are then combined in the proper proportion to give the desired frequency response. Low-pass, band-pass, and band-rejection filters can be synthesized, all at constant time delay.

A discussion of the transient response of non-minimum-phase-shift networks is given.

## INTRODUCTION

IN amplifiers, such as are used in television equipment, it is often desirable that the transient response to a unit-step function be symmetrical about the fifty per cent point. This usually increases the apparent detail contrast and the sharpness or quality of the picture in the transitions from black to white, resulting in a high-quality picture.

An introductory theory of the transient response of low-pass filters having minimum net phase shift will be given, and then by moving zeros of the transfer function successively to the right half of the complex frequency plane, the theory of non-minimum-phase-shift networks will be developed. Following this theory the performance of constant-time-delay networks will be discussed. It will be shown how the selectivity curve can be expanded in a Fourier series and the desired curve synthesized by a term-by-term combination of the successive terms of the Fourier series. An additive method of synthesis as well as a cascade method will be presented and experimental results obtained with such equipment will be shown.

---

\* Decimal Classification: R143.4.

† A substantial part of this paper was presented at the National Electronics Conference, Chicago, Illinois on September 28, 1953 and was published in the 1953 issue of the Proceedings.

## SHUNT PEAKING CIRCUITS

If a tuned circuit has a very low  $Q$ , there will be a slight rise in the selectivity curve when the circuit is resonant to the driving force. In Figure 1 let the peaking coil  $L$  be added in series with the load resistor  $R$ . The normalized impedance of this circuit is

$$\begin{aligned} \frac{Z}{R} &= \frac{1 + \frac{pL}{R}}{1 + pRC + p^2LC} \\ &= \frac{1 + Qp}{1 + p^2Q + p} \end{aligned} \quad (1)$$

where  $\omega_0 = \frac{1}{RC}$ ,  $p = \frac{j\omega}{\omega_0}$ , and  $Q = \frac{\omega_0 L}{R}$ .

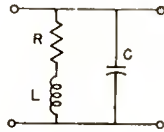


Fig. 1—Low-pass filter with shunt peaking coil.

If the  $Q$  of the circuit is varied by changing the inductance,  $L$ , of the peaking coil, the selectivity curves for  $k$  circuits in cascade will be as shown by Figure 2. For a single circuit,  $k = 1$ .  $Q = 0$  corresponds to  $L = 0$  and is the usual  $RC$  characteristic. All curves start out flat at low frequencies and are asymptotic to the same dotted line of unit slope (20 decibels per decade) going through unit gain at  $\omega/\omega_0 = 1$ . The frequency of greatest gain decreases as  $Q$  increases, since the  $LC$  product increases with  $L$ . The dotted line is for a semi-infinite constant-slope low-pass filter.<sup>1</sup> The corresponding phase curves are given by Figure 3. The phase shift from zero to very high frequencies is ninety degrees per section of filter.

The time delay in seconds for such a filter will be defined as minus one times the phase shift in radians divided by the angular frequency in radians per second. The curves of Figure 4 show the normalized time delay per section of filter. All curves are flat at the origin, and

<sup>1</sup> Hendrik W. Bode, *Network Analysis and Feedback Amplifier Design*, D. van Nostrand Company, Inc., New York, N. Y., 1945. Chapter 15.

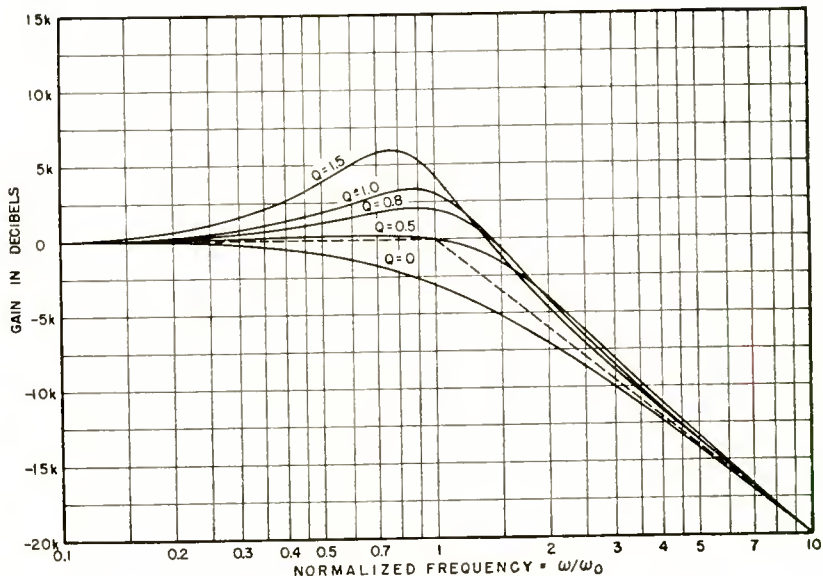


Fig. 2—Amplitude characteristics for low-pass filter.

the initial value is  $1 - Q$ . When  $Q > 1$  the time delay is negative at low frequencies. All curves approach the zero time delay axis asymptotically at high frequencies.

The response of these filters to a unit-step function can be computed

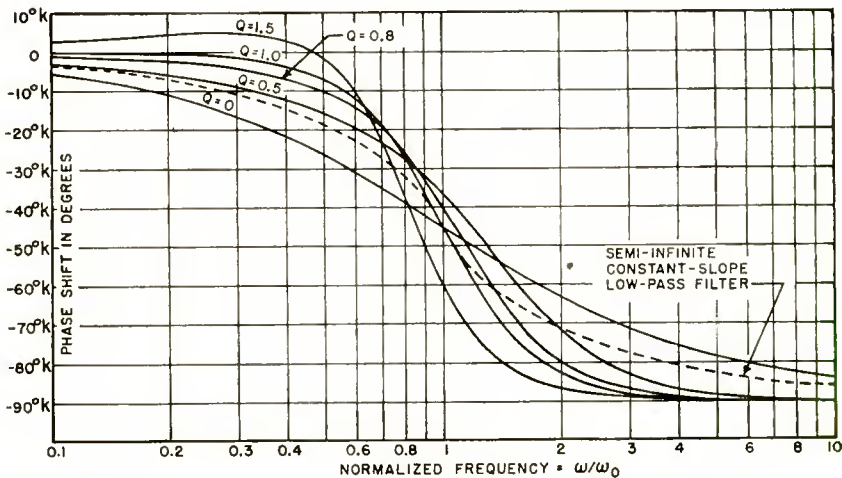


Fig. 3—Phase curves for low-pass filter.

from Equation (1) by means of the usual Laplace transform tables.<sup>2</sup> The curves of Figure 5 show these results for a single section of filter,  $k=1$ . The time axis is in radians at the cutoff frequency  $\omega_0$ .  $Q=0$  is the usual  $RC$  charging curve which, like the others, starts out with unit slope. As  $Q$  is increased, the overshoot increases rapidly; the ringing becomes more and more pronounced. The curve for  $A_1(\alpha)$  is for a semi-infinite constant-slope filter.<sup>3</sup> The maximum  $Q$  that will not produce overshoot is 0.25.

TRANSFER FUNCTION OF LATTICE NETWORK

If a lattice has impedances  $Z_1$  and  $Z_3$  in the series arms and  $Z_2$  and

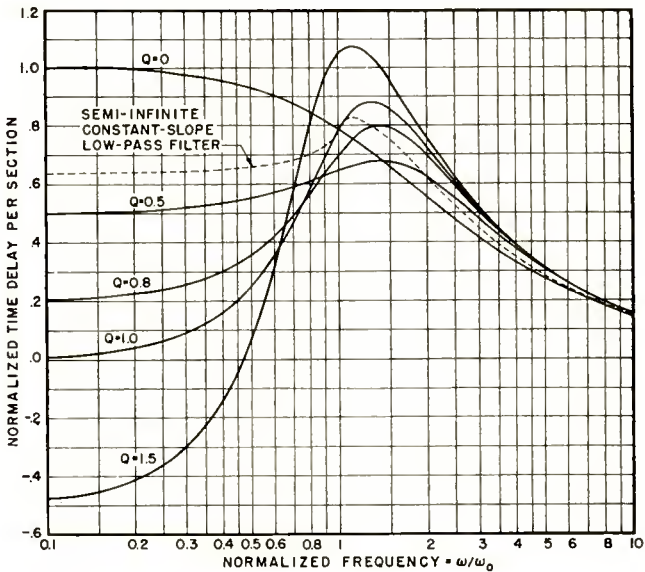


Fig. 4—Time-delay curves for low-pass filter.

$Z_4$  in the shunt arms, as shown by Figure 6, the network has the transfer function

$$\frac{e_2}{e_1} = \frac{Z_2 Z_4 - Z_1 Z_3}{(Z_1 + Z_4)(Z_2 + Z_3)} \tag{2}$$

<sup>2</sup>Murray F. Gardner and John L. Barnes, *Transients in Linear Systems*, Vol. I, John Wiley & Sons, Inc., New York, N. Y., 1942, Appendix A, pp. 332-356.

<sup>3</sup>Murlan S. Corrington, "Transient Response of Filters," *RCA Review*, Vol. 10, pp. 397-429, September, 1949.

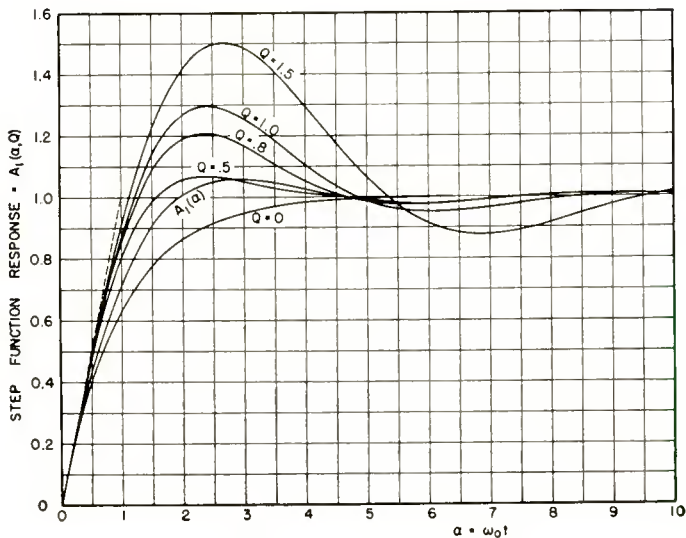


Fig. 5—Response of low-pass filter to unit-step function.

where  $e_1$  is the input voltage,  $e_2$  is the output voltage, and the  $Z$ 's may be any complex impedance. For the symmetrical lattice let  $Z_1 = Z_3$  and  $Z_2 = Z_4$  to give the transfer function

$$\frac{e_2}{e_1} = \frac{Z_2 - Z_1}{Z_2 + Z_1} \tag{3}$$

In the special case where  $Z_1 = \frac{1}{pC}$  and  $Z_2 = R$ , shown by Figure 7(a), the transfer function is

$$\frac{e_2}{e_1} = \frac{p - \frac{1}{RC}}{p + \frac{1}{RC}} \tag{4}$$

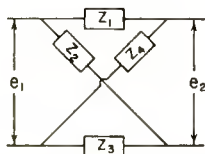


Fig. 6—Lattice network.

which is an all-pass lattice, since the absolute value is one at all frequencies. It is thus evident that if such a symmetrical lattice is used in cascade with the low-pass filter, the lattice will have no effect on the selectivity curve.

By means of the Laplace transform tables<sup>2</sup> the unit-step response is

$$A(t) = 2e^{-\frac{t}{RC} - 1} \tag{5}$$

which is shown by Figure 7(b). The zero of Equation (1) is at  $p = -1/Q$ . If  $RC = Q$  in Equation (4), the lattice will cancel the zero on the axis in the left half of the complex frequency plane and move it to the corresponding point on the axis in the right half of the complex frequency plane. Thus it is possible to have more than one phase curve for a given amplitude response, and the transient responses will then be different. Similar results can be obtained by letting  $Z_1 = R$  and  $Z_2 = pL$ . It should be noticed that interchanging  $Z_1$  and  $Z_2$  in the symmetrical lattice merely changes the polarity of the output and has

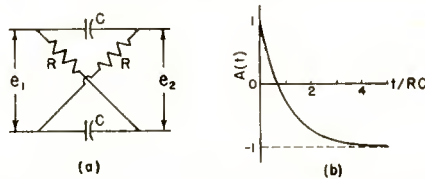


Fig. 7—Transient response of symmetrical lattice.

no other effect on either the amplitude or phase responses. If we let  $Z_1 = 2a$  and  $Z_2 = p + (a^2 + b^2)/p$ , as shown by Figure 8(a), the transfer function becomes

$$\frac{e_2}{e_1} = \frac{Z_2 - Z_1}{Z_2 + Z_1} = \frac{p - a - ib}{p + a - ib} \cdot \frac{p - a + ib}{p + a + ib} \tag{6}$$

which moves the conjugate zeros  $p = -a \pm ib$  to  $p = +a \pm ib$ . The response of this lattice to a unit-step function can be derived by the usual Laplace transformation as follows:

$$\frac{1}{p} \frac{(p - a)^2 + b^2}{(p + a)^2 + b^2} = \frac{1}{p} - \frac{4a}{(p + a)^2 + b^2} \tag{7}$$

The inverse transform is the response to a unit-step function

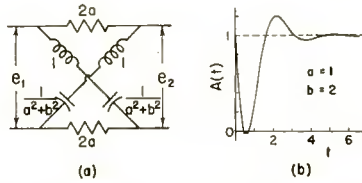


Fig. 8—Transient response of symmetrical lattice.

$$A(t) = U(t) - \frac{4a}{b} e^{-at} \sin bt. \tag{8}$$

where  $U(t)$  is the unit-step function. This is plotted on Figure 8(b) for  $a = 1$  and  $b = 2$ .

EFFECT OF MOVING ZEROS ON UNIT-STEP RESPONSE

If the network of Figure 1 is used in cascade with the lattice of Figure 7 and the constants are adjusted so the zero is moved from the left half of the complex frequency plane to the right, the resulting response to a unit-step function, for a single section,  $k = 1$ , is as shown by Figure 9. The curves start out with a negative precursory swing followed by the rise to the final value of unity. When  $Q$  does not exceed 0.25, the curve approaches the final value of unity with no oscillation.

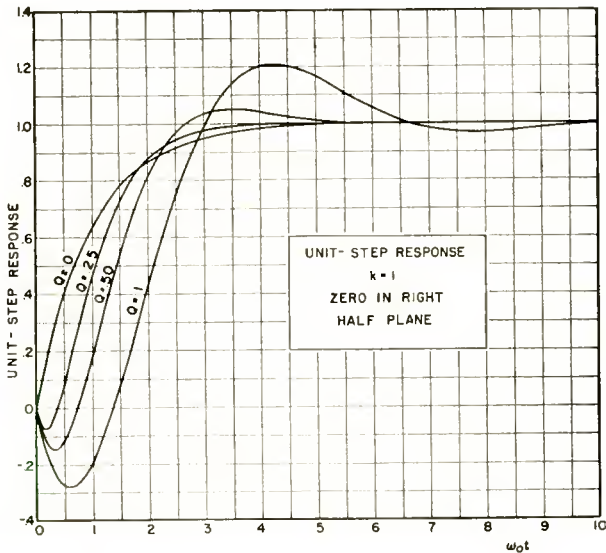


Fig. 9—Effect of moving one zero to right half plane,  $k = 1$ .

For higher values of  $Q$  there is an overshoot followed by a rapidly decreasing oscillation about the final value.

When Figure 9 is compared with Figure 5, they show that moving the zero to the right half of the complex frequency plane adds a negative precursory swing to the response to the unit-step function, following which the curve increases to its final value of unity in a manner similar to that of the minimum-phase network. For the higher  $Q$ 's, this negative overshoot of Figure 9 is somewhat similar in amplitude and shape to the positive overshoot which follows the main rise to unity.

If two low-pass circuits of Figure 1 are cascaded with a single lattice of Figure 7, the effect is to move one of the zeros to the right

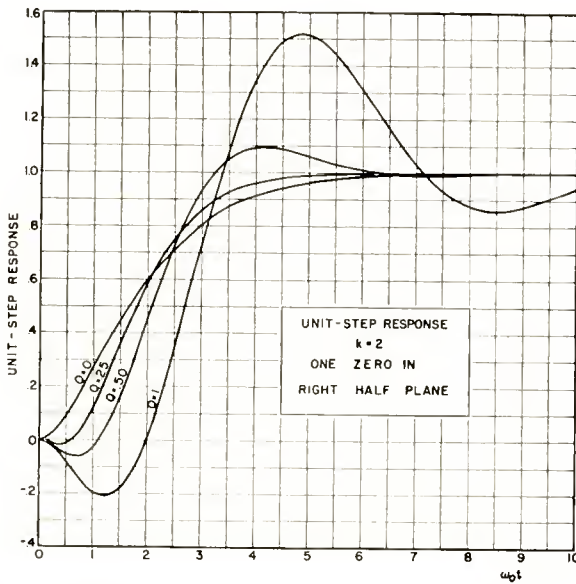


Fig. 10—Effect of moving one zero to right half plane,  $k=2$ .

half plane, leaving the other in the left half plane as before. The unit-step response is shown by Figure 10. As before, there is a precursory swing in the negative direction before the circuit begins its rise to the final value of unity.

If two sections of the lattice of Figure 7 are cascaded with two sections of the filter of Figure 1, the effect is to move both of the zeros from the left half plane to the right half. The curves of Figure 11 show the unit-step response of such a network. There is a small positive swing, followed by a negative one, before the circuit begins its main positive swing to its final value of unity. Here again there is consid-

erable symmetry between the large negative ripple and the positive overshoot which follows the main rise to the final value.

The precursory ripple can be explained in terms of the charging up of the lattice of Figure 7(a). When a positive unit-step of voltage is applied to the upper input terminal it goes right through the series capacitor, making the upper output terminal positive. Later on, when the transient is over, the capacitor will no longer conduct current and the lower terminal becomes positive. This is why the output voltage starts out in one direction and then reverses after the lattice is charged up. In a similar manner two lattices in cascade will cause two such reverses, as shown by Figure 11.

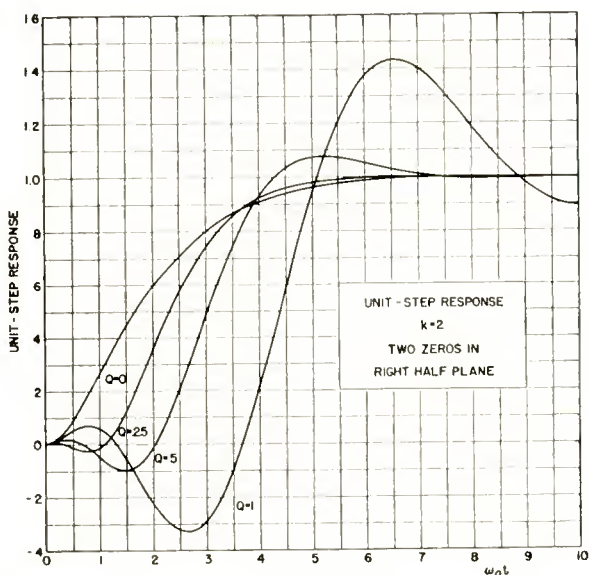


Fig. 11—Effect of moving two zeros to right half plane,  $k = 2$ .

#### CONSTANT-TIME-DELAY NETWORKS

The preceding discussion shows that in order to produce a transient response where there is a negative swing of voltage followed by a main rise and a positive overshoot followed by a rapid approach to the final value of unity, it is desirable to use non-minimum-phase-shift networks. It can be shown by means of the Fourier integral for the response to a unit-step function<sup>4</sup> that for the response to be sym-

<sup>4</sup> W. L. Sullivan, "Analysis of Systems With Known Transmission-Frequency Characteristics by Fourier Integrals," *Elec. Eng.*, Vol. 61, pp. 248-256, May, 1942.

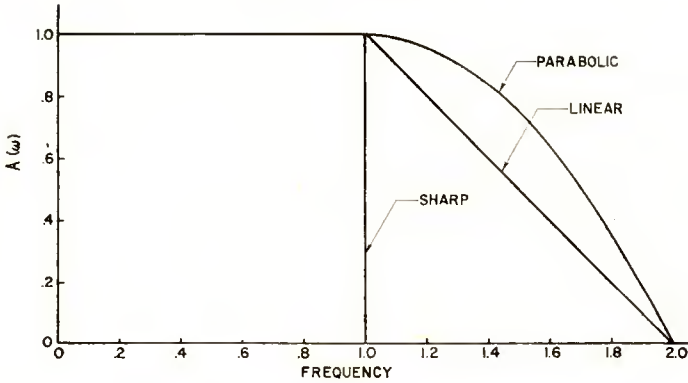


Fig. 12—Constant-time-delay filters.

metrical about the fifty per cent point it is necessary that the network have phase shift proportional to frequency, or that the time delay be constant.

If we assume a low-pass filter which has a constant time delay and various rates of cutoff, such as shown by Figure 12, it is possible to use the Fourier integral to compute the response to a unit-step function as shown by Figure 13. These filters are not physically realizable since they have infinite attenuation over a finite bandwidth, but are used to simplify the analysis. In a practical case there will be small ripples in the response beyond cutoff.

A filter which is flat to unit frequency and then cuts off sharply will have the response to unit-step function shown by the curve marked "sharp cutoff" in Figure 13. This curve is symmetrical about the

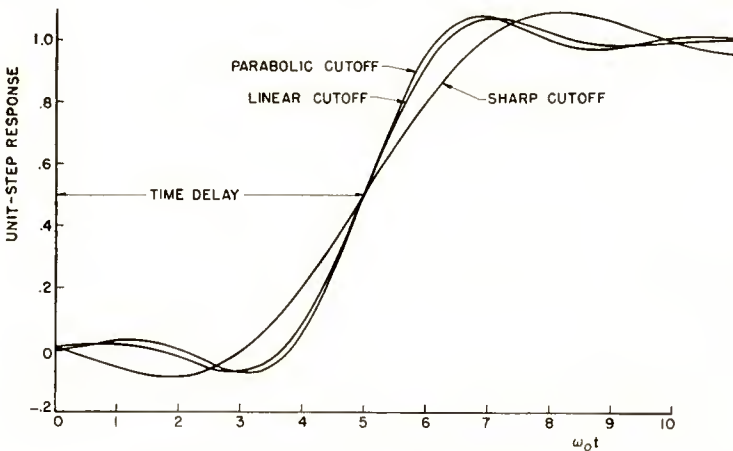


Fig. 13—Unit-step response of filters.

fifty per cent point and is delayed in time by an amount equal to the time delay of the filter. There is a negative and a positive overshoot of approximately nine per cent. If the bandwidth of the filter is increased by adding a linear cutoff, as shown by Figure 12, the response will be somewhat more rapid, as shown by the curve marked "linear cutoff" in Figure 13. As before, the response is symmetrical about the fifty per cent point, having a negative and positive overshoot of approximately seven per cent. If the bandwidth is further increased by letting the rolloff be parabolic, the rise is somewhat more rapid, but the overshoot is approximately the same, as shown by the curve marked "parabolic cutoff" in Figure 13.

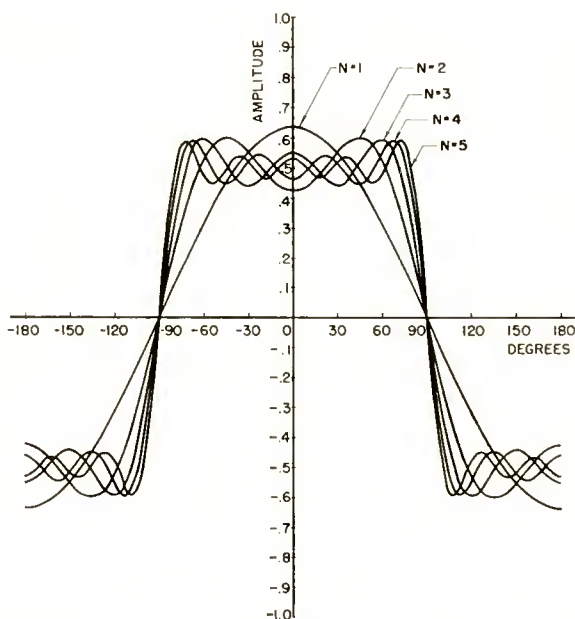


Fig. 14—Square-wave response, sharp-cutoff filter.

The response of the sharp-cutoff filter of Figure 12 to a square wave is as shown by Figure 14. If the repetition rate is so high that only the fundamental component of the square wave can be passed by the filter, the response will be a sine wave, shown by the curve  $N = 1$ . If the repetition rate is decreased so that two terms of the Fourier series for the square wave can be passed by the filter, the output will be shown by the curve  $N = 2$ . In a similar manner, by further decreasing the repetition rate until more harmonics are passed, the response

will more nearly approximate the square wave, as shown by curves labeled  $N = 3, 4,$  and  $5$ . In a similar manner, if a square wave is applied to the linear filter, Figure 12, such that the repetition rate occurs at the frequency  $\omega_0 = 1$ , the third harmonic will occur at a frequency equal to three, and is therefore stopped by the filter.

Since only the fundamental component is passed, the response is a simple sine wave shown by Figure 15. If the repetition rate is decreased so that the fundamental frequency is  $1/2$ , the third harmonic will be passed with an amplitude equal to  $0.5$  and the resulting response is shown by the curve of Figure 15 labeled  $\omega_0 = 1/2$ . If the repetition

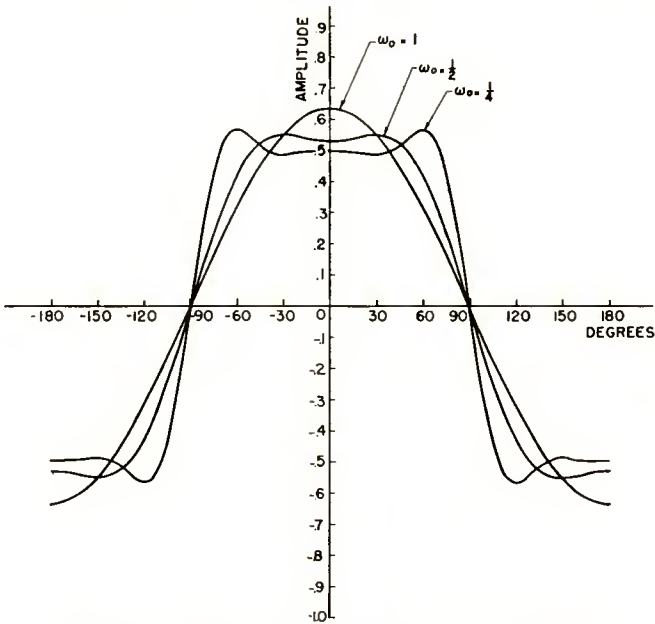


Fig. 15—Square-wave response, linear-cutoff filter.

rate of the square wave is one-fourth of the cutoff frequency of the linear filter of Figure 12, the third harmonic will be passed with full amplitude, the fifth harmonic at  $3/4$  amplitude, and the seventh harmonic at  $1/4$  amplitude, to give the response shown by the curve labeled  $\omega_0 = 1/4$  in Figure 15.

#### FOURIER SYNTHESIS OF SELECTIVITY CURVES

The selectivity curves of Figure 12 can be expanded in a Fourier series with frequency as the independent variable. For the sharp-

cutoff case the fundamental component will be as shown by the curve labeled  $N = 1$  of Figure 14, except that the X-axis is now frequency instead of degrees. Two terms of the series will give the curve labeled  $N = 2$ , and additional terms are shown by the curves labeled  $N = 3, 4$ , and 5. A constant term can be added to move the origin from the point shown to  $-0.5$  on the vertical amplitude axis. The curves of Figure 14 then represent low-pass filters where the abscissa corresponds to frequency. In a similar manner, the linear-cutoff low-pass filter of Figure 12 can be approximated by 1, 2, or 4 terms of the Fourier series, as shown by Figure 15. In the general case, where the equation for the amplitude response is not known but where the points are obtained from laboratory measurements, or where the formula is too complicated to evaluate the Fourier coefficients easily, the amplitudes can be found by means of harmonic analysis schedules.<sup>5</sup>

The successful synthesis of filters by means of a Fourier series representing the selectivity curve requires elements which correspond electrically to individual terms or to groups of terms of the desired Fourier series. For constant-time-delay filters these elements must each have the required selectivity curve, while at the same time each must have constant time delay. The amplitudes of the individual selectivity curves are then adjusted to correspond with the terms of the series to be synthesized.

Transducers having selectivity at constant time delay are well known. For instance, they are found in television systems wherever light energy is converted into electrical energy with a finite scanning-spot size. The finite magnitude of the scanning spot used in pick-up and reproducing devices such as iconoscopes, image orthicons, kinescopes, etc., causes aperture distortion, since the finite spot cannot scan fine lines properly. The resulting resolution or selectivity is related to the spot size and velocity, the scanning repetition rate, and other factors.<sup>6</sup>

In the early stages of experimental work with systems having symmetrical transients, aperture distortion response functions were used in conjunction with so-called aperture corrector circuits to obtain sharp-cutoff low-pass filter sections. Their usefulness is, however,

---

<sup>5</sup> R. P. G. Denman, "36 and 72 Ordinate Schedules for General Harmonic Analysis," *Electronics*, Vol. 15, pp. 44-47, September, 1942. Corrections by F. W. Grover, Wave Analysis Schedules, *Electronics*, Vol. 16, pp. 214-215, April, 1943. In addition to the errors listed, in column one, p. 215, for "Column for  $B_{11}$  and  $B_{25}$ , line for  $\alpha = 20^\circ$ , for  $\Delta_2$ , read  $\Delta_3$ ," read ". . . for  $\Delta_3$ , read  $-\Delta_2$ ."

<sup>6</sup> Pierre Mertz, "Television—The Scanning Process," *Proc. I.R.E.*, Vol. 29, pp. 529-537, October, 1941.

severely limited and they are cumbersome and expensive. A simpler element having a cosine amplitude function of frequency is desirable to obtain exact correspondence with the Fourier series for the selectivity curve.

#### TRANSMISSION-LINE THEORY

Low-loss transmission lines open at the receiving end and driven from their characteristic impedance have the following property. As shown in the Appendix, if a transmission line  $d$  electrical units long has inductance  $L$  per unit length and capacitance  $C$  per unit length, then at a frequency  $\omega$  the voltage at a point  $x$  units from the receiving end, as shown by Figure 16, is

$$E_x = E_g e^{-i\theta d} \cos \theta x. \quad (9)$$

This is a voltage of amplitude  $E_g \cos \theta x$  having a lagging phase angle of  $\theta d$  radians, which gives a constant-time-delay of  $(LC)^{1/2}d$ .

The sending end voltage is

$$E_d = E_g e^{-i\theta d} \cos \theta d. \quad (10)$$

The receiving end voltage is

$$E_0 = E_g e^{-i\theta d}. \quad (11)$$

From Equations (9), (10), and (11) it is seen that the voltage at any point on the line lags the generator voltage by the same phase angle  $\theta d$ .

#### ADDITIVE METHOD

Figure 16 shows a schematic presentation of how such voltages may be combined to yield successive terms of a Fourier series. The taps are equally spaced so the voltage on the  $n$ th tap is  $E_n = E_g e^{-i\theta d} \cos n\theta$ . All the terms with positive signs are collected on a bus, after proper attenuation; similarly all the terms with negative signs are collected on another bus and are then inverted in polarity. The two groups of terms are combined in accord with the harmonic-analysis schedule of the selectivity curve.

This method yields only a finite number of terms and is therefore not a precise equivalent of the Fourier development of the selectivity curve, except in those cases where this development is a finite series. Experience has shown that the approximations are acceptable for practical purposes because, by proper choice of the "repetition rate"

of the selectivity curve, rapidly converging Fourier series can be obtained.

In Figure 16 it is implied that the attenuating sections do not significantly load the line, and their impedance must accordingly be high compared to the impedance of the line. The conventional coaxial transmission line is difficult to tap for this type of filter. A parallel-conductor type of line is easier to use, but experience has shown that well-designed lumped-constant lines are suitable for this purpose. It must be clearly understood that the passband of such a filter must always be less than the passband of the individual elements of which it is made. For the filter to have constant time delay in its working band, the elements must be used over only that portion of their bandwidth for which the phase is linear.

Such crude approximations to transmission lines as filters of the constant-k type are usable whenever they have sufficient inherent bandwidth to permit linear-phase operation of the filter over its passband. The sole disadvantage is the waste of impedance entailed by working the elements over the small linear-phase portion of their bandwidth. More complex structures can overcome this disadvantage to a startling degree.<sup>7-9</sup>

#### CASCADE METHOD

A finite Fourier series for the selectivity curve can be rewritten in terms of a series of powers of harmonic functions rather than in terms of functions of multiple angles. For instance, consider the finite series

$$\begin{aligned}
 S &= \frac{1}{2} + \frac{2}{\pi} \cos \beta - \frac{1}{3\pi} \cos 3\beta \\
 &= \frac{1}{2} + \frac{3}{\pi} \cos \beta - \frac{4}{3\pi} \cos^3 \beta.
 \end{aligned} \tag{12}$$

This is the equation of the curve marked  $\omega_0 = 1/2$  in Figure 15, with the frequency axis moved down 0.5 unit. Let it represent a selectivity curve for a low-pass filter with repeated responses beginning at  $270^\circ$ .

<sup>7</sup> Marcel J. E. Golay, "The Ideal Low-Pass Filter in the Form of a Dispersionless Lag Line," *Proc. I.R.E.*, Vol. 34, pp. 138-144, March, 1946.

<sup>8</sup> Heinz E. Kallmann, "Equalized Delay Lines," *Proc. I.R.E.*, Vol. 34, pp. 646-657, September, 1946.

<sup>9</sup> A. J. Ferguson, "Note on Phase Correction in Electrical Delay Networks," *Canadian Journal of Research*, A, Vol. 25, pp. 68-71, January, 1947.

Equation (12) can be factored to give

$$S = -\frac{4}{3\pi} (\cos \beta + 0.64279) (\cos \beta - 1.71429) (\cos \beta + 1.07149). \quad (13)$$

Inspection of this equation indicates that three cascaded elements, each corresponding to one of the expressions in the brackets of Equation (13), and a gain of  $4/(3\pi)$  can furnish an exact equivalent of the finite Fourier series for the selectivity curve  $S$  of Equation (12). The cutoff rate of the filter can be increased by using more terms in the series of Equation (12), resulting in additional factors in Equation (13).

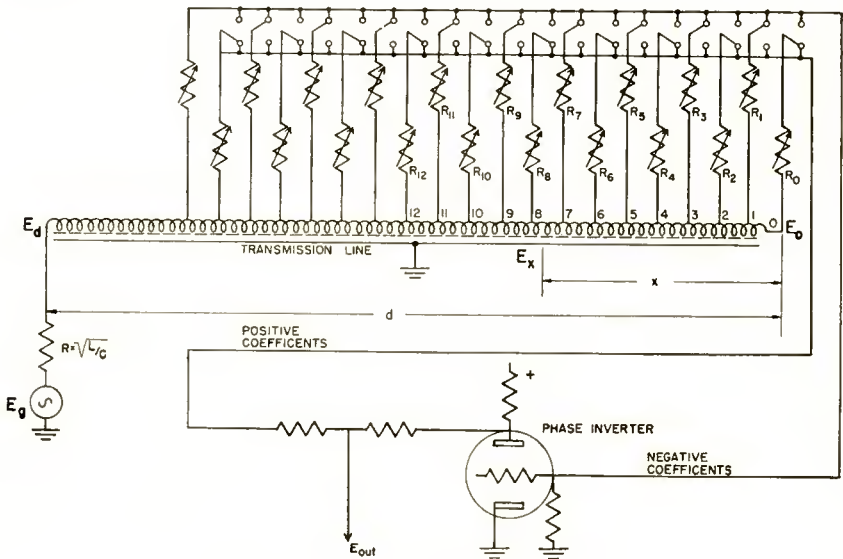


Fig. 16—Transmission-line filter.

It can be shown that the Fourier series for a real function having even symmetry about the origin can only have cosine terms, and that all coefficients must be real numbers. When cosine functions of multiple angles are replaced by power functions of the cosine, in order to obtain a polynomial in  $\cos \beta$ , a polynomial with real coefficients results. The roots of such a polynomial are either real or occur in conjugate pairs. Real roots may be either positive or negative, resulting in cascade element factors of the type  $(\cos \beta - a)$  or  $(\cos \beta + a)$ . These are readily constructed as will be shown in the following section.

Pairs of conjugate complex roots correspond to cascade elements of

the type  $(\cos \beta - a - ib)$  and  $(\cos \beta - a + ib)$ . Upon multiplying the two together, a real number is obtained.

$$\begin{aligned}
 &(\cos \beta - a - ib) (\cos \beta - a + ib) \\
 &= \frac{1}{2} \cos 2\beta + \frac{1}{2} - 2a \cos \beta - b^2 + a^2. \tag{14}
 \end{aligned}$$

Cascade filter elements for this type of factor are also available, as is shown in a later section.

SYNTHESIS FOR REAL ROOTS

In Figure 17(a) a transmission line open at the receiving end and driven from its characteristic impedance at the sending end is shown. From Equations (10) and (11) the sending and receiving end voltages are

$$E_d = E_g e^{-i\theta d} \cos \theta d$$

and

$$E_0 = E_g e^{-i\theta d}$$

respectively.

If the network consisting of  $R_a$  and  $R_b$  in Figure 17(a) is connected to the transmission line as indicated by the dotted lines, and if  $R_a$  and  $R_b$  are much greater than the line impedance so that the loading is negligible, the voltage  $E$  at the junction of  $R_a$  and  $R_b$  is seen to be

$$\begin{aligned}
 E &= \frac{R_a}{R_a + R_b} E_0 + \frac{R_b}{R_a + R_b} E_d \\
 &= \frac{R_b}{R_a + R_b} E_g (\cos \theta d + \frac{R_a}{R_b}) e^{-i\theta d} \tag{15}
 \end{aligned}$$

which is the form required for negative real roots, resulting in cascade terms of the form  $k(\cos \beta + a)$  and a delay angle  $\theta d$ .

Figure 17(b) shows a delay line with a differential amplifier, where the differential voltage is between the grid and cathode. It is assumed that the cathode impedance is sufficiently low compared to the plate load  $R_L$  that it produces negligible cathode impedance feedback. The voltage applied to the input to the line is

$$E_d = \left(\frac{R}{R_c}\right) E_g e^{-i\theta d} \cos \theta d \tag{16}$$

where 
$$R = \frac{R_c (R_a + R_b)}{R_c + R_b + R_c}$$

is the equivalent resistance of  $R_c$  in parallel with  $R_a$  and  $R_b$  in series, and is the termination of the line.

The voltage applied to the cathode is

$$E_k = \frac{R_a R}{R_c} E_g e^{-i\theta d} \cos \theta d. \tag{17}$$

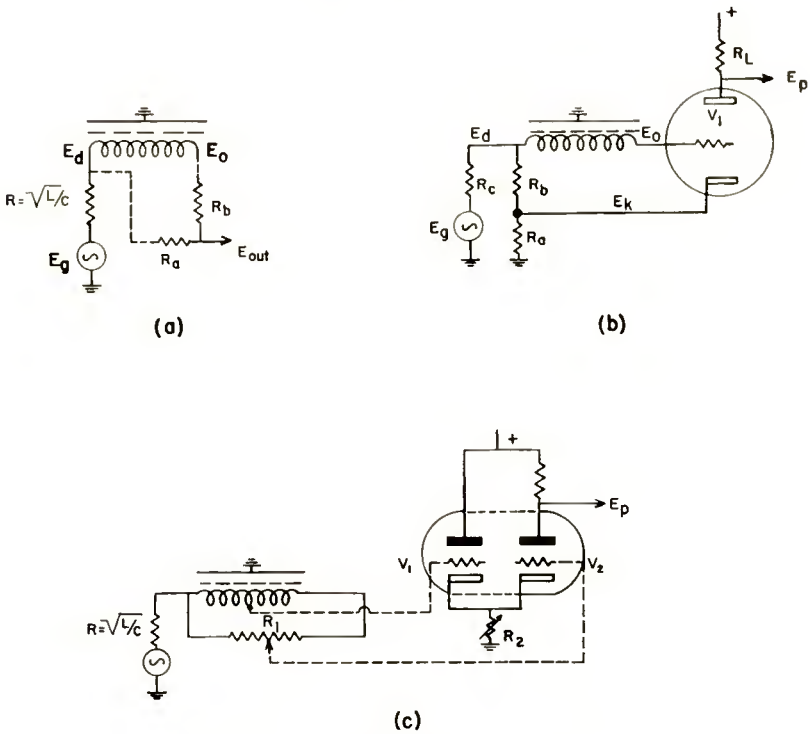


Fig. 17—Synthesis of cascade terms.

The grid voltage is

$$E_0 = \left(\frac{R}{R_c}\right) E_g e^{-i\theta d}. \tag{18}$$

The grid-cathode voltage is

$$E_{gk} = E_0 - E_k = \frac{R_a}{R_a + R_b + R_c} E_g \left[ \left( 1 + \frac{R_b}{R_c} \right) - \cos \theta d \right] e^{-i\theta d}. \quad (19)$$

The plate output voltage is

$$E_p = -\mu E_{gk} \frac{R_L}{R_L + R_p} \quad (20)$$

where  $\mu$  is the amplification factor of the tube,  $R_L$  is the load resistor, and  $R_p$  is the plate resistance of the tube.

$$E_p = \mu \frac{R_L}{R_L + R_p} \frac{R_a}{R_a + R_b + R_c} E_g \left[ \cos \theta d - \frac{R_a + R_b}{R_a} \right] e^{-i\theta d} \quad (21)$$

which is of the form  $k(\cos \beta - a)$  where  $k$  and  $a$  are constants. This is the form required for positive real roots.

SYNTHESIS FOR CONJUGATE ROOTS

Complex conjugate root pairs present a somewhat more difficult problem. Consider the complex conjugate factors  $(\cos \beta - a - ib)$  and  $(\cos \beta - a + ib)$ . A network can be found to represent the conjugate pair of roots accurately. In Figure 17(c) a transmission line with a

center tap is shown. In Equation (9), let  $x = \frac{1}{2}d$  so

$$E_{\frac{1}{2}d} = E_g e^{-i\theta d} \cos \frac{1}{2} \theta d. \quad (22)$$

If connections are made to the grids of the differential amplifier  $V_1 - V_2$ , the output voltage  $E_p$  will be of the required form when  $R_1$  and  $R_2$  are set for the proper coefficients. This type of differential amplifier is well known.<sup>10</sup>

Resistor  $R_1$  allows variable ratio addition of sending and receiving

end voltages to obtain the terms  $\frac{1}{2} \cos 2\beta + \frac{1}{2} + a^2 + b^2$  in accord with

<sup>10</sup> George E. Valley, Jr. and Henry Wallmann, *Vacuum Tube Amplifiers*, M.I.T. Radiation Laboratory Series, Vol. 18, McGraw-Hill Book Company, Inc., New York, N. Y., 1948, p. 442.

Figure 17(a). Resistor  $R_2$  permits subtraction of the term  $2a \cos \beta$  by selecting the proper amount of the center tap voltage. The output voltage is therefore

$$E_p = k \left( \frac{1}{2} \cos 2\beta - 2a \cos \beta + \frac{1}{2} + a^2 + b^2 \right) \quad (23)$$

where  $\beta = \frac{1}{2} \theta d$ .

According to these results an approximation to the Fourier development of the selectivity curve obtained by taking the first  $n$  terms of the series can be accurately obtained from  $n$  circuits in cascade. When possible, they should be cascaded directly by stepping up impedance levels between elements to prevent loading effects. In general, however, an isolating amplifier between sections is highly desirable.

Comparison of the cascade and additive methods indicates that the additive method offers a more straightforward approach due to the ready availability of elements representing the terms of the Fourier series directly. It has the disadvantage that a great number of gain settings have to remain fixed in order to maintain the proper relationship between the coefficients of the Fourier development of the selectivity curve. The cascade method has the advantage that the gain of the different cascade elements may vary, one with respect to the other, without affecting the selectivity curve. It has the disadvantage that more mathematics is required to obtain the cascade elements which represent the desired Fourier series. The number of terms required for a good approximation to a desired selectivity curve will usually be the deciding factor in choosing which of these methods is to be employed in a specific case.

#### SUPPRESSION OF MULTIPLE RESPONSES

In Figure 14 it is seen that the selectivity curve is a repetitive function with symmetry about the zero-frequency ordinate. It is generally desirable to obtain only one passband or one stopband. One possible way of doing this is to adjust the Fourier development in such a manner that undesired repetitions of the selectivity curve fall outside the passband of the remaining portions of the system with which the filter is to be associated, since band limiting is inherent in most systems. Where such band limiting is not present to an adequate degree, and multiple response regions are widely separated, it is usually found that

the Fourier series does not converge very rapidly, so that a great many filter elements are required to obtain the desired response function. Another and more expedient approach is available. The elements themselves may be given bandwidths in excess of the bandwidth of the composite filter by an amount sufficient only to maintain linear phase over the pass region of the composite filter. The cutoffs of the elements are then designed so the attenuation is rapid outside the passband. Certain lumped-constant approximations to transmission lines are suitable since it is possible to obtain essentially constant time delay from them over extended portions of their passband.<sup>7-9</sup>

A third possibility is for the filter to be followed by a conventional filter of good phase characteristics over the desired selectivity curve and high attenuation in the undesired response regions. This is generally possible since, according to the Fourier development, passbands and stopbands occur alternately and there is no restriction on the phase of the supplementary conventional filter for frequencies in the stopband of the Fourier development filter.

#### EXPERIMENTAL RESULTS

Filters based on the principles discussed above have been constructed and their actual performance has been found to be in substantial agreement with the theory. They have been advantageously used for band limiting and band splitting in color television applications, and have been adapted to perform the functions of linear-phase high-frequency peaking as well.

To design a line to give a low-pass filter of specified bandwidth it is usually desirable that the low-pass bandwidth of Figure 14 correspond to approximately one-half the width of the band rejection which follows. This gives rapid convergence of the Fourier series. For a line of lumped constants, the fundamental component of the Fourier series requires a length of line determined by  $\theta = \pi/2$  or  $LC = 1/(16 f_0^2)$  where  $f_0$  is the first point of infinite rejection of the filter.

The line is designed by selecting the characteristic impedance desired, which gives  $L/C$ . The  $L$  and  $C$  values are then selected to give a reasonable size wire and spacing. For constant delay the usual theory of the distortionless line is used. The articles by Golay,<sup>7</sup> Kallmann,<sup>8</sup> and Ferguson<sup>9</sup> give the details of the design.

For laboratory purposes it is useful to have a filter built according to Figure 16. Each tap can be connected to either side of the line by the double-throw switch. Each amplitude is adjustable by the variable resistor. If the fundamental is taken from tap 1, the second harmonic

from tap 2, etc., a certain bandwidth will be obtained which can be varied some by proper choice of the resistors  $R_1$ ,  $R_2$ , etc. By such a process a wide variety of bandwidths can be synthesized rapidly by proper choice of taps.

Figure 18(a) shows the square-wave response of a  $\frac{\sin \omega}{\omega}$  filter that

was designed to give a linear response to a unit-step function, followed by a sharp corner and a constant value following the rise. The amplitude response to a linear sweep is shown above the square-wave response. Figure 18(b) shows a filter that has a sharp linear cutoff. The two markers on the selectivity curve, which is the upper curve,

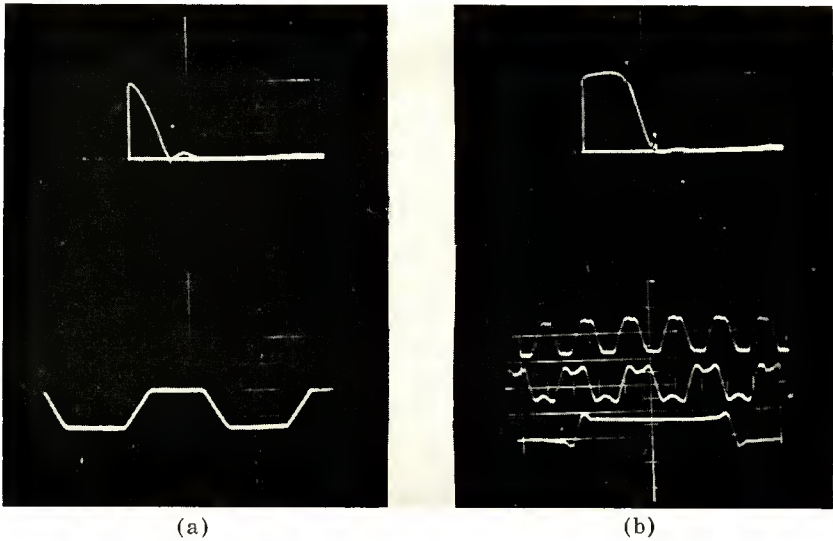


Fig. 18—Amplitude and square-wave responses of filters.

are at 2100 and 2700 kilocycles respectively. Starting at the bottom of Figure 18(b), the first curve is the response to a 150-kilocycle square wave. The next one is 700 kilocycles and the last one has a 900-kilocycle repetition rate. As the repetition rate of the square wave is speeded up it approaches a sine wave smoothly as the higher harmonics are stopped by the filter. The symmetry of the response function is to be especially noted and the relative rate of filter cutoff is indicated by the rapid change in wave shape of the response for square waves between 700 and 900 kilocycles. These responses are in substantial agreement with those of Figure 15 with which they should be compared.

## APPLICATIONS

Constant-time-delay filters are ideal for television systems where band limiting is a necessary feature of the system. They have applications in frequency-interlaced color television systems where the original signal must be encoded in circuits of different bandwidths prior to multiplexing and where the decoded signals from the several circuits must all arrive simultaneously at the reproducer. This requires the same constant time delay in each channel. They are generally desirable wherever symmetrical transients result in signals with greater intelligibility than signals with the nonsymmetrical transients of variable-time-delay filters. They are suitable for aperture correction circuits.

In addition to these uses, they are adaptable to use as linear-phase band-stop and band-pass circuits with many applications in communications. In transmission networks it is possible to correct the phase linearity by any network available, without regard to the resulting amplitude response. The selectivity curve can then be adjusted separately without any effect on the phase linearity.

## CONCLUSIONS

A method has been developed for producing symmetrical transients by means of constant-time-delay networks. These networks are not of the minimum-net-phase-shift type so it is possible to have selectivity curves which are independent of the phase response. Such filters have many applications in television systems.

A laboratory filter has been designed with which any desired selectivity curve can be obtained by merely throwing double-throw switches to the proper polarity and by adjusting the values of variable resistors. All such filters have linear phase throughout the passband. They are therefore very useful in correcting the amplitude response of a filter after the phase linearity has been compensated by conventional methods.

These symmetrical transients increase the detail contrast and sharpness of both monochrome and color television pictures without introducing objectionable ringing. They are useful in any other communication system where a symmetrical pulse response increases the intelligibility or resolution of the system.

## APPENDIX

In a lossless transmission line let  $E_x$  be the voltage at a point  $x$  units from the receiving end,  $I_x$  the current at point  $x$ ,  $L$  the inductance per unit length,  $C$  the capacitance per unit length, and let  $\omega$  be the

applied frequency. Then

$$\frac{dE_x}{dx} = i\omega LI_x \quad (24)$$

and

$$\frac{dI_x}{dx} = i\omega CE_x \quad (25)$$

since there are no losses. These equations can be solved to give

$$I_x = A_1 e^{i\theta x} + A_2 e^{-i\theta x} \quad (26)$$

$$E_x = A_1 \left( \frac{L}{C} \right)^{\frac{1}{2}} e^{i\theta x} - A_2 \left( \frac{L}{C} \right)^{\frac{1}{2}} e^{-i\theta x} \quad (27)$$

where  $A_1$  and  $A_2$  are constants and  $\theta = \omega(LC)^{\frac{1}{2}}$ .

Let the generator voltage be  $E_g$  with internal impedance  $R = \left( \frac{L}{C} \right)^{\frac{1}{2}}$ .

Then for an open-ended line

$$I_0 = 0 = A_1 + A_2$$

so

$$A_1 = -A_2. \quad (28)$$

The voltage at the sending end is

$$E_d = 2A_1 \left( \frac{L}{C} \right)^{\frac{1}{2}} \cos \theta d = E_g - I_d \left( \frac{L}{C} \right)^{\frac{1}{2}} \quad (29)$$

where  $I_d$  is the sending-end current.

From Equation (26)  $I_d = 2A_1 i \sin \theta d$ .

Substituting in Equation (29)

$$A_1 = \frac{1}{2} E_g \left( \frac{L}{C} \right)^{-\frac{1}{2}} \cdot e^{-i\theta d}. \quad (30)$$

This gives

$$E_x = E_g \cos \theta x \cdot e^{-i\theta d}. \quad (31)$$

# SYNTHETIC-PATTERN GENERATOR FOR THE SOLUTION OF CERTAIN INSTRUMENTATION PROBLEMS IN TELEVISION\*

BY

RICHARD C. WEBB†

*Summary*—A new television test-pattern generator has been designed that will produce a wide variety of calibrated patterns directly from vacuum-tube oscillators, multivibrators, etc. The instrument has a number of features which add to its usefulness to the broadcaster, manufacturer and research laboratory, and make it an extremely useful reference signal source for setting up new equipment or maintaining video systems. For example, it enables quick measurement or adjustment of video amplifiers, equalizers, and transmission lines. Transient characteristics of transmission circuits as well as their gray-scale performance are readily visualized. In addition, a selection of bar patterns are available for adjusting the scanning linearity of cameras, monitors, and receivers.

## INTRODUCTION

COMPREHENSIVE testing and adjustment of television transmission systems is not accomplished with the same ease and precision that has come to be commonplace in the field of sound transmission. This is primarily due to the fact that in television an inherently two-dimensional transmission medium (amplitude/time) must be multiplexed in order to carry information concerning two space dimensions in addition to a point-by-point measure of brightness values. The basic elements of this multiplexing structure are the vertical and horizontal blanking intervals which punctuate the transmission of a brightness-amplitude/time function that is, in other respects, similar to an audio signal except for the fact that its transient nature requires a frequency band approximately 267 times wider and includes components extending to direct current. Advantage is taken of the fundamental timing structure in order to obtain direct-current setting in television transmission equipment, and for this reason it is usually necessary to include a standard blanking pedestal with all test signals, since only with this provision can the equipment respond just as it would when pictures are being carried.

---

\* Decimal Classification: R355.913.5.

† Formerly, Research Department, RCA Laboratories Division, Princeton, N. J. Now with Denver Research Institute, University of Denver, Denver, Colo. The work described in this paper was done while the author was with RCA.

In addition to the frequency- and phase-response measurements that are normally made on all types of communication systems, it is customary to test the linearity of the amplitude response as well. In high-quality audio equipment, each element of the system is expected to be a precisely linear device. Therefore, critical amplitude distortion measurements are made either with a wave analyzer or by observing the magnitude of the intermodulation components that are produced when two test signals are applied to the system simultaneously. Television equipment, however, includes certain elements that are inherently nonlinear while others are linear. Furthermore, although the desired over-all transfer characteristic is frequently linear (unity gamma), occasionally some prescribed nonlinear transfer relation may be sought. Measurements of such a characteristic are most readily accomplished with the aid of a test signal comprised of a number of discrete amplitude levels arranged in a known manner as in a photographic gray scale.

One additional requirement in television measurements that has no counterpart in audio work is the determination of scanning linearity both at the camera and at the receiver, since a combination of these two characteristics determines the geometric distribution of picture components in the received image. These measurements are generally made with the aid of a set of timing markers that are seen in the display as a grid of parallel lines.

From the preceding it is evident that the best way to test a television transmission system is with a television picture; hence, the widespread use of test charts and monoscope patterns throughout the industry. In practice, this type of testing is quite useful since in the end the human eye will be the final judge of picture quality. However, the technique borders on the line of listening tests on audio equipment although it is undoubtedly more quantitative. One of the chief objections to the method is the fact that small defects inherent in cameras are included in the test signal. Such things as beam noise, shading, limited resolution, gray-scale errors, and scanning inaccuracies, although reduced to trivial amounts by viewing standards, should certainly be avoided in establishing a reference standard test signal.

A synthetic-pattern generator has been designed to fulfill the need for an effective television test signal source, free of the limitations of electro-optical devices and capable of producing many of the idealized test patterns that have been found useful by the industry as set forth in both the IRE and RTMA standards on television testing.<sup>1-5</sup>

---

<sup>1</sup> IRE 22 S1 Standards on Television: Methods of Testing Television Transmitters, 1947.

<sup>2</sup> IRE 22 S1 Standards on Television: Methods of Testing Television Receivers, 1948. (Adopted by ASA, C16, 13-1949)

## PATTERN GENERATORS

The synthetic-pattern generator shown in Figure 1 was built as part of a thesis program at Purdue University. The instrument provides the same type of television signal that might be found on the cable from a studio camera or a monoscope. Signal levels up to 2 volts peak-to-peak across 75 ohms are available in either blacks negative or whites negative polarity. In addition, a selection can be made of the actual source impedance of the output stage to facilitate studies of the termination requirements of long lines, etc. Source impedance levels of 50, 75, 100, 300 and 1000 ohms are available.

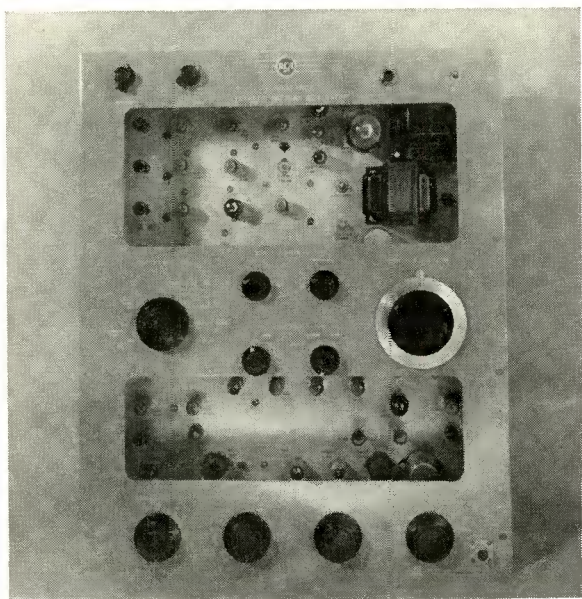


Fig. 1—First model of the synthetic pattern generator.

The frequency response of the output circuit is 10 megacycles wide, but a high frequency de-emphasis network can be selected which has the slope of a single R-C section with a time constant ranging from

<sup>3</sup> IRE 23 S1 Standards on Television: Methods of Measurement of Television Signal Levels, Resolution, and Timing of Video Switching Systems, 1950.

<sup>4</sup> IRE 23 S2 Standards on Television: Methods of Measurement of Time of Rise, Pulse Width, and Pulse Timing of Video Pulses in Television, 1950.

<sup>5</sup> RMA Standards TR-104, "Electrical Performance Standards for Television Broadcast Transmitters, Channels 1 to 13," *Proc. I.R.E.*, pp. 932-938, July, 1948,

0.7 microsecond to 1.5 microseconds in 0.1-microsecond steps. This latter feature makes it possible to send test patterns through the very first stage of camera preamplifiers and other equipment where frequency equalizers or "high peakers" are used simply by selecting the appropriate time constant in the output amplifier of the test generator.

#### TEST PATTERNS

Any of the following adjustable test patterns may be chosen by means of a selector switch:

1. Horizontal bars, black on white, 5 to 20
2. Horizontal bars, white on black, 5 to 20
3. Vertical bars, black on white, 5 to 20
4. Vertical bars, white on black, 5 to 20
5. Combination bars, black on white, 5 to 20
6. Combination bars, white on black, 5 to 20
7. Horizontal gray scale, 5 to 20
8. Vertical gray scale, 5 to 20
9. Sine waves at spot frequencies of 100, 200, 300, 400, 500 kilocycles, and continuously adjustable from 0.6 to 10 megacycles.

A second model of the instrument, which was built at the RCA Laboratories, is shown in Figure 2. In addition to the above patterns, this provides a test pattern consisting of six arbitrary sample spot-frequency sine-wave bursts along each horizontal scanning line.

#### EXTERNAL DRIVING SIGNALS

Horizontal and vertical driving pulses must be supplied to the instrument from the studio sync generator in order to lock in the otherwise free-running internal multivibrators to synchronous operation with the standard television scanning rates. The instrument produces its own blanking signals, but no provision is made for associating sync signals with the video within the unit. Wherever this is required it would be done in one of the studio sync mixing amplifiers just as in the case of a monoscope or any other camera.

#### BAR PATTERNS

Figure 3 shows a sample photograph taken from the screen of a monitor kinescope illustrating one of the bar patterns generated by the instrument (combination bars, black on white). Oscillograms taken at both line and field scanning rates are also shown. Either vertical or horizontal bars may be selected alone or combined as shown, and the

number of bars is adjustable in either direction from 5 to about 20. The spacing between bars is held precisely constant by means of multi-vibrator-type circuits. On a receiver having proper interlace, the horizontal bars will be seen to occur on adjacent scanning lines (one line in each field) thus forming a bar 2 picture elements wide. The length of the horizontal bars may be adjusted by a panel control from about  $\frac{1}{2}$  of the width of the screen to several screen widths. The latter long bars appear on subsequent pairs of scanning lines thus permitting the bar to grow in thickness as the control is advanced. Figure 4 shows these horizontal bars when adjusted to be 2 lines wide with a length of about  $\frac{1}{2}$  of the screen width. Incidentally, this type of pattern

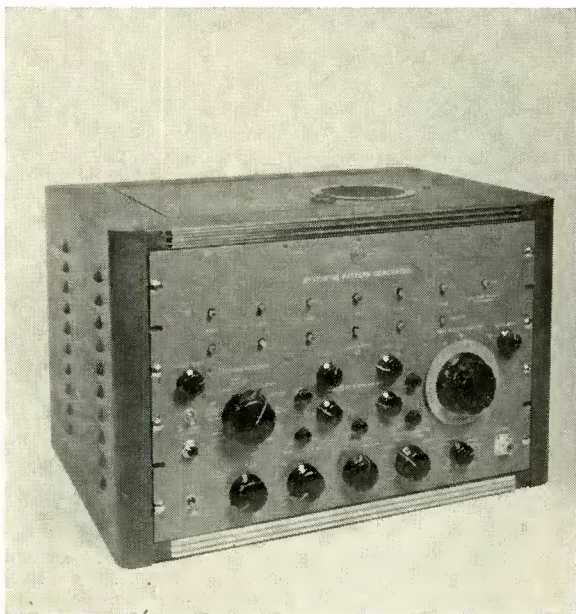


Fig. 2—Later model of the synthetic pattern generator.

provides a very sensitive check on medium-low-frequency performance of video circuits as indicated by any streaking that may follow to the right of the bar segment.

The vertical bars are available in three widths. The narrowest bars are approximately 2 picture elements wide (0.162 microsecond) as shown in Figure 3. The intermediate width is roughly 1.5 microseconds and the widest bars are about  $\frac{1}{3}$  of the screen width. All of the bar signals are passed through a very effective clipper, so that

their edges are sharp enough to provide a good square-wave test of a transmission system. The rise time of the bar signals is about 0.05 microsecond.

#### GRAY SCALES

One of the most useful signals produced by the instrument is the stair step or gray-scale pattern. In addition to its use in making dynamic transfer measurements, adjusting gamma-correction amplifiers, etc., the horizontal step signal is particularly useful in examining

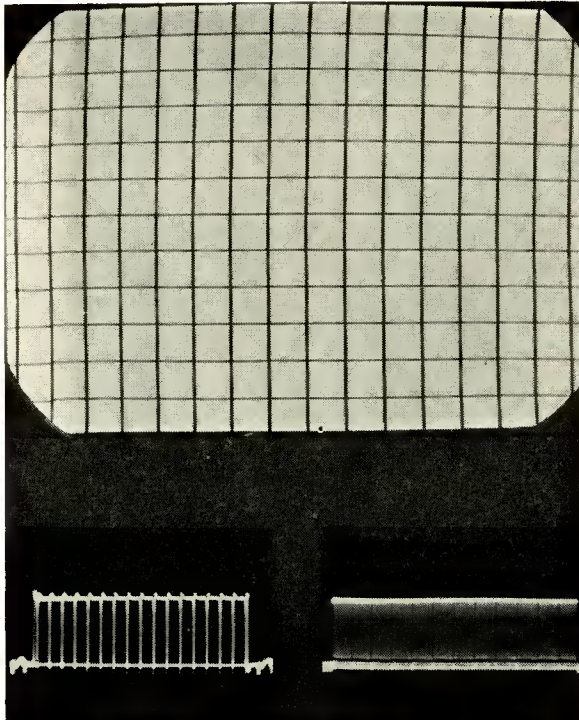


Fig. 3—Sample bar pattern; line sweep (lower left) and field sweep (lower right).

the low-frequency performance of transmission circuits, since even the slightest low-frequency phase shift is visible as a tilt in the step waveform when viewed on a cathode-ray-oscilloscope at field sweep rate. Figure 5 shows the horizontal step wedge adjusted for 5 steps.

The vertical stair step pattern shown in Figure 6 serves the same general purpose as the horizontal steps. However, the frequencies present in its waveform are much higher and the slots that are cut

down to black level between steps are useful in giving an indication of the transient response of nonlinear circuits such as gamma correction amplifiers since it provides a sample square wave at various amplitude levels.

#### SINE-WAVE TEST SIGNALS

A very useful form of sine-wave signal source has been developed as one feature of the pattern generator. It consists of a three-phase ring-type R-C phase-shift oscillator<sup>6,7</sup> keyed to quiescence during the



Fig. 4—Short horizontal bars two lines high; line sweep (lower left) and field sweep (lower right).

vertical and horizontal blanking intervals. Each time the oscillator is turned on at the start of a new horizontal line, it begins in the same phase position that it had at the start of the preceding line. Thus a stationary pattern of vertical lines spaced in inverse proportion to the

<sup>6</sup> E. L. Ginston and L. M. Hollingsworth, "Phase-Shift Oscillators," *Proc. I.R.E.*, Vol. 29, pp. 43-49, February, 1941.

<sup>7</sup> Chance, Hughes, MacNickel, Sayre, and Williams, *Wave Forms*, MIT Radiation Series, Vol. 19 (McGraw-Hill, 1949, pp. 110-115).

frequency setting of the oscillator is obtained. Figure 7 shows the pattern as it appears at 0.75 megacycle.

The synchronous feature of this test signal extends its usefulness beyond the frequency-response measurements for which it was primarily intended. It has been found useful in the precision measurement of horizontal-scanning linearity; measurement of short time intervals; and measurement of the limiting resolution of kinescopes, storage tubes, recording systems, etc. For example, a studio camera might be set up to scan a regular grating of vertical lines thus obtain-

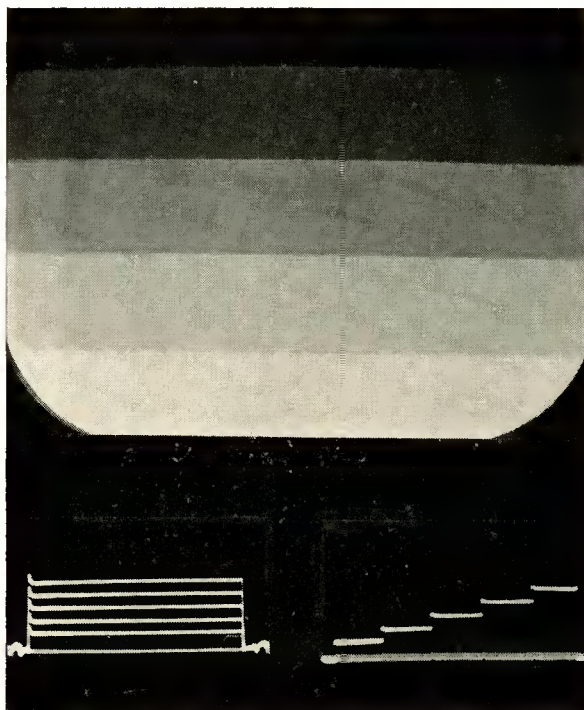


Fig. 5—Horizontal gray scale pattern; line sweep (lower left) and field sweep (lower right).

ing a video signal having a fundamental component of perhaps 2.0 megacycles. The signal from the pattern generator set at 2.0 megacycles is then mixed with the camera output and the combination viewed on a monitor. The equivalent of interference fringes or a bold beat pattern between the uniform signal from the pattern generator and that developed by the camera can then be seen. At 2.0 megacycles, a scanning error of one part in 214 produces one fringe.

In color television research, where video sampling, subcarriers, and high-low filters are involved, the synchronous sine-wave pattern has proven to be a particularly useful laboratory tool. A frequency range of 0.6 to 10 megacycles can be covered in one sweep of the dial, and any point can be set to an accuracy of  $\pm 2$  per cent. The signal amplitude is automatically held constant within  $\pm 3$  per cent over the entire range, and there is no amplitude instability in case the tuning dial should be rocked rapidly through a portion of its range. Point-by-point frequency-response measurements can readily be made using a

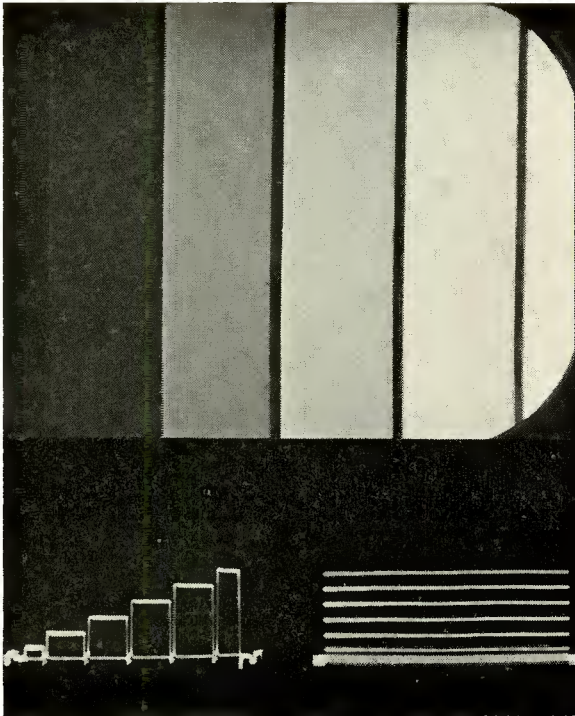


Fig. 6—Vertical gray scale pattern; line sweep (lower left) and field sweep (lower right).

wide-band oscillograph as a detector. In some cases, however, where only a quick performance check of a circuit is required, the monitor kinescope itself can be used as the detector. The background control of the kinescope is backed off so that the positive tips of the sine-wave pattern produce a low-brightness pattern on the screen. As the frequency control is swung over the video band, any peaks or valleys in the frequency response become visible as a brightness change on the screen.

## SINE-BURST GENERATOR

The pattern produced by the sine-burst generator is shown in Figure 8. It consists of short bursts of sine-wave test signals at various spot frequencies arranged in sequence along each horizontal line. The frequencies in this case are approximately 0.5, 1.0, 2.0, 3.0, 3.5, and 4.0 megacycles. This pattern makes it convenient to examine the frequency-response characteristic of transmission systems rapidly by displaying the oscillogram of the signal at line scanning rate upon

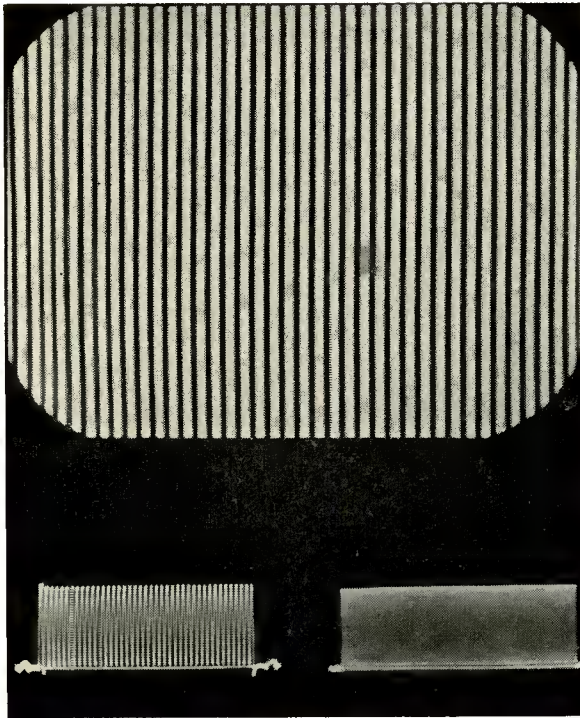


Fig. 7—Sine-wave test signal set at 0.75 megacycle; line sweep (lower left) and field sweep (lower right).

a wide-band oscilloscope. The performance of the circuit under test is interpreted in terms of the relative heights of the bursts much as the cathode-ray-oscilloscope trace is studied when sweep-frequency equipment is used. Moreover, this signal has the advantage of being able to pass through all types of television circuits without modification. However, since discrete frequencies are used, errors might be made in cases where abrupt changes occur in the frequency characteristic

under test. Nevertheless, the signal has considerable value in giving a rapid indication of the general trend.

A video test-signal generator of this kind was recently developed by Morrison, Borkan, and Reddeck<sup>8</sup> and a modified version of their design is incorporated in the second model of the pattern generator. For calibration of the burst frequencies, the continuously variable sine-wave pattern generator can be switched on simultaneously and adjusted to zero beat with each of the sine bursts in turn.

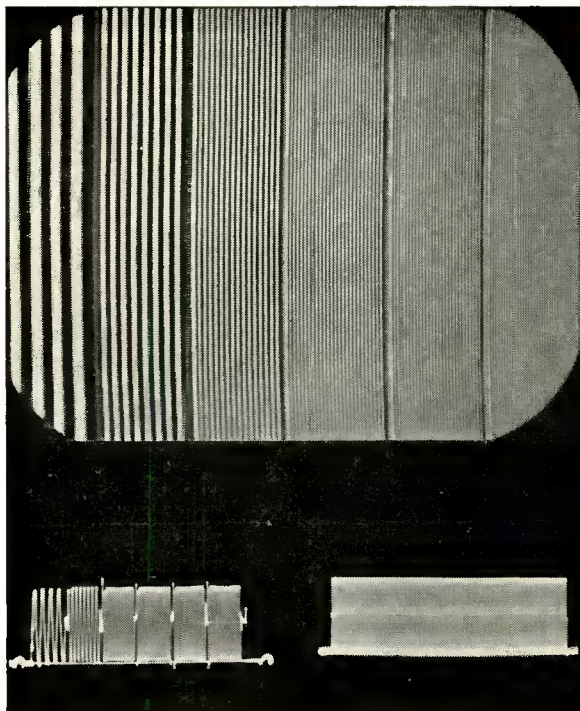


Fig. 8—Sine-burst signal, 0.5, 1.0, 2.0, 3.0, 3.5, and 4.0 megacycles; line sweep (lower left) and field sweep (lower right).

#### OPERATION OF THE INSTRUMENT

Figure 9 shows the functional relationships between various circuit groups within the instrument. All of the individual generator circuits are brought to the pattern selector switch at 500 ohms impedance level

<sup>8</sup> W. C. Morrison, H. Borkan, and J. G. Reddeck, "A Video Test Signal Generator," *Electronics*, Vol. 25, pp. 139-141, September, 1952.

and at this point the signal amplitude is controlled. The first stage of the output amplifier is arranged to minimize capacitive loading on the amplitude control potentiometer as can be seen in the lower left hand portion of the schematic diagram, Figure 11. Simple shunt peaking is employed in the second stage of the amplifier V-14, and the high-frequency de-emphasis circuit is arranged to shunt the plate load resistor at this point. The third stage is a compensated picture-polarity inverter which is switched simultaneously with the bias for the output stage as it is applied via the clamping diodes. This is done in order to place picture black level at the foot of the most linear range of the output tubes for both signal polarities.

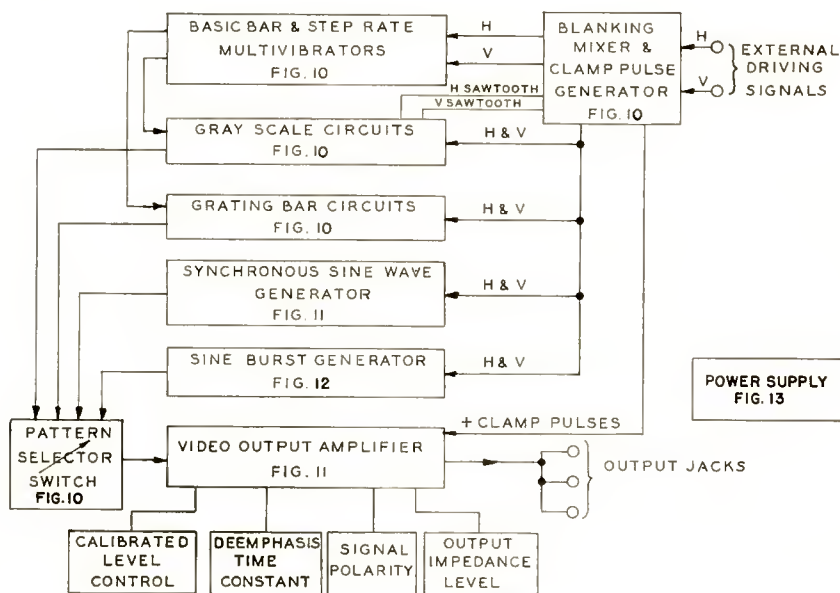


Fig. 9—Block diagram of pattern generator.

Since pentode tubes are used in the output stage, the basic internal impedance of the pattern generator approximately equals the final plate load resistor of 1000 ohms. In order to make the instrument have other apparent internal impedances so that long transmission lines, filters, etc., may be conveniently terminated on both ends during tests, a selection of shunting resistors is provided to establish additional source impedance levels of 50, 75, 100, and 300 ohms.

Both of the gray-scale patterns are generated by adding two sawtooth waveforms together. The lower of the two provides the basic period of the wave (1/60 second for horizontal and 1/15,750 second

for vertical patterns) while the higher frequency sawtooth wave added in reverse polarity produces identical stepwise increments. Thus at the top of Figure 10, multivibrators V-20 and V-23 provide the basic period for the horizontal and vertical step patterns while V-35 and V-27 supply the higher frequency components to their respective summation circuits.

The same variable speed multivibrator circuits which are used as above to develop the gray-scale patterns also provide the pulses for the grating bar patterns, and hence the number and adjustment of the bar and step-wedge signals are identical. The final waveform clipping of the bar signals is accomplished with the use of crystal diodes between V-40 and V-41A in the left center part of Figure 10.

The schematic diagram of the keyed sine-wave oscillator is shown at the top of Figure 11. Tubes V-9, V-10 and V-11 comprise the three-phase ring oscillator, with frequency being determined by variable shunt capacitor  $C_2$  and the 680-ohm plate-load resistors. V-8 is supplied with positive-going blanking pulses so that during each pulse it draws all of the plate current it can for zero grid volts and remains cut off thereafter. The plate current for V-8 is taken through the load resistors of oscillator tubes V-9 and V-11 with appropriate isolating resistors. Thus during blanking a large negative pulse is produced on the grid of V-10, cutting off this tube and opening up the oscillatory ring. At the end of blanking, conditions for oscillations are re-established and the signal begins again, unchanged in amplitude and always in the same phase position. Thus a stationary sine-wave pattern is obtained at any frequency setting. The signal may be conveniently viewed on an oscillograph running at line-sweep rate or directly upon the monitoring kinescope.

Since the frequency of this oscillator is inversely proportional to the value of  $C_2$ , a tuning range of 17 to 1 may be accomplished directly with a three-gang capacitor having a natural range of 13 to 603 micro-microfarads. Additional lower spot frequencies can be obtained by adding fixed capacitors to shunt  $C_2$ .

Amplitude control of the oscillator is accomplished by allowing the three oscillator tubes to take a "bite" of grid current during the positive peaks of the grid swing. It has been found that with the circuit constants given, the tubes take so small a "bite" that the waveform distortion attributable to this cause is negligible.

The circuit of the sine-burst generator is shown in Figure 12. Tubes V-53 through V-58 produce sine-wave bursts as they are pulsed by the multivibrator circuits above. The six burst signals ranging from 0.5 to 4 megacycles, are gathered on a common bus and applied

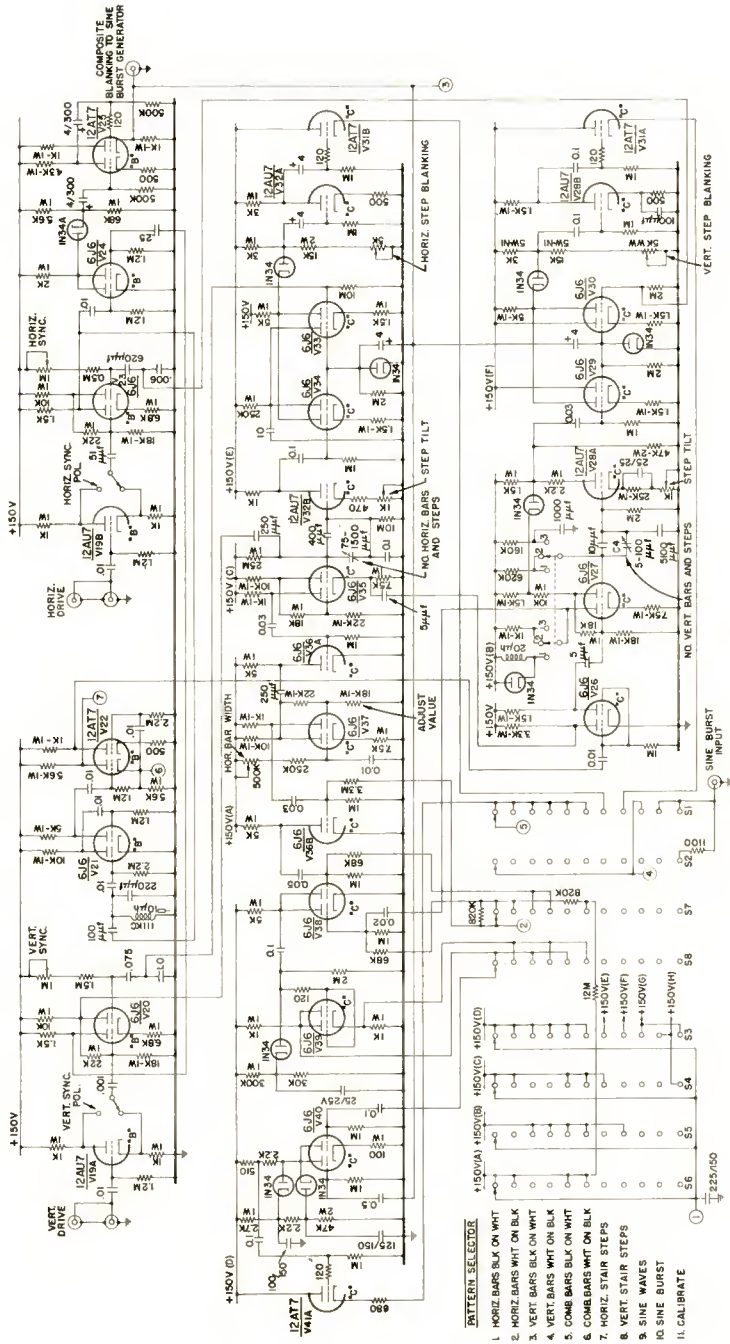


Fig. 10—Bar and step-wedge generator.

to amplifier and blanking mixer tube V-52 before passing to the pattern selector switch via cathode follower V-42B. The tandem chain of mono-stable multivibrators V-43 through V-48 form the driving pulses for the burst oscillators after amplification in buffer stages V-49 through V-51. These latter tubes also serve to isolate the individual tandem multivibrator stages and provide a one-microsecond delay between bursts.

The pattern-selector switch through which all of the signals must pass to reach the video output amplifier also switches the power-supply voltage to the necessary portions of the circuit for any given pattern. The possibility of cross talk from undesired patterns is thus eliminated,

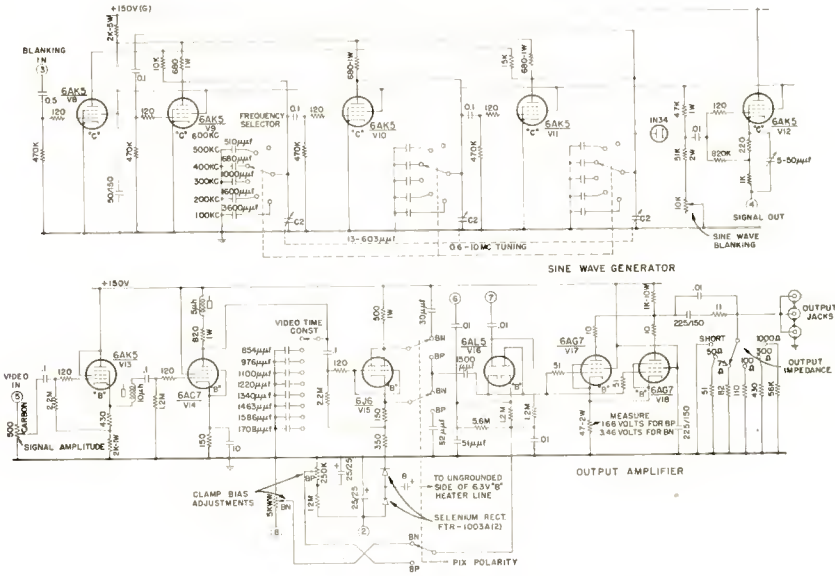


Fig. 11—Keyed sine-wave generator and output amplifier.

since only one pattern circuit is active at any one time except when it is desired to calibrate the sine-burst generator by noting zero beats with the variable frequency sine wave source. In this case, both circuits are made operative and the signals are applied in parallel to the output amplifier.

Plate-supply voltage for the instrument is taken from an extremely well regulated 150-volt power supply shown schematically in Figure 13. The maximum current requirement is approximately 275 milliamperes.





# BROADBANDING OF RESONANT-TYPE MICROWAVE OUTPUT WINDOWS\*

BY

T. S. CHEN

Tube Division, Radio Corporation of America,  
Harrison, N. J.

*Summary*—This paper discusses the development of a broadband window assembly for use as the output of moderate-power tunable magnetrons. The assembly is required to provide free transmission of microwave energy over a maximum bandwidth consistent with minimum reflections throughout the band.

The resonant-type output window used in these magnetrons consists of a thin ceramic plate brazed across the waveguide between two frames containing rectangular openings. Broadbanding of this window has been accomplished by the addition of a resonant iris at a fixed distance on each side of the ceramic plate. Bandwidths of 1000 and 1570 megacycles, with center frequency respectively at 9150 and 9350 megacycles, have been obtained for two different kinds of ceramic. The voltage-standing-wave ratio was below 1.10 in both cases and response was uniform throughout the transmission region. The principle of broadbanding is substantiated by the theory of maximally flat filters. Design formulas and procedures are presented to facilitate the selection of proper proportions for the window elements and the prediction of the performance of the assemblies.

## INTRODUCTION

THE output window in a multi-cavity magnetron serves as a vacuum seal through which power at microwave frequencies is transmitted to the load. The type of window discussed in this paper consists of a thin ceramic plate cut to the internal dimensions of the output waveguide and sandwiched between two iris diaphragms. The entire structure is brazed in position across the guide. The window structure behaves like a parallel tuned circuit; at resonance, the incident power from the magnetron is almost wholly transmitted to a matched load. At frequencies a little off resonance, however, appreciable reflection occurs. Because a magnetron cannot operate successfully into a mismatch presented by a voltage-standing-wave ratio exceeding 1.5, this type of window must be broadbanded over the tunable frequency range of the tube with which it is associated.

In view of its selective characteristics, the window assembly described above is designated as a resonant-type output window. With proper broadbanding methods, this resonant-type window can be made

---

\* Decimal Classification: R339.2.

to have a reflection coefficient which is substantially zero over a wide band of frequencies. In a series of output windows in which AlSiMag 243\* was used as the ceramic material, a 1050-megacycle bandwidth having a voltage-standing-wave ratio below 1.10 and a center frequency of 9150 megacycles has been obtained consistently after broadbanding. When an experimental blend of forsterite ceramic composition is substituted, the center frequency is raised to 9350 megacycles and the broadband characteristic is extended to a range of 1510 megacycles over which the reflections are uniformly low. The bandwidth attainable and the insertion loss of the assembly can be predicted from the theory discussed in this paper. The method for the proper proportioning of the window structure and the matching elements and for the determination of their relative position to obtain the proper interaction is also described. In addition, performance data for complete window assemblies are included. These performance data indicate satisfactory agreement between the actual test results and the theoretical calculations.

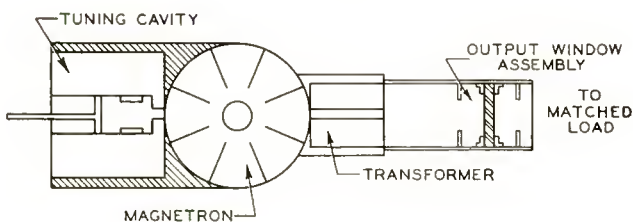


Fig. 1—Diagram of magnetron and associated components showing position of output window assembly.

#### PRINCIPLES UNDERLYING THE METHOD OF BROADBANDING

The resonant-type output window can be made to transmit a sufficiently wide range of frequencies by the application of principles developed in connection with the design of microwave bandpass filters. In filters, however, the region of free transmission is comparatively narrow and attenuation is high outside that region. In window assemblies, it is desired to obtain a maximum bandwidth with low reflections, attenuation outside the pass band being incidental.

Figure 1 shows the position of the output window assembly in relation to the magnetron and its tuning accessories. The window is connected to a matched load on the right and to the magnetron on the left. The low impedance of the magnetron is transformed to the high-

\* Trademark registered by American Lava Corporation, Chattanooga, Tennessee.

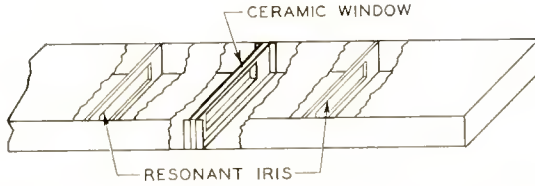


Fig. 2—Diagram of output window assembly showing relative position of ceramic window and resonant irises.

impedance level of the waveguide by means of a transformer. It may be assumed in the design and analysis that the window assembly works into a pure resistance on each side.

A diagram of the window assembly is shown in Figure 2. The two outer matching elements in this diagram are resonant irises. The performance of the window may be simulated by a parallel resonant circuit, such as that shown in Figure 3(a), in the form of a two-terminal-pair network. An open resonant iris, as a microwave component, is also equivalent to a parallel tuned circuit. If two identical irises having the same resonant frequency as the window are spaced a quarter wavelength on either side of the window, as shown in Figure 2, the lumped-constant analog of the assembly appears as illustrated in Figure 3(b). This equivalent network consists of three parallel susceptances interposed by quarter-wavelength lines. The quarter-wavelength coupling line transforms the shunt admittance into a series impedance, and changes the shunt branches representing the open irises to series resonant branches, as shown in Figure 3(c). If the resonant angular frequency of the series branches is made equal to the anti-resonant angular frequency of the shunt branch, or

$$\omega_0 = \frac{1}{\sqrt{L_1 C_1}} = \frac{1}{\sqrt{L_2 C_2}},$$

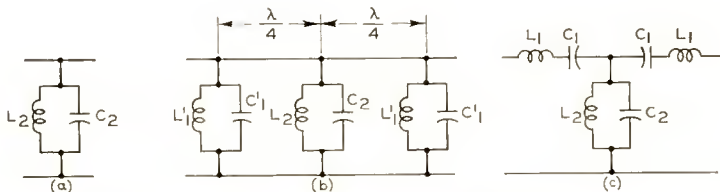


Fig. 3—(a) Schematic representation of ceramic window. (b) Schematic representation of output window assembly having resonant irises spaced a quarter wavelength on either side of ceramic window. (c) Equivalent circuit for output window assembly shown in (b).

then Figure 3(c) may be recognized as the prototype of a T-termination bandpass filter having a single pass band.

The window-and-iris assembly, therefore, may be considered as a filter composed of resonant irises coupled by quarter-wavelength lines,<sup>1</sup> and the theory of microwave filters may be employed in its design. Because of the difference in selectivity between the ceramic window and the open iris, the theory of maximally flat filters<sup>2-9</sup> is particularly adaptable to the window-assembly design. In this class of filters, the loss characteristics are notably flat over the range of free transmission and do not have the resonant effects usually encountered in filters of the conventional constant-K type.

Because the three components making up the window assembly can be represented by parallel tuned circuits, the properties of these circuits will be discussed before the functioning of the entire structure and the calculation of its over-all performance are considered.

#### CHARACTERISTICS OF PARALLEL TUNED CIRCUITS

Although the individual iris may be represented by a parallel  $L$ - $C$  circuit, it is usually not feasible to determine the values of the inductance and capacitance by experimental means. An analysis may be made, however, in terms of the resonant frequency and the loaded  $Q$  of the separate branches of which the final network is composed.

The  $r^{\text{th}}$  branch in a network, for example, consists of an inductance,  $L_r$ , and a capacitance,  $C_r$ , in parallel. The combination is intended for insertion between a constant-current source,  $I$ , having parallel internal resistance,  $R$ , and a load of equal resistance, as shown in Figure 4. The loaded  $Q$  of the  $r^{\text{th}}$  branch may be expressed as follows:

---

<sup>1</sup> G. L. Ragan (Editor), *Microwave Transmission Circuits*, MIT Radiation Laboratory Series, Vol. 9, pp. 677-709, McGraw-Hill Book Co., New York, N. Y.

<sup>2</sup> E. L. Norton, "Constant Resistance Networks with Applications to Filter Groups," *Bell Sys. Tech. Jour.*, Vol. XVI, pp. 178-193, April, 1937.

<sup>3</sup> E. L. Norton, U. S. Patent #1,788,538, January 13, 1931.

<sup>4</sup> W. R. Bennett, U. S. Patent #1,849,656, March 15, 1931.

<sup>5</sup> S. Butterworth, "On the Theory of Filter Amplifiers," *Experimental Wireless and the Wireless Engineer*, London, Vol. VII, #85, pp. 536-541, October, 1930.

<sup>6</sup> V. D. Landon, "Cascade Amplifiers with Maximal Flatness," *RCA Review*, Vol. V, pp. 347-362, January, and pp. 481-497, April, 1941.

<sup>7</sup> W. W. Mumford, "Maximally Flat Filters in Waveguide," *Bell Sys. Tech. Jour.*, Vol. XXVII, pp. 684-713, October, 1948.

<sup>8</sup> W. W. Mumford, U. S. Patent #2,540,488, February 6, 1951.

<sup>9</sup> H. J. Riblet, "Synthesis of Narrow-Band Direct-Coupled Filters," *Proc. I.R.E.*, Vol. 40, pp. 1219-1223, October, 1952.

$$\begin{aligned}
 Q_r &= \omega_0 \frac{\text{peak energy stored}}{\text{average loss}} \\
 &= \omega_0 \frac{\frac{1}{2} C_r E^2}{\left(\frac{E}{\sqrt{2}}\right)^2 \left(\frac{2}{R}\right)} = \frac{\omega_0 R C_r}{2} = \frac{R}{2} \sqrt{\frac{C_r}{L_r}} \quad (1)
 \end{aligned}$$

where  $\omega_0$  = anti-resonant angular frequency of the branch in radians per second =  $\frac{1}{\sqrt{L_r C_r}}$ ,

$E$  = maximum voltage across the branch.

The admittance,  $Y$ , in mhos, at the right of terminals  $T-T'$  in Figure 4 may be expressed as follows:

$$Y = G + jB = \frac{1}{R} \left[ 1 + j \omega_0 C_r R \left( \frac{f}{f_0} - \frac{f_0}{f} \right) \right] = Y_0 \left[ 1 + j2 Q_r \left( \frac{f}{f_0} - \frac{f_0}{f} \right) \right] \quad (2)$$

where  $G$  = conductance in mhos,

$B$  = susceptance in mhos,

$f$  = operating frequency in cycles per second,

$f_0$  = resonant frequency in cycles per second, and

$Y_0$  = termination admittance in mhos.

If both sides of Equation (2) are divided by  $Y_0$ , the normalized admittance,  $g + jb$ , of the branch is obtained.

$$g + jb = 1 + j2 Q_r \left( \frac{f}{f_0} - \frac{f_0}{f} \right) \quad (3)$$

Differentiation of the normalized susceptance given in Equation (3) with respect to frequency gives the loaded  $Q$  of the parallel branch when resistance termination is used:

$$Q_r = \frac{f_0}{4} \left( \frac{db}{df} \right)_{f=f_0} \quad (4)$$

The slope of the susceptance curve is evaluated at the resonant frequency,  $f_0$ . Expression (4) is particularly convenient for use in the determination of the loaded  $Q$  of a broadband element such as an iris.

In the circuit shown in Figure 4, the power delivered to the load is reduced when the parallel tuned circuit is added. The load power,  $P_0$ , available from a generator having an internal resistance,  $R$ , equal to the load termination is expressed as follows:

$$P_0 = \frac{1}{4} RI^2 \tag{5}$$

where  $I$  is the current delivered by the generator.

When the susceptance,  $jB$ , is inserted as indicated in Figure 4, the load current is changed to

$$I_R = \frac{I}{2 + jBR} \tag{6}$$

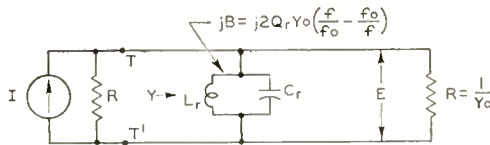


Fig. 4—Parallel tuned circuit representing individual resonant iris inserted between a constant-current source,  $I$ , having parallel internal resistance,  $R$ , and a load of equal resistance.

The power in the load,  $P_L$ , can be shown to be

$$P_L = \frac{I^2 R}{4 + B^2 R^2} \tag{7}$$

The power insertion ratio,  $P_0/P_L$ , which is also called the loss function, can be determined from Equations (5) and (7),

$$\frac{P_0}{P_L} = 1 + \frac{1}{4} B^2 R^2 = 1 + \left( \frac{B}{2 Y_0} \right)^2, \tag{8}$$

where  $Y_0 = 1/R$ .

The insertion loss in decibels,  $\alpha$ , may be written as follows:

$$\alpha = 10 \text{Log}_{10} \left[ \left( \frac{B}{2 Y_0} \right)^2 + 1 \right] \quad (9)$$

If the imaginary part of Equation (2) is substituted in Equation (8), the loss function can be expressed in the alternative form,

$$\frac{P_0}{P_L} = 1 + Q_r^2 \left( \frac{f}{f_0} - \frac{f_0}{f} \right)^2 \quad (10)$$

The conventional definition of the loaded  $Q$  may be deduced from Equation (10).

If  $f_c$  is the frequency in cycles per second at which  $\frac{P_0}{P_L} = 2$ , Equation (10) may be rewritten as follows:

$$Q_r = \frac{1}{\left| \frac{f_c}{f_0} - \frac{f_0}{f_c} \right|} = \frac{f_0}{f_{c2} - f_{c1}} = \frac{\frac{1}{\lambda_0}}{\frac{1}{\lambda_{c2}} - \frac{1}{\lambda_{c1}}} \quad (11)$$

In this expression,  $f_{c2}$  and  $f_{c1}$  are, respectively, the upper and lower half-power frequencies and  $\lambda_0$ ,  $\lambda_{c2}$ , and  $\lambda_{c1}$  are the free-space wavelengths corresponding to  $f_0$ ,  $f_{c2}$ , and  $f_{c1}$ , respectively. Because both the iris and the window possess broadband characteristics, Equation (4) is used in preference to Equation (11) in the evaluation of  $Q$  to avoid a wide coverage of frequencies in the standing-wave ratio test.

If the series combination of  $L_r$  and  $C_r$  is inserted between a constant-voltage generator having internal resistance  $R$  and an equal load resistance, the loaded  $Q$  of the series combination is as follows:

$$Q_r = \frac{\omega_0 L_r}{2R} = \frac{1}{2R} \sqrt{\frac{L_r}{C_r}} \quad (12)$$

The normalized impedance of this series branch terminated by a resistance,  $R$ , is

$$\frac{Z}{R} = 1 + j2Q_r \left( \frac{f}{f_0} - \frac{f_0}{f} \right) \quad (13)$$

Equation (10) still gives the power insertion ratio for the series branch provided the value of  $Q_r$  given in Equation (12) is used.

#### THEORY OF THE MAXIMALLY FLAT FILTER

A filter is generally composed of reactive elements arranged to form an iterative network which transmits energy in certain frequency bands and discriminates against other bands. The selective property of such a network is a result of the substantial reflections suffered by the incident wave at the terminal load. In wave-transmission systems involving smooth lines or cascaded networks, it is necessary for uniform transmission that the load impedance be substantially equal to the characteristic impedance of the line or network at all frequencies in the desired transmission range. The characteristic impedance of the constant-K filter is not constant with frequency except at frequencies remote from cutoff. When such a structure is used with a terminal apparatus having constant resistance, wave reflections occur at the junction and cause irregularities in the transmission region.

These undulations in the passband may be eliminated by an arrangement of the selective branches of the network to form a tapered line which gives a response with greatest flatness. The circuit in Figure 5 comprises equal terminal resistances,  $R$ , and  $n$  other branches,  $Z_1, Z_2, \dots, Z_n$ , disposed alternately in series and in shunt to form a ladder structure. The nature of these branches provides the desired selective characteristics and their values vary from section to section in accordance with a prescribed law.<sup>3,4</sup>

- (1) The branch impedances are made of purely reactive elements.
- (2) The series impedances are all of similar character, and the shunt impedances are similar to each other, their exact nature depending on the function the filter is called upon to perform.
- (3) The impedances of the series arms increase in value progressively from both ends toward the center, while the impedances of the shunt arms vary in an inverse manner. The series impedance may be expressed

$$Z_1 = a_1 \lambda R, Z_3 = a_3 \lambda R, \dots, Z_{n-1} = a_{n-1} \lambda R \quad (14)$$

and the shunt impedances

$$Z_2 = \frac{R}{a_2 X}, Z_4 = \frac{R}{a_4 X}, \dots Z_n = \frac{R}{a_n X}. \tag{15}$$

In Expressions (14) and (15),  $R$  is the common value of the terminal resistances, and the factors  $a_1, a_2, \dots a_n$  are related to the imaginary parts of the  $2n^{\text{th}}$  root of  $-1$ . The factor  $X$  describes the law of variation of the branch impedances with frequency. The factor  $X$  is equal to  $j \left( \frac{f}{f_c} \right)$  for a low-pass filter and  $j \left( \frac{f_c}{f} \right)$  for a high-pass filter,  $f$  being the operating frequency and  $f_c$  the cutoff frequency in both cases.

When this method is used to determine the proportions of the branches, the current  $I$  in the load resistance  $R$  due to the source voltage  $E$  in Figure 5 may be expressed as follows:<sup>4</sup>

$$|I| = \frac{|E|}{2R\sqrt{1 + |X|^{2n}}}. \tag{16}$$

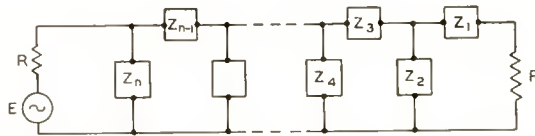


Fig. 5—Block diagram of maximally flat filter network consisting of equal terminal resistances,  $R$ , and  $n$  other branches,  $Z_1, Z_2, \dots Z_n$ , in a ladder structure.

As long as the value of  $|X|$  is less than unity, the value of the current in the load resistance is close to that of the fraction  $\frac{E}{2R}$ , which is the current in the load when it is matched to the internal resistance of the generator. When the value of  $|X|$  exceeds unity, the current in the load resistance becomes very small, particularly when  $n$  is a large number. The critical frequencies which form the demarcation of transmission and attenuation can be found from the following relations:

$$X = j, \text{ and } X = -j. \tag{17}$$

Within the transmission band, the current varies gradually with no maxima or minima whatever.

The insertion of a structure such as that shown in Figure 5 between a generator and its matched load produces a loss function,

$$\frac{P_0}{P_L} = 1 + |X|^{2n} \tag{18}$$

which depends only on the frequency factor,  $X$ , and the number of branches involved,  $n$ . If a bandpass filter is desired, the series branches should consist of resonant circuits and the shunt branches of anti-resonant circuits. The resonant frequencies of the series-arms are equal to the anti-resonant frequencies of the shunt arms, because these branches all contain the same frequency factor. If the cutoff frequencies of the passband are denoted by  $f_{c1}$  and  $f_{c2}$ , the frequency factor may be expressed as follows:<sup>3,4</sup>

$$X = j \left( \frac{f}{f_0} - \frac{f_0}{f} \right) \left( \frac{f_{c2}}{f_0} - \frac{f_0}{f_{c2}} \right)^{-1} \tag{19}$$

where  $f_0 = \sqrt{f_{c1} f_{c2}}$  = the mid-frequency of the filter.

The preceding discussion has been concerned primarily with networks having lumped parameters. In adapting the theory of maximal flatness to microwave filters, Mumford introduced the concept of the loaded  $Q$  of the total filter,  $Q_T$ , and defined this factor as follows:

$$Q_T = \frac{1}{\left| \frac{f_c}{f_0} - \frac{f_0}{f_c} \right|} \tag{20}$$

Mumford derived the loss function for the filter,  $\frac{P_0}{P_L}$ , in terms of the loaded  $Q$ ,

$$\frac{P_0}{P_L} = 1 + \left( \frac{f}{f_0} - \frac{f_0}{f} \right)^{2n} \left( \frac{f_c}{f_0} - \frac{f_0}{f_c} \right)^{-2n} = 1 + Q_T^{2n} \left( \frac{f}{f_0} - \frac{f_0}{f} \right)^{2n} \tag{21}$$

The frequency  $f_c$  in both Equations (20) and (21) represents the cutoff frequency of the filter at the half-power points.

The series-resonant and shunt-antiresonant branches in a bandpass filter are simulated in microwave work by cavities or resonant irises separated by quarter-wavelength lines. The quarter-wavelength coupling line transforms alternate shunt admittances into series impedances. These normalized series impedances or shunt admittances, as shown previously, are all expressible in terms of the resonant frequency and the loaded  $Q$ . Because the resonant frequencies of the microwave components are made to coincide, only their loaded  $Q$ 's are graded in accordance with the requirements set in Expressions (14) and (15), as follows:<sup>7</sup>

$$\left. \begin{aligned} Q_1 &= Q_T \sin \frac{\pi}{2n} = Q_n \\ Q_2 &= Q_T \sin \frac{3\pi}{2n} \\ \dots\dots\dots \\ Q_r &= Q_T \sin \left( \frac{2r-1}{2n} \right) \pi \end{aligned} \right\} \quad (22)$$

Uniform efficiency of transmission over the passband is obtained, therefore, by choosing the microwave elements in such proportions that they have a common resonant frequency and their bandwidths decrease progressively from both ends toward the center of the structure.

#### CHARACTERISTICS OF RESONANT IRISES AND CERAMIC WINDOWS

When the window-and-iris assembly is viewed as a maximally flat filter, the window forms the shunt branch in the middle, and the two outer irises, after transformation by the connecting lines, form the series branches of a three-branch ladder. The ceramic window is more selective than the open iris and, consequently, has a higher  $Q$ . The loaded  $Q$ 's of the three elements can be proportioned to satisfy Equations (22) when  $n$  has a value of 3. Pertinent characteristics for these elements are their resonant frequencies, their loaded  $Q$ 's, and their susceptances as a function of frequency.

A resonant iris having the dimensions  $a' \times b'$  in a waveguide having internal dimensions  $a \times b$  is illustrated in Figure 6(a). The longitudinal view is shown in Figure 6(b), the iris being a transverse diaphragm having an opening concentric with the cross section of the

waveguide. Electrically, these irises act as parallel tuned circuits in shunt to the line, as illustrated in Figure 6(c). Certain aspects regarding their properties are of significance.

- (1) Part of the waveguide associated with the iris also stores energy.<sup>1</sup>
- (2) The anti-resonant equivalent circuit should be changed to a four-terminal T-network having series-arm impedances to account for the finite thickness of the iris plate.<sup>10,11</sup> In this analysis, the effect due to the thickness of the iris plate is included in the magnitude of its loaded  $Q$ .
- (3) The ratio of the effective volume to the surface in a resonant iris is low, and its  $Q$  is necessarily small. This low value of  $Q$  causes the inherent characteristic of broad bandwidth in the window assembly.

An approximate expression for the resonant wavelength of an open

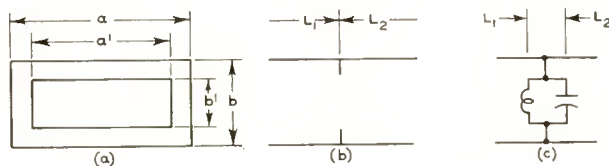


Fig. 6—Resonant iris having dimensions  $a' \times b'$  in a waveguide having internal dimensions  $a \times b$ , and its equivalent circuit.

iris can be obtained by matching the characteristic impedance of a waveguide having internal dimensions  $a$  and  $b$  to the impedance of a guide having dimensions  $a'$  and  $b'$ . By the use of this process,<sup>12</sup> the resonant wavelength,  $\lambda$ , is related to these dimensions in the following expression:

$$\frac{a}{b} \sqrt{1 - \left(\frac{\lambda}{2a}\right)^2} = \frac{a'}{b'} \sqrt{1 - \left(\frac{\lambda}{2a'}\right)^2} \quad (23)$$

In tests made on irises having a thickness of 0.020 inch and different

<sup>10</sup> J. W. Miles, "The Equivalent Circuit for a Plane Discontinuity in a Cylindrical Waveguide," *Proc. I.R.E.*, Vol. 34, pp. 728-742, October, 1946.

<sup>11</sup> N. Marcuvitz, *Waveguide Handbook*, MIT Radiation Laboratory Series, Vol. 10, McGraw-Hill Book Co., New York, N. Y., 1951.

<sup>12</sup> J. C. Slater, *Microwave Transmission*, McGraw-Hill Book Co., New York, N. Y., 1942.

opening in waveguides  $0.900 \times 0.400$  inch, the resonant wavelengths agreed more closely with the following empirical relation:

$$\frac{a}{b} \sqrt{1 - \left(\frac{\lambda}{1.97a}\right)^2} = \frac{a'}{b'} \sqrt{1 - \left(\frac{\lambda}{1.97a'}\right)^2} \quad (24)$$

Consideration of Expressions (23) and (24) reveals that different combinations of  $a'$  and  $b'$  are available for resonance at any particular wavelength. This fact may be used to advantage in the selection of a set of values that provides the desired  $Q$ .

An analytical expression derived by Lewin<sup>13</sup> gives the normalized susceptance of a resonant iris in a rectangular waveguide as

$$\begin{aligned} \frac{B}{Y_0} = & -\left(\frac{\lambda_g}{a}\right) \cot^2\left(\frac{\pi a'}{2a}\right) + \\ & \left[\frac{\pi(a^2 - a'^2)}{4aa' \cos\left(\frac{\pi a'}{2a}\right)}\right]^2 \left\{ \left(1 - \frac{\lambda^2}{4a'^2}\right) \left(1 - \frac{\lambda^2}{4a^2}\right)^{-1} \left(\frac{4b}{\lambda_g}\right) \log \csc\left(\frac{\pi b'}{2b}\right) + \right. \\ & \left. \frac{\lambda_g}{aa'^2} \left(\frac{b^2}{3} + \frac{b'^2}{2} - \frac{8bb'}{\pi^2}\right) \right. \\ & \left. 2 \left[\frac{b}{\pi}\right]^2 \sum_1^{\infty} J_0^2\left[\frac{n\pi b'}{b}\right] K\left[2n\pi \frac{(a-a')}{b}\right] \right\} \frac{1}{n^2} \quad (25) \end{aligned}$$

where  $J_0$  is the Bessel function of zero<sup>th</sup> order and  $K$  denotes a special function.

The first term in Equation (25) can be recognized as the first-order term for the susceptance of a symmetrical inductive diaphragm having a slit of width  $a'$ . The first part of the second term, involving the logarithm, gives the main portion of the capacitive susceptance of the resonant iris, and the remaining parts form a small correction to this term.

The principal terms in Equation (25) may be used to calculate satisfactorily accurate values of the iris susceptance as a function of frequency. From this susceptance and the relation given in Equation (4), the loaded  $Q$  of the iris can be determined graphically, or an expression can be derived for  $Q$  in terms of the dimensions.

<sup>13</sup>L. Lewin, *Advanced Theory of Waveguides*, Iliffe and Sons, Ltd., London, 1951.

If the principal terms in Equation (25) are set to zero and the result is solved for  $\lambda$ , an implicit expression for the resonant wavelength is obtained.

$$\frac{4}{\pi^2} \left( \frac{a}{b} \right) \frac{a'^2 \lambda^2}{(a^2 - a'^2)^2} \cot^2 \left( \frac{\pi a'}{2a} \right) \cos^2 \left( \frac{\pi a'}{2a} \right) = \left( 1 - \frac{\lambda^2}{4a'^2} \right) \log \csc \frac{\pi b'}{2b}. \quad (26)$$

The use of this equation yields a resonant wavelength in close agreement with the result obtained by the use of Equation (24) for irises having a thickness of 0.020 inch.

In an experimental study, the ceramic output window employed was composed of a  $0.900 \times 0.400 \times 0.040$ -inch ceramic plate brazed across the waveguide between two metal frames of the resonant-iris type. The window structure may be considered as two resonant irises coupled by a short length of ceramic-filled waveguide. However, tests show that this structure acts as an anti-resonant circuit and it simplifies matters to consider the unit as a parallel tuned circuit.

Because the electrical characteristics of the ceramic window are less amenable to analytical treatment than those of the open iris, it is expedient to resort to experimental means for their determination. It was found that the following empirical formula for the resonant wavelengths of windows could be used in the frequency range 8300 to 9200 megacycles.

$$\frac{a}{b} \sqrt{1 - \left( \frac{\lambda}{1.097a} \right)^2} = \frac{a'}{b'} \sqrt{5.42 - \left( \frac{\lambda}{1.097a'} \right)^2} \quad (27)$$

In this equation, the number 5.42 is the dielectric constant of the ceramic AlSiMag 243 at about 10,000 megacycles per second.<sup>14</sup> Values of  $\lambda$  obtained with the use of Equation (27) checked satisfactorily with experimental results for windows having various opening dimensions in  $0.900 \times 0.400$  inch waveguides. The material used for the window frames was 52-alloy having a thickness of 0.005 inch, and the ceramic plate was 0.040 inch thick.

The susceptance of such obstacles as the output window or the

<sup>14</sup> A. Von Hippel, "Tables of Dielectric Materials," MIT Laboratory of Insulation Research, NDRC Report 14-237, February, 1945, Report 14-425, June, 1945.

resonant iris can be determined by measurement of their voltage-standing-wave ratios. The obstacle is introduced in a waveguide terminated with a matched load, as shown in Figure 7(a), and the standing-wave ratio at different frequencies is found by the use of a slotted section. For example, if

$S$  = voltage-standing-wave ratio,

$$K = \frac{S - 1}{S + 1} = \text{magnitude of the reflection coefficient,}$$

$P_0$  = incident power (power delivered to matched load),

$P_r$  = reflected power caused by the insertion of the obstacle, and

$P_L$  = power delivered to the load with the inclusion of the obstacle,

then the power received by the load when the window or the iris is inserted may be expressed as follows:

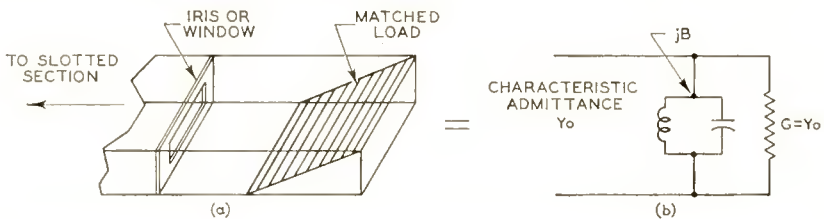


Fig. 7—(a) Diagram showing resonant iris or output window in waveguide terminated by a matched load. (b) Equivalent circuit for arrangement shown in (a).

$$P_L = P_0 - P_r = P_0(1 - K^2) = P_0 \frac{4S}{(1 + S)^2}. \quad (28)$$

In terms of the standing-wave ratio, therefore, the loss function due to the insertion may be written as,

$$\frac{P_0}{P_L} = 1 + \frac{(S - 1)^2}{4S}. \quad (29)$$

If Expressions (29) and (8) are equated, the absolute value of the normalized susceptance may be determined.

$$\left| \frac{B}{Y_0} \right| = \frac{S - 1}{\sqrt{S}}. \quad (30)$$

When the susceptance is plotted against frequency in the vicinity of resonance, the loaded  $Q$  of the obstacle concerned may be computed by an application of Equation (4).

### TRANSFORMATION PROPERTY AND SELECTIVITY OF CONNECTING LINES

The two outer resonant irises and the middle window in Figure 2 are spaced along the waveguide at distances approximately equal to one quarter of the guide wavelength. The connecting guide serves a dual purpose in providing a coupling link and in effecting the proper impedance transformation. It is well known that a quarter wavelength of lossless line transforms a normalized load impedance into a normalized admittance of equal value.<sup>15</sup> Figure 8 illustrates a microwave filter in which the selectivity,  $Q$ , and the resonant frequency,  $f_0$ , are

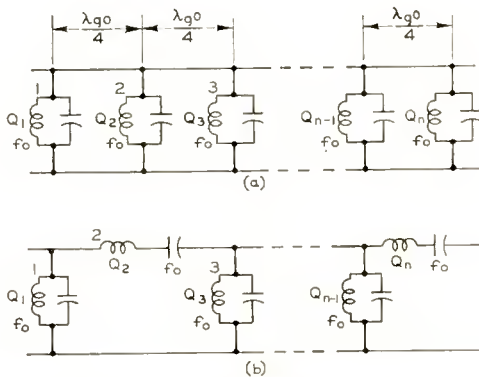


Fig. 8—(a) Microwave bandpass filter using resonant irises coupled by quarter-wavelength lines. (b) Ladder-type equivalent network for (a).

used to describe the behavior of each element. Starting at the left of Figure 8, the first shunt branch of (b) is identical with the first one in (a). Because of the impedance transformation of the quarter-wavelength section, the shunt branch 2 in (a) appears as the series branch 2 in (b). The shunt branch 3 in (a) undergoes two successive transformations as a result of the two quarter-wavelength sections and appears in (b) in its original form as a shunt branch. In this manner, the maximally flat ladder is simulated by shunt elements spaced at quarter-wavelength intervals.

<sup>15</sup> R. M. Fano and A. W. Lawson, "Microwave Filters Using Quarter-Wave Coupling," *Proc. I.R.E.*, pp. 1318-1323, November, 1947.

The impedance transformation property is perfect only at a frequency at which the line length is exactly one quarter of the guide wavelength. At other frequencies, the line transforms a purely resistive load into one having both resistive and reactive parts. In other words, the line possesses frequency sensitivity which can be measured in terms of an equivalent  $Q$ . Mumford<sup>7</sup> obtained an all-frequency circuit representation of a parallel tuned circuit inserted between a quarter-wavelength line and a resistance termination, as shown in Figure 9. The two correction networks on each side of the universal quarter-wavelength line account for the frequency sensitivity of the line. The line selectivity, on the basis of wavelength, may be derived for a quarter-wavelength section as

$$Q'_L = \frac{\pi}{8}$$

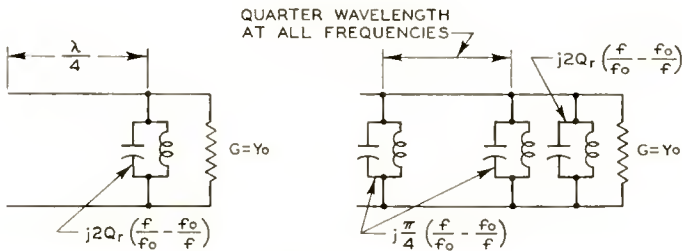


Fig. 9—(a) Equivalent circuit representing the selectivity of a quarter-wavelength line. (b) Correction network to account for line sensitivity.

This expression can be changed as follows to give a  $Q$  based on frequency:<sup>7</sup>

$$Q_L = \frac{\pi}{8} \left( \frac{\lambda_{g0}}{\lambda_0} \right)^2 \tag{31}$$

The guide wavelength,  $\lambda_{g0}$ , and the free-space wavelength,  $\lambda_0$ , are evaluated at the resonant frequency.

An end branch which has a quarter-wavelength line on one side requires a correction of  $Q_L$ ; a mid-branch having lines on both sides requires a correction of  $2Q_L$ . In narrow-band filters, the  $Q$ 's of the elements are high and the line selectivity has negligible effect. In the broadband windows, this selectivity is comparable in magnitude to that of the elements themselves and exerts a considerable effect on the performance of the assembly.

LENGTH OF CONNECTING LINES IN WINDOW ASSEMBLIES AND  
INTERACTION BETWEEN WINDOW ELEMENTS

In quarter-wavelength coupled filters in which the resonant cavity is made of two susceptances connected by a section of waveguide, there is an excess phase associated with the cavity.<sup>7</sup> If inductive susceptances are used to make up the cavity, the theoretical length of the guide coupling two adjacent cavities should be shortened by an amount equal to the excess phase. In window assemblies, improved bandwidth with lowered reflection is obtained when the connecting line is reduced from a quarter of the guide wavelength by a short distance. This distance is in the order of the range of fringing fields near the iris and window openings. Practically, the optimum spacing,  $d$ , between the ceramic window and the iris is equal to approximately the average of one quarter of the guide wavelength,  $\lambda_{g0}$ , and one quarter of the free-space wavelength,  $\lambda_0$ .

$$d = \frac{1}{2} \left( \frac{\lambda_{g0}}{4} + \frac{\lambda_0}{4} \right). \quad (32)$$

In addition to the beneficial effect on bandwidth and reflection loss, a shortened spacing yields a lighter and more compact structure. This fact is an important consideration in the window assembly where space and weight are at a premium.

Because of this reduction in the spacing and the interaction due to the proximity of the window components in the assembly, the mutual impedance effect between the components becomes noticeable. As a consequence, the mid-band frequency of the assembly is raised above the resonant frequency of the individual component by about three per cent. Measurements made on finished window assemblies show a consistent amount of increase in mid-band frequency. In the design, allowance must be made for this effect to obtain a proper location of the passband in the frequency spectrum.

## BANDWIDTH OF THE WINDOW ASSEMBLY

If the selectivities of the window components are proportioned in accordance with Equations (22) and their resonant frequencies are equal, a uniform transmission band is obtainable with the assembly provided the spacing between the elements is properly chosen. The frequency limits within which the voltage-standing-wave ratio is less than a prescribed value can be estimated and, as a result, the bandwidth of the assembly can be ascertained. In the general case of an assembly

comprising  $n$  branches, the loss functions, Equations (21) and (29), may be equated, thus defining a factor,  $F$ :

$$\frac{f}{f_0} - \frac{f_0}{f} = \left( \frac{S-1}{2\sqrt{S}} \right)^n \left( \frac{1}{Q_T} \right) = F. \quad (33)$$

If the above equation is solved for  $f$ , the lower and upper frequency limits are obtained:

$$f_{c1} = \frac{f_0}{2} (\sqrt{F^2 + 4} - F),$$

$$f_{c2} = \frac{f_0}{2} (\sqrt{F^2 + 4} + F). \quad (34)$$

The bandwidth  $w$  within which the standing-wave ratio is below an assigned value,  $S$ , is given by

$$w = f_0 F. \quad (35)$$

In Equations (34) and (35),  $f_0$  is the mid-band frequency of the assembly. Equations (33) and (35) show that a low  $Q_T$  results in a wide band coverage. The inherently low  $Q$ 's of the iris and the window proper are responsible for the broadband characteristics of the assembly.

#### PERFORMANCE OF WINDOW ASSEMBLIES

Tests conducted on finished window assemblies showed consistent and predictable performance. In one type of tunable magnetron, the center frequency was fixed at 9150 megacycles. In view of mutual effects between the components, the resonant frequency of the window was chosen at 8900 megacycles. In accordance with Equation (24), an iris opening of  $0.706 \times 0.140$  inch gave a resonant frequency of 8900 megacycles for the open irises. The AlSiMag 243 ceramic having a dielectric constant of 5.42 was used in the 0.040-inch-thick ceramic plate. When the window-frame openings were  $0.474 \times 0.250$  inch, the use of Equation (27) gave 8900 megacycles as the resonant frequency of the ceramic window.

The standing-wave ratio-characteristics of the ceramic window and one of the two resonant irises are plotted in Figure 10; their susceptance curves are shown in Figure 11. In accordance with Equation (4),

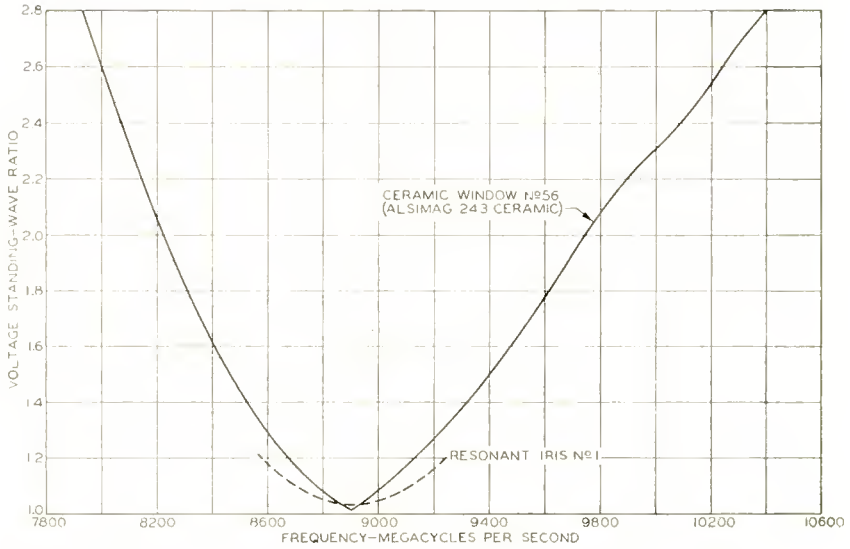


Fig. 10—Standing-wave-ratio characteristics of AlSiMag 243 ceramic window and one resonant iris.

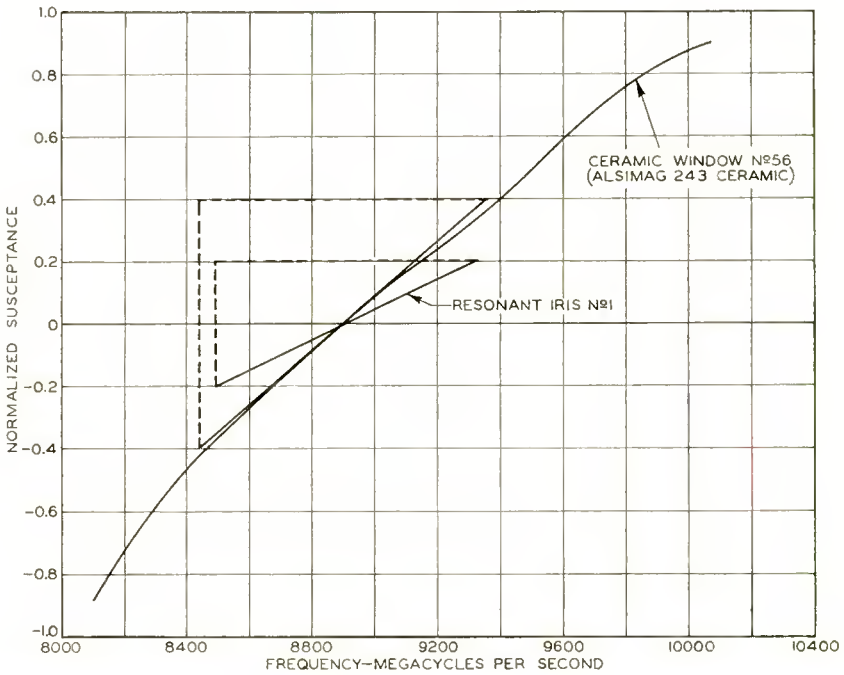


Fig. 11—Susceptance curves of AlSiMag 243 ceramic window and one resonant iris.

the loaded  $Q$  of the ceramic window has the value

$$Q'_2 = \frac{f_0}{4} \frac{d}{df} \left( \frac{B}{Y_0} \right)_{f=f_0} = \frac{8900 \times 10^6}{4} \times \frac{0.80}{935 \times 10^6} = 1.907.$$

Similarly, the loaded  $Q$  of the resonant iris,  $Q'_1$ , is found to be 0.978, which is approximately one half of the loaded  $Q$  of the window.

On the basis of frequency, the selectivity of the quarter-wavelength line is determined by the use of Equation (31):

$$\frac{\pi}{8} \left( \frac{\lambda_g}{\lambda} \right)^2 = \frac{\pi}{8} \left( \frac{4.72}{3.28} \right)^2 = 0.808.$$

The length of the coupling line in the window assembly was 0.41 inch, or materially less than one quarter of the guide wavelength. The line selectivity, compensated for this shortening, is

$$0.808 \left( \frac{\frac{d}{\lambda_g}}{\frac{1}{4}} \right) = 0.808 \left( \frac{0.410}{0.465} \right) = 0.708.$$

Therefore, the loaded  $Q$  of the ceramic window together with its associated line selectivity becomes

$$Q_2 = 1.907 + 2 \times 0.708 = 3.323.$$

The same quantity for the resonant iris is

$$Q_1 = 0.978 + 0.708 = 1.686.$$

When a value of 3 is substituted for  $n$  in Equation (22),

$$Q_1 = Q_T \sin \frac{\pi}{6}, \quad Q_T = 2Q_1 = 3.372$$

and

$$Q_2 = Q_T \sin \frac{3\pi}{6}, \quad Q_T = Q_2 = 3.323.$$

When the voltage-standing-wave ratio is less than 1.10, the response curve of the window assembly is substantially uniform. When it ex-

ceeds this value, the insertion loss rises abruptly and produces the sharp attenuation characteristic commonly found in filters. A ratio of 1.10, therefore, may be used to demark the attenuation and the transmission bands.

If  $Q_T = 3.323$ ,  $n = 3$ ,  $S = 1.10$ , and  $f_0 = 9150$  megacycles, then

$$F = \left( \frac{S-1}{2\sqrt{S}} \right)^{\frac{1}{n}} \left( \frac{1}{Q_T} \right) = 0.1091.$$

The lower cutoff frequency is

$$f_{c1} = \frac{9150}{2} [\sqrt{(0.1091)^2 + 4} - 0.1091] = 8640 \text{ megacycles,}$$

and the upper cutoff frequency is

$$f_{c2} = \frac{9150}{2} [\sqrt{(0.1091)^2 + 4} + 0.1091] = 9640 \text{ megacycles.}$$

The bandwidth is

$$w = f_0 F = 9150 \times 0.1091 = 1000 \text{ megacycles.}$$

For other assigned values of standing-wave ratio, the lower and upper frequency limits can be calculated in a similar fashion. The computed values are plotted in Figure 12, which also shows the complete performance determined by test on the assembly.

The kind of ceramic material used exerts a great influence on the performance of the window assembly, changing both its resonant frequency and its selectivity. One window assembly in which an experimental blend of forsterite composition was used for the ceramic plate had a resonant frequency of 9100 megacycles. The loaded  $Q$  of the window structure together with the selectivities of its associated line was 2.426. Resonant irises used with this output window were constructed from 0.020-inch copper and had openings  $0.680 \times 0.125$  inch. The resonant irises resonated at 9100 megacycles and had a selectivity of 0.649. When values of  $Q_T = 2.426$  and  $f_0 = 9350$  megacycles were used, the calculated upper and lower frequencies of the band within which the standing-wave ratio is less than different assigned values were as shown in Figure 13. In view of the broadband nature of the assembly, the agreement between the theoretical prediction and the experimental result is satisfactory.

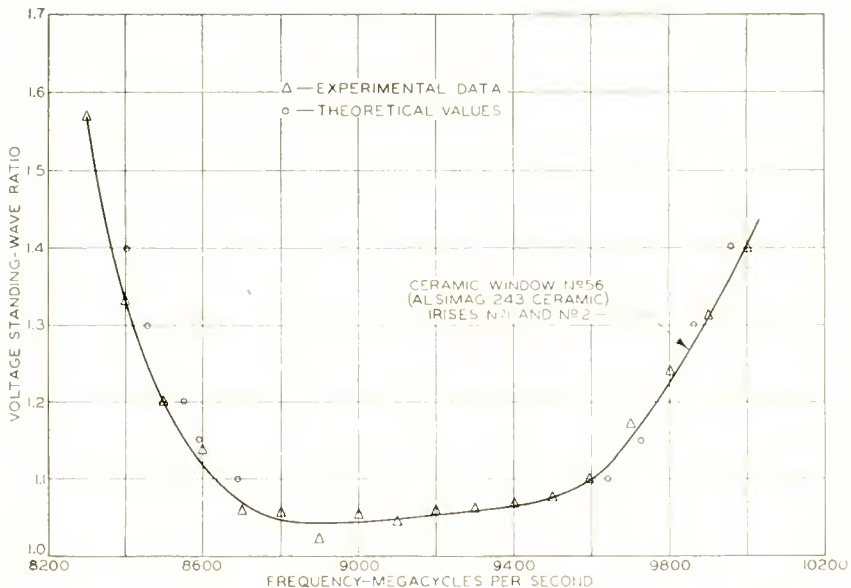


Fig. 12—Performance of AlSiMag 243 ceramic output window assembly over a 1000-megacycle bandwidth (8640 to 9640 megacycles).

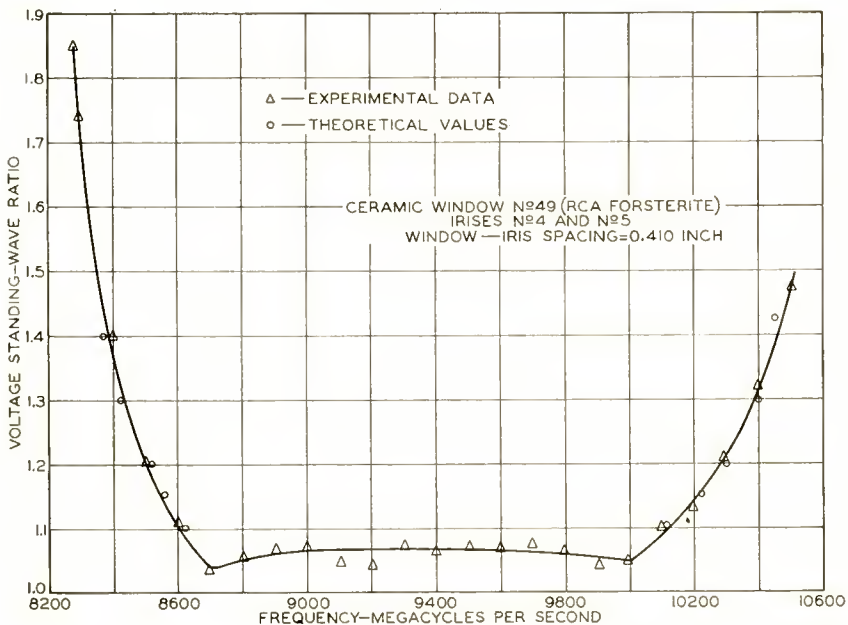


Fig. 13—Performance of forsterite ceramic output window assembly over a 1500-megacycle bandwidth (8600 to 10,100 megacycles).

VARIATION OF BANDWIDTH AND MID-BAND FREQUENCY WITH WINDOW-TO-IRIS SPACING

The broadband characteristics of a ceramic output-window assembly made as shown in Figure 2 were tested with different window-to-iris spacings; the results are shown in Figure 14. This output window used a second blend of ceramic and had iris-frame openings  $0.498 \times 0.250$  inch. The irises, except #1-1, were made of 0.020-inch copper and had  $0.706 \times 0.140$ -inch openings. The window and all irises used in the test, with the exception of iris #1-1, resonated at 8900 megacycles.

Curve A in Figure 14 shows that when the spacing is 0.47 inch,

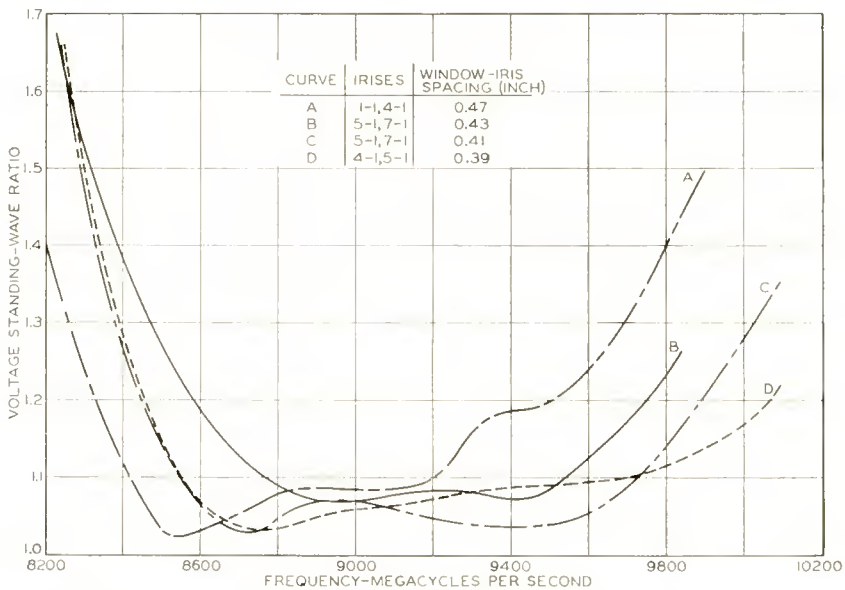


Fig. 14—Variation of bandwidth and mid-band frequency with window-to-iris spacing.

or near the value  $\lambda_g/4$ , the bandwidth occupies the low side of the frequency scale and the mid-frequency is close to the resonant value of each of the window elements. As the spacing,  $d$ , is decreased to 0.43 inch, a substantial upward shift of the transmission band occurs, and the mid-band frequency arises, as is evidenced by curve B. If the spacing is decreased further to 0.41 inch, an optimum condition is attained which gives a maximum bandwidth, low voltage-standing-wave ratio in the band, and mid-band frequency of desired value, as shown in curve C. Beneficial effects do not accrue from a further reduction in spacing to 0.39 inch, as illustrated by curve D.

### EFFECT OF STAGGERING THE RESONANT FREQUENCIES OF WINDOW ELEMENTS

The response shown by curve A in Figure 14 is not symmetrical, the window elements interacting properly near the lower limit of the band, but not functioning well in the neighborhood of the upper limit. The reason is that iris #1-1 resonated at 9100 megacycles, while the ceramic window and the iris #4-1 used in the combination resonated at 8900 megacycles. This staggering in resonant frequencies of the elements is detrimental to the filtering action and results in a lack of symmetry in the response curve, high standing-wave ratio, and irregularities in the reflections over the passband.

### EFFECT OF THE THICKNESS OF THE IRIS PLATE

In a series of tests, irises having a thickness of 0.005 inch were used in the broadbanding process. The performance curves for these irises lacked the distinct cutoff characteristic obtained for 0.020-inch irises, and the bandwidth was reduced from 1000 to 700 megacycles. Because the effective volume-to-surface ratio is lower in the 0.005-inch iris, its  $Q$  is less than the value required. Appropriate tapering of the  $Q$ 's requires the higher selectivity of the 0.020-inch irises, which, along with other unaccounted-for effects, contributes to improving the over-all performance of the assemblies incorporating thicker iris diaphragms.

### EVALUATION OF RESULTS

Tests on a 200-watt continuous-wave tunable magnetron using this window assembly indicate that the life of the window is satisfactory. Because of the presence of capacitive slits in both the resonant iris and the window frame, the breakdown voltage of the waveguide is reduced and there is a consequent reduction in the power-handling capacity. Breakdown of the assembly has occurred at 10 kilowatts for pulse-type operation.

Because both the resonant iris and the ceramic window are frequency-sensitive elements, close tolerances should be maintained on their opening dimensions and their spacing in the waveguide. The maintenance of vacuum in the magnetron precludes the use of tuning screws or other conventional means to adjust the resonant frequencies of the elements and to obtain some degree of flexibility in the spacing.

### CONCLUSIONS

The resonant-type output window can be broadbanded by applica-

tion of the principles included in this article. With the aid of some experimental determinations, the performance of such assemblies can be predicted with satisfactory accuracy. Use of AlSiMag 243 for the ceramic plate gives a consistent bandwidth of more than 1000 megacycles with a voltage-standing-wave ratio below 1.10. When the experimental blend of forsterite ceramic is employed, the bandwidth is extended to 1570 megacycles. The response is uniform and free from undulations over the transmission region.

Although the performance of mica windows with chokes<sup>16</sup> is superior to that of the resonant-type output window as regards high power-handling capacity and absence of abrupt attenuation, the drastic reduction in material and the great saving in cost of manufacture effected with the resonant-type window makes its adoption in continuous-wave magnetrons very desirable. This ceramic output window is particularly suitable for applications in which space and weight are factors of prime concern.

#### ACKNOWLEDGMENTS

The writer wishes to express his thanks to B. B. Brown for providing guidance and advice, and to H. K. Jenny, L. Kovach, and F. E. Vaccaro for rendering assistance in the course of this program. A. Leutwyler has helped to conduct many of the measurements. The Physical and Chemical Laboratory at Harrison supplied the experimental blend of ceramic and the Development Shop made all the finished window assemblies.

---

<sup>16</sup> Pp. 221-222 of Reference (1).

# DESIGN CONSIDERATIONS FOR FREQUENCY-SHIFT-KEYED CIRCUITS\*

BY

WALTER LYONS

Engineering Department, RCA Communications, Inc.,  
New York, N. Y.

*Summary*—Long-range radiotelegraph communications requires operation during marginal conditions and the maximum utilization of the frequency spectrum. Therefore the usual precept of trading bandwidth for noise does not hold, and methods for frequency-shift keying are examined to establish an optimum shift and keying-wave shape. Methods for implementing the suggested modes of operation are given.

Specifically, it is found that a considerable gain in signal-to-noise ratio can be realized by using sine-wave keying and unity deviation ratio. At high speeds, multipath delay distortion precludes the use of sine-wave keying and therefore an optimum keying speed is determined for maximum frequency utilization.

## INTRODUCTION

THERE are two primary reasons for the adoption of frequency-shift keying (FSK) almost to the exclusion of on/off keying in long-range radiotelegraph communications. The first is economy due to a comparative power gain; and the second is conservation of frequency spectrum due to means, readily and cheaply available, to control the shape of the keying pulse and thus to limit the extent of the keying side frequencies.<sup>1</sup>

Unfortunately, there has been a great deal of reluctance to adopt those design factors which give optimum performance with respect to the two objectives, particularly as to the choice of the amount of frequency shift, which determines the modulation index. It is possible that this attitude has been primarily due to a failure to appreciate the fact that there is a gain in signal-to-noise ratio (S/N) as the spectrum is narrowed, for small values of the ratio.<sup>2</sup>

For sinusoidal frequency modulation, the equation of the wave is

---

\* Decimal Classification: R423.3.

<sup>1</sup> H. O. Peterson, J. B. Atwood, H. E. Goldstine, Grant E. Hansell, and Robert E. Schock, "Observations and Comparisons on Radio Telegraph Signaling by Frequency Shift and On/Off Keying," *RCA Review*, Vol. VII, p. 11, March, 1946.

<sup>2</sup> Murray G. Crosby, "Frequency Modulation Noise Characteristics," *Proc. I.R.E.*, Vol. 25, p. 472, April, 1937.

$$e = E_o \sin (\omega t + m \sin pt). \tag{1}$$

This may be written

$$e = E_o [J_o (m) \sin \omega t + J_1(m) \sin (\omega + p)t - J_1(m) \sin (\omega - p)t + J_2(m) \sin (\omega + 2p)t + J_2(m) \sin (\omega - 2p)t + J_3(m) \sin (\omega + 3p)t - J_3(m) \sin (\omega - 3p)t + \dots] \tag{2}$$

in which  $E_o$  = maximum amplitude of the wave (unmodulated carrier amplitude),

$\omega = 2\pi$  times the frequency of the unmodulated carrier,

$p = 2\pi$  times the fundamental keying frequency,

$$m = \text{deviation ratio} = \frac{\text{shift frequency}}{2 \times \text{keying frequency}}$$

$$= \text{modulation index} = \frac{\text{deviation of frequency}}{\text{frequency of modulation}}$$

$J_n(m)$  = Bessel function of 1st kind of argument  $m$  and  $n$ th order  
 = Amplitude, relative to unmodulated carrier of the  $n$ th order sideband.

Figure 1 is a plot of  $J_n(m)$ .

In Equation (2), the frequencies present are the carrier, or mid-frequency,  $\omega$ , the first order sidebands  $\omega \pm p$ , etc. These components are analogous to amplitude modulation, differing, however, in that the amplitude of the carrier in FSK varies, and is dependent upon the modulation index. For on/off keying, if it were feasible to key sinusoidally, there would only exist one pair of side frequencies, corresponding to  $\omega \pm p$  when transmitting reversals. In FSK many side frequency pairs exist for sine-wave keying if the modulation index is high.<sup>3</sup> It can be seen from Figure 1, however, that at a modulation index of unity, second and higher order sideband components are 20 or more decibels down and can be neglected since 20 decibels down represents only 1 per cent of the power. If the deviation ratio were to be reduced below unity, nothing would be gained since the receiver

<sup>3</sup> Gilbert S. Wickizer, "Relative Amplitude of Side Frequencies in On/Off and Frequency Shift Telegraph Keying," *RCA Review*, Vol. VIII, p. 158, March, 1947.

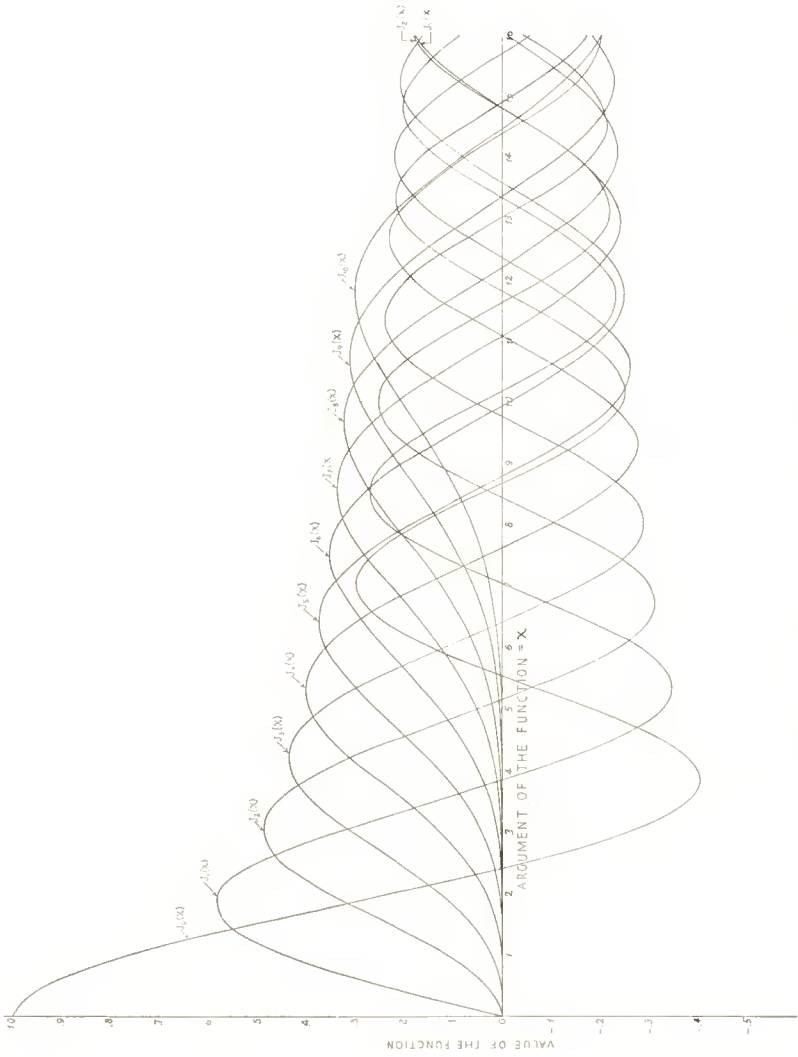


Fig. 1—Bessel functions for the first ten orders.

must be able to accept the first-order side frequencies and therefore receiver bandwidth could not be reduced. Also, the amplitudes of these sidebands decrease nearly linearly with the modulation index below unity.

Unity deviation ratio is, as shown above, unique, and establishes the first criterion for FSK working. The analysis was predicated, however, on sine-wave keying pulse shape, which departs from usual practice on two major counts. First, unless reversals are being transmitted, ordinary traffic is composed of "mark" and "space" pulses which are generally several baud elements duration rather than a single element of time. Therefore the deviation ratio may increase momentarily to a value greater than unity; first order side frequencies may then decrease but second- and third-order side frequencies will rise to restore the energy distribution in the spectrum. This will not, however, increase the bandwidth of the transmitted signal.

Second, multipath delay distortion, which increases or decreases the pulse width, is greater for sine-wave keying pulses than for rectangular pulses. This is due to greater amplitude changes in the sine-wave pulse after detection, but is significant only at keying speeds in excess of 50 cycles per second. At lower keying speeds, where the pulse width is greater than 10 milliseconds, multipath delay is not significant and considerable advantage in signal-to-noise ratio can be gained by sine-wave keying because the bandwidth may be constricted to include only first-order side frequencies. Moreover, it is reasonable to expect greater deterioration of a rectangular pulse due to selective fading since the loss of the energy in the several component side frequencies will result in less total energy than that in the simple sidebands for sine-wave keying. A loss of the significant side frequencies of sine-wave keying would be more likely to cause switching in a system employing diversity reception.

This leads to the conclusion that in the interests of obtaining higher S/N and better spectrum conservation, FSK should be shaped to correspond to sine-wave reversals on the transitions between mark and space. Since most frequency-shift-keying exciters in use today utilize reactance-tube modulation, this can be accomplished simply by inserting a low-pass filter before the reactance tube. The characteristics of this filter should be such as to pass the fundamental frequency of the highest keying speed, and to attenuate higher frequencies in a manner that does not cause phase distortion which gives rise to key clicks.

Due to the presence of a "mark" wave and a "space" wave in FSK working, this mode of operation suffers greater multipath delay distortion than the on/off mode. It is for this reason that facilities

should be made available for quickly changing over from FSK to on/off. This may be particularly important during the coming high sunspot cycle. At the present time we are in a low sunspot cycle, and operational requirements rarely necessitate on/off working on a normal FSK circuit.

Under ordinary circumstances and with customary operating frequencies, the maximum multipath distortion is taken to be approximately 2.5 milliseconds. This figure establishes the minimum duration of a pulse to be 5.0 milliseconds if a signal element which is 50 per cent of normal length is to be identified. This leads to the conclusion that the highest practical speed for FSK working is roughly 200 bauds which is equivalent to 100 cycles per second fundamental keying frequency and to 300 words per minute when using a 5-unit code.

With the system design criteria established, it is of interest to consider the factors and design techniques involved in the construction of suitable equipment. For the transmission of FSK signals of narrow shift and sine-wave shape, it is required that the transmitter frequency stability be of a high order, or that receiver automatic frequency control be used so that bias distortion is kept low, particularly when a two-filter-type discriminator is used. To achieve greater stability, it is helpful to use push-pull modulators. All sources of instability which affect the two reactance modulators equally, such as filament current changes and temperature changes, will cause cancelling effects. When using the tone-division (frequency division) multiplex system over a single sideband circuit, it is helpful to phase the tones so as to avoid addition of all or most tones in phase, which would result in high peak values. Band-pass filtering of the keyed tones of each channel can assure sinusoidal shape of the transmitted signals.

Receivers should incorporate automatic frequency control in order to take full advantage of signal-to-noise ratio improvement afforded by narrow shift without increasing operating attention, as well as to avoid distortion. This is a primary requirement since it allows the use of the narrowest bandwidth, obtaining the maximum S/N. Bandwidth thus may be only wide enough to receive the first-order sidebands. These are determined by the fundamental keying rate or the shift frequency for unity deviation ratio assuming sine-wave keying without multipath distortion. For 300 word-per-minute operation, during periods of multipath distortion, second-order components become considerable, and it is therefore required that the bandwidth before detection be about twice what it would ordinarily be on the basis of keying speed and deviation ratio alone. For speeds of 150 words per minute or less, multipath distortion need not be taken into account,

since a 2.5-millisecond maximum delay has been assumed. Thus the bandwidth requirement is determined by keying speed alone (unity deviation ratio and neglecting third-harmonic keying components required at high speed). By halving the keying speed, a gain of about 6 decibels in S/N accrues, since the bandwidth may be reduced to about one quarter of the former value, partly because of the lower keying speed and partly because half-baud elements are no longer encountered. Especially careful consideration should therefore be given to determining the necessary speed of a communications circuit before investment in equipment is made. This is most important when contemplating the use of powerful transmitters.

Additional filtering, of low-pass type, is required after detection in order to limit the cross-modulation products produced by detection, which are higher than the necessary band of frequencies. As in the case of band-pass filtering, the low-pass filters for 300 word-per-minute traffic must not cut off below 200 cycles per second. If this were to occur, the build-up time would not be short enough to reproduce these fast pulses which have suffered fifty per cent multipath distortion.

High gain and good limiting before demodulation are necessary so that adequate sensitivity will be obtained when using discriminator detection for small frequency shifts. Good limiting is especially required so that the rejection characteristics will act efficiently in the reduction of interference and noise.

Two types of detection of FSK are currently popular, "mark" and "space" filters each connected to its own rectifier, and the discriminator. These two methods are essentially similar especially if there is limiting after detection. The discriminator has the advantage of greater linearity for better reduction of white noise and for better fidelity. The "mark" and "space" filter type is somewhat more expensive but requires less limiting in the amplifier following. If, as is not uncommon, trigger circuits follow detection, then discriminator detection is favored. In the above discussion automatic frequency control was assumed. If automatic frequency control is not employed, then use of the discriminator is preferable since its linearity will allow drifting along its length without loss of sensitivity and margin, provided it is a-c coupled to the amplifier and means are incorporated to hold a "mark" condition when keying stops. Operation on narrow-shift FSK without automatic frequency control is not recommended because the necessary bandwidth allowance for drift defeats the original purpose.

Since both limiting and high gain are desirable and since pulse regeneration is frequently used, use of sensitive trigger circuits is indicated. For maximum protection against noise or interference, the

triggering potentials for "mark" condition and for "space" condition should logically be half the maximum "mark" and maximum "space" potentials, respectively. The output will then be a rectangular pulse reproducing the original telegraph signal.

Both space and frequency diversity are often employed in communications. Consideration of the type of diversity switching for FSK reception must take cognizance of the limiting before detection which precludes selection of the stronger signal in the common detector load. Therefore, in order to exclude the contribution of noise from the weaker signal path, switched diversity action is indicated so that only one receiver contributes to the load — the one with the highest signal intensity. To accomplish this, gate tubes may be used to couple the output of each detector to the trigger circuits described above. The gate tubes, of which there is one per receiver in diversity connection, can be made conducting or nonconducting by trigger tubes, so that only one is carrying the signal. Obviously, the decision to switch must be made ahead of the limiting. The decision to switch, and actual switching, should be as short as practicable to avoid distortion of the received pulse, and care must be exercised to avoid the possibility of the diversity switching causing false characters. As before, taking the shortest pulse to be five milliseconds, and with a five per cent limit for distortion, maximum switching time must be limited to 0.25 millisecond.

There has been considerable disagreement within the industry as to the optimum number of receivers for diversity reception. Recent tests indicate that the contribution of the third receiver decreases as conditions worsen, so that at error levels which barely may be considered commercial, the help of the third receiver is very little. An economic consideration will show that the expense of the additional facilities required for triple diversity as opposed to dual might better be applied to either a higher powered transmitter or better receiver and transmitter antennas.

#### CONCLUSIONS

The following procedures appear to be desirable in the interest of economy of operation and frequency conservation.

1. Frequency shifting should be sinusoidal for alternate element reversals.
2. The deviation ratio (modulation index) should be unity on reversals.
3. Two-receiver space diversity reception is indicated.

4. Automatic frequency control is a prime system requirement.
5. Filtering should be designed to pass only first-order frequencies except for speeds utilizing pulse elements shorter than 10 milliseconds. For the latter, filtering should pass no higher than second-order frequencies.

With this mode of operation, as opposed to the present practice of using rectangular pulse elements and a deviation ratio of five, it appears that a gain of about 6 decibels is obtained. In addition, the transmitted spectrum is reduced by about 70 per cent when measured between points 40 decibels down.

#### ACKNOWLEDGMENT

The author gratefully acknowledges the help he received from C. W. Latimer in discussions of the subject matter, and the assistance of J. L. Finch, who edited the paper critically.

# APPLICATION OF BREWSTER'S ANGLE TO THE DESIGN OF COAXIAL-LINE COMPONENTS FOR MICROWAVES\*

BY

B. A. DAHLMAN†

*Summary*—The boundary surface between two dielectrics can be used to refract electromagnetic waves. In principle, a uniform TEM wave can be refracted without reflections over an infinitely wide frequency band (the "Brewster Angle" effect). An investigation has been made of the application of this effect to the transition between a coaxial and a conical line. Experimental results show that fairly low reflections can be obtained over very wide frequency bands. Conical lines are very useful as adapters between different types of coaxial systems. An adapter between a 7/8-inch and a 3/8-inch coaxial line, both with 50 ohms impedance, was built and tested. The voltage-standing-wave ratio was less than 1.06 in the frequency range from 2000 to 5800 megacycles. Some suggestions are made for other applications.

## INTRODUCTION

IF a uniform transverse electromagnetic (TEM) wave,‡ traveling in one dielectric ( $\epsilon_1$ ) impinges upon a plane boundary surface between this dielectric and another dielectric ( $\epsilon_2$ ) (see Figure 1), it may, under certain conditions, be transmitted through the surface without any reflections. These conditions are that the wave be polarized in the plane of incidence, and that the angle of incidence be:

$$\theta_1 = \arctan \sqrt{\frac{\epsilon_2}{\epsilon_1}}. \quad (1)$$

From a physical or field point of view this simply means that we can satisfy the boundary conditions at the surface by assuming only one

\* Decimal Classification: R310.

† Formerly Research Department, RCA Laboratories, Princeton, N. J.

‡ A uniform TEM wave is one for which  $\vec{E}$  and  $\vec{H}$  are constant in a plane normal to the direction of propagation. It can exist only in free space, or between two parallel infinite conductive planes. The TEM wave in a coaxial line is nonuniform because  $\vec{E}$  and  $\vec{H}$  vary over a plane normal to the direction of propagation.

incident and one transmitted wave. However, we can also explain the Brewster angle effect from a transmission line point of view. This will be demonstrated.

For waves other than uniform TEM waves, the Brewster angle effect generally does not occur. There is, for instance, no equivalent phenomenon for TE or TM waves in hollow waveguides. However, the TEM mode in a coaxial line, although it is a nonuniform wave according to the definition given previously, can be refracted with small reflections by a dielectric boundary surface cut at Brewster's angle. Reflections from certain kinds of discontinuities can be minimized in this way. It will be shown how this effect can be applied to the design of certain microwave components.

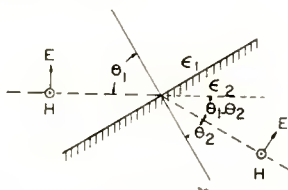


Fig. 1—A uniform TEM-wave impinging upon the boundary surface between two dielectrics at Brewster's angle.

#### EXPLANATION OF BREWSTER'S ANGLE FROM A TRANSMISSION-LINE POINT OF VIEW

Figure 1 shows a uniform TEM wave impinging at Brewster's angle upon a boundary surface between two dielectrics. The boundary conditions at the surface require that the tangential components of  $E$  and  $H$  be continuous at the boundary surface and that the normal component of  $E$  be inversely proportional to the dielectric constant. It is easily shown that these conditions are satisfied by only one incident and one transmitted wave for which

$$\frac{\sin \theta_1}{\sin \theta_2} = \sqrt{\frac{\epsilon_2}{\epsilon_1}}. \quad (2)$$

Conducting planes may be inserted perpendicular to the  $E$ -lines without disturbing the field. If two such planes are inserted in each dielectric in such a way as to intersect on the boundary surface, as shown in Figure 2, the result is two infinite parallel-plane transmission lines connected at the surface. Since the field is not disturbed, no reflections will occur at the junction between the lines. For the relation between  $b$  and  $a$ , the following equation holds:

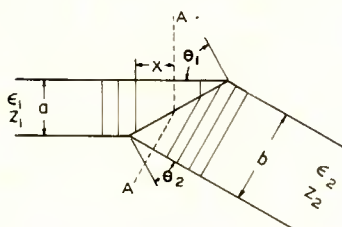


Fig. 2—The Brewster angle effect applied to transmission lines consisting of two infinite parallel planes.

$$\frac{b}{a} = \frac{\cos \theta_2}{\cos \theta_1}. \quad (3)$$

If Equations (1) and (2) are substituted in Equation (3),

$$\frac{b}{a} = \sqrt{\frac{\epsilon_2}{\epsilon_1}}. \quad (4)$$

The characteristic impedances of the lines are

$$Z_1 = k \frac{a}{\sqrt{\epsilon_1}}, \quad Z_2 = k \frac{b}{\sqrt{\epsilon_2}}.$$

By combining these expressions with Equation (4),

$$Z_1 = Z_2.$$

This circuit is shown in Figure 3.

#### APPLICATION OF BREWSTER'S ANGLE IN COAXIAL STRUCTURES

##### Two Basic Arrangements

If the projection of a parallel-plane line, as shown in Figure 2, is rotated about an axis parallel to the direction of propagation in one of the lines, it will generate a coaxial structure of the type shown in



Fig. 3—Equivalent circuit for Figure 2.

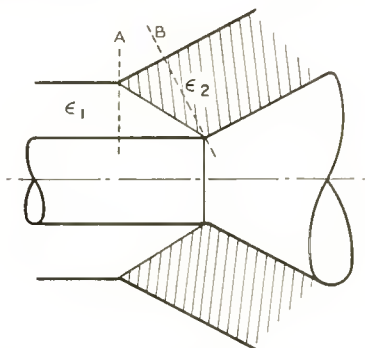


Fig. 4a—Transition between a coaxial line and a conical line. The outer and inner conductors in the conical line have the same top angle.

Figure 4a. A TEM wave traveling in the cylindrical line toward the boundary surface has a plane wave front, and Equation (1) can be applied to determine the slope of the dielectric face which will refract the wave into the conical line. A more complicated situation is found in the conical section of the line. It might be anticipated that a wave would travel along the cone with a conical wave front perpendicular to the two guiding surfaces, but it can be shown that such a wave cannot exist. (See Appendix I.) The consequence is that a wave entering at the small end of the cone must undergo a transformation to a different mode having a longitudinal component of electric field. This produces an effect similar to that of a distributed shunt capacitance in the vicinity of the boundary surface. (See Appendix II.) There are several ways in which this structure, including the shunt capacitance, can be represented by an equivalent circuit; one such representation is shown in Figure 4b. Here the shunt capacitance is concentrated in lumps at A and B.

The second of the two basic arrangements is illustrated in Figure 5a. This diagram represents the junction of a cylindrical coaxial line with a conical line of constant characteristic impedance.\* The wave in the conical line has a spherical wave front. The question then arises as to whether the dielectric boundary surface should be cut at the Brewster's angle appropriate to a plane wave front in the cylindrical

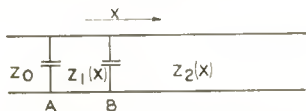


Fig. 4b—Equivalent circuit for Figure 4a.

\* The impedance is constant along the conical line if the vertices of the cones lie at the same point on the axis.

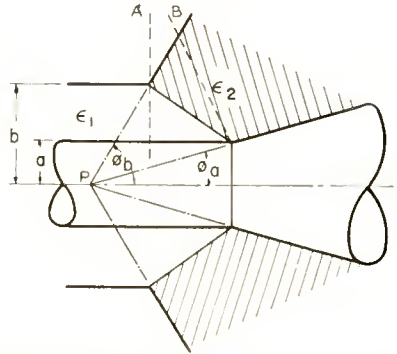


Fig. 5a—Transition between a coaxial line and a conical line of constant impedance.

line, or at the angle required by the wave in the conical line. The first leads to a conical boundary surface, and the second to a curved surface generated by revolving an exponential spiral around the axis of the lines. It is also possible to effect a compromise between the two boundary shapes. All three methods have been tested experimentally, and the results, which will be discussed subsequently, show that the first approach leads to the best result. In a design based on the first approach, the slope of the boundary surface depends only on the ratio of dielectric constants in the two line sections. The angles  $\phi_a$  and  $\phi_b$  (Figure 5a) are determined by placing the vertices of the two cones at the point P on the axis which makes the impedance of the conical line equal to that of the coaxial line. Formulas for the calculation of these angles will be found in Appendix III. In this case, as in the previous one, the wave which is delivered to the conical line at the junction is not exactly what is required for propagation between the two conical boundary surfaces, and therefore there must be a mode transformation which takes place mostly in the region between A and B. The equivalent circuit therefore includes two lumped capacitances, as shown in Figure 5b. The E component perpendicular to the B surface is larger than that found in Figure 4a, and therefore the shunt capacitances in the equivalent circuit are larger than those in Figure 4b. In either construction the effect of the shunt capacitances can be reduced by cutting off the sharp tip of dielectric at the plane A.

Since there is an approximation involved in determining the slope of the dielectric face, it is not to be expected that microwave devices



Fig. 5b—Equivalent circuit for Figure 5a.

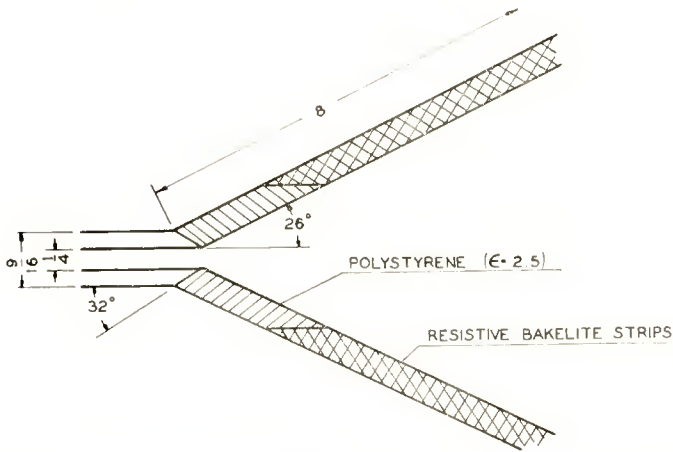


Fig. 6—Connection between coaxial line and nonuniform conical line.

designed according to the principles described above will be completely reflectionless. However, the results obtained with the experimental devices, which are described in the following section, show that very good performance can be obtained over wide frequency ranges.

#### Experimental Data

To check the performance of the couplings several experimental models were designed. Figure 6 shows a coupling between a 48-ohm air-dielectric coaxial line and a conical taper of the kind shown in Figure 4a. A termination was made of tapered strips of resistive bakelite inserted in radial slots in the polystyrene. The line was too short however for the strips to be a good match below about 6000 megacycles. A signal generator and a slotted line were connected to the coaxial line and the voltage-standing-wave ratio (VSWR) was measured at several frequencies. The results are plotted in Figure 7.



Fig. 7—VSWR for the connection shown in Figure 6, accurate to within  $\pm .02$ .

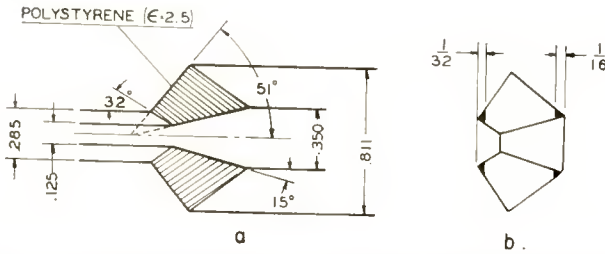


Fig. 8—(a) Adapter between two 50-ohm coaxial lines of different dimensions; (b) shape of refracting dielectric.

The increase in VSWR for lower frequencies is due partly to increased reflections from the termination and partly to the fact that the change in characteristic impedance of the conical line per wavelength along the line increases with the wavelength. The very low reflections at higher frequencies show that the lumped shunt capacitances in Figure 4b are small.

Figure 8a shows an adapter between two 50-ohm lines of different dimensions in which the characteristic impedance of the conical line is 50 ohms. This corresponds to the second basic arrangement. It was pointed out that there could be some question as to which shape of the dielectric boundary surface would be most suitable in this case. Three different shapes, which are shown in Figure 9, were tried. Curve I is for the cone, wherein the cone angle is chosen so that the wave in the coaxial line impinges upon the boundary surface at Brewster's angle. Curve II is the shape that corresponds to Brewster's angle for the spherical wave in the conical line. Curve III was designed as a compromise between Curves I and II. This design was started by dividing the structure into several concentric zones, and considering the action of waves arriving at the boundary surface from the two directions. Each facet of the dielectric surface was sloped so as to achieve the minimum reflection of waves arriving from either direction, and to balance the reflections over the whole surface so that cancellation could be assumed to occur. The net effect, if the theory had been correct, would have been almost complete cancellation of reflections at the boundary.

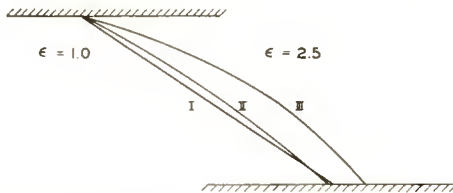


Fig. 9—The shapes of the dielectric boundary surface, corresponding to the curves in Figure 10.

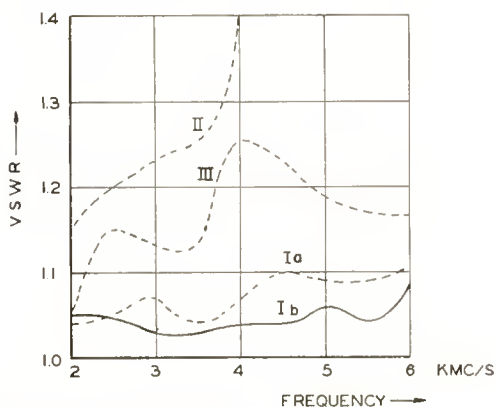


Fig. 10—VSWR for the adapter shown in Figure 8, accurate to within  $\pm .02$ .

The VSWR of the adapter measured with a slotted line in the smaller line when the bigger line was terminated in a matched load is shown in Figure 10, where Ia, II and III correspond to different shapes of the dielectric. It is obvious that curve Ia is the best. In order to compensate for the shunt capacitances, part of the dielectric was cut off. These parts are shown dark in Figure 8b. The resulting VSWR curve is plotted in Figure 9 curve Ib. The VSWR for the same adapter without the dielectric was 2.5 at 6,000 megacycles.

#### *Some Circuit Elements Using Brewster's Angle in Coaxial Systems*

We have already described an adapter between two transmission lines of the same impedance and with the same dielectric but with different dimensions. Figures 11-13 show ideas for other possible applications. Figure 11 is a transformer between two coaxial lines having different characteristic impedances. The figure shows the case where the dielectric constant for the material in the taper is higher than for the material in the lines. In case the lines are filled with dielectric, the material in the taper can have a lower dielectric constant. The boundary surface then has to be cut in a somewhat different way. (The left end of the taper in Figure 13b is an example of this case.)

Figure 12 shows how a wave can be guided around a right angle

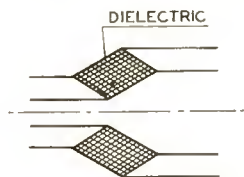


Fig. 11—Transformer between coaxial lines of different impedance, using Brewster's angle.

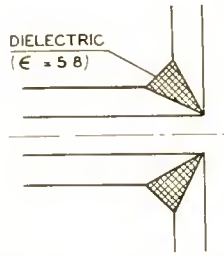


Fig. 12—Adapter between coaxial line and radial line, using Brewster's angle.

bend into a radial line. In the case shown in the figure the radial line has the same dielectric as the coaxial line. The direction of propagation changes by  $45^\circ$  at each boundary surface.

Using the nomenclature of Figure 1 we have

$$\theta_1 - \theta_2 = 45^\circ$$

$$\tan \theta_1 = \sqrt{\frac{\epsilon_2}{\epsilon_1}} \text{ and } \tan \theta_2 = \sqrt{\frac{\epsilon_1}{\epsilon_2}}$$

Thus,

$$\tan (\theta_1 - \theta_2) = \frac{\tan \theta_1 - \tan \theta_2}{1 + \tan \theta_1 \tan \theta_2} = \frac{\sqrt{\frac{\epsilon_2}{\epsilon_1}} - \sqrt{\frac{\epsilon_1}{\epsilon_2}}}{2} = \tan 45^\circ = 1$$

$$\epsilon_2 / \epsilon_1 = 5.8.$$

Thus the ratio of the dielectric constants in the adapter to that of the lines should be either 5.8 or  $1/5.8$ . The first of these cases is shown in Figure 12.

Figure 13a shows a transformer between a dielectric-filled and an air-filled coaxial line with the same characteristic impedances. The

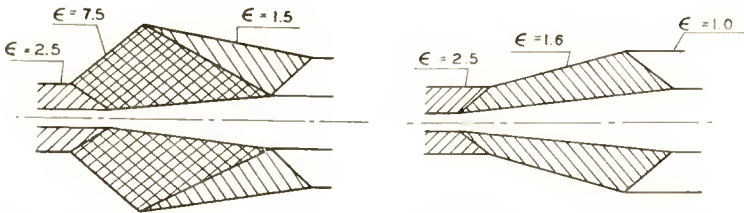


Fig. 13a (left) and b (right)—Adapters between dielectric-filled and air-filled coaxial lines of equal impedance, using Brewster's angle.

dimensions of the conical lines are determined by the dielectric they contain in accordance with Appendix III. These dielectrics should be chosen so that the condition for the Brewster's angle effect are approximately satisfied at the intersection of the cones. A simpler and probably better design is shown in Figure 13b. In order that the conical wave in the taper be transformed back to the TEM-wave in the coaxial line, the dielectric constant in the taper should be equal to the square root of the product of those in the lines. An adapter between a RG-8/U cable and 7/8-inch coaxial line, for instance, could be made in this way.

#### APPENDIX I — PROOF OF THE NONEXISTENCE OF TEM-MODE PROPAGATION IN A CONICAL LINE

A conical coordinate system, illustrated in Figure 14, is used. The coordinate lines are given as intersections between coordinate surfaces ( $u$ -cones,  $v$ -cones and  $w$ -planes). Thus  $u$ -lines (lines where  $v$  and  $w$  are constant) are intersections between  $v$ -cones and  $w$ -planes, and so on for  $v$ -lines and  $w$ -lines. The top angle ( $2\alpha$ ) for the  $u$ -cones is equal to the top angle for the cones in the conical line. The top angle for the  $v$ -cones is  $\pi - 2\alpha$ .

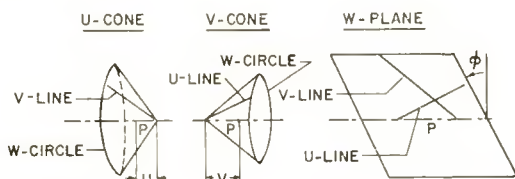


Fig. 14—Elements of a conical coordinate system.

Schelkunoff's method<sup>1</sup> for evaluating the vector derivatives in Maxwell's equations for this coordinate system is used. The lengths of a short line-element  $dS$  along a coordinate line is given by

$$\begin{aligned} dS_u &= du \cos \alpha = e_1 du & e_1 &= \cos \alpha \\ dS_v &= dv \sin \alpha = e_2 dv & e_2 &= \sin \alpha \\ dS_w &= dw (u + v) \sin \alpha \cos \alpha = e_3 dw & e_3 &= \sin \alpha \cos \alpha (u + v) \end{aligned}$$

Div and curl for a vector  $F = (F_u, F_v, F_w)$  is then given by

$$\operatorname{div} F = \frac{1}{e_1 e_2 e_3} \left[ \frac{\partial}{\partial u} (e_2 e_3 F_u) + \frac{\partial}{\partial v} (e_1 e_3 F_v) + \frac{\partial}{\partial w} (e_1 e_2 F_w) \right]$$

<sup>1</sup> S. A. Schelkunoff, *Electromagnetic Waves*, D. Van Nostrand Co., Inc., 1943, pp. 9-12.

$$\text{curl}_u F = \frac{1}{e_2 e_3} \left[ \frac{\partial (e_3 F_w)}{\partial v} - \frac{\partial (e_2 F_v)}{\partial w} \right]$$

$\text{Curl}_v$  and  $\text{curl}_w$  are obtained from  $\text{curl}_u$  by cyclic permutation. We will assume a TEM-wave with radial symmetry and show that such a wave does not satisfy Maxwell's equations. For the symmetrical TEM-wave we have

$$\begin{aligned} E_u &= 0, \quad \frac{\partial E_u}{\partial u} = \frac{\partial E_u}{\partial v} = \frac{\partial E_u}{\partial w} = 0 \\ E_v &= E, \quad \frac{\partial E_v}{\partial u} = \frac{\partial E}{\partial u}, \quad \frac{\partial E_v}{\partial v} = \frac{\partial E}{\partial v}, \quad \frac{\partial E_v}{\partial w} = 0 \\ E_w &= 0, \quad \frac{\partial E_w}{\partial u} = \frac{\partial E_w}{\partial v} = \frac{\partial E_w}{\partial w} = 0 \\ H_u &= 0, \quad \frac{\partial H_u}{\partial u} = \frac{\partial H_u}{\partial v} = \frac{\partial H_u}{\partial w} = 0 \\ H_v &= 0, \quad \frac{\partial H_v}{\partial u} = \frac{\partial H_v}{\partial v} = \frac{\partial H_v}{\partial w} = 0 \\ H_w &= H, \quad \frac{\partial H_w}{\partial u} = \frac{\partial H}{\partial u}, \quad \frac{\partial H_w}{\partial v} = \frac{\partial H}{\partial v}, \quad \frac{\partial H_w}{\partial w} = 0 \end{aligned}$$

Using these expressions to evaluate the div and the curl, and inserting the result in Maxwell's equations, we obtain, finally

I  $\text{Div } E = 0$

$$\frac{1}{\sin \alpha} \left[ \frac{\partial E}{\partial v} + \frac{E}{u+v} \right] = 0. \quad (1)$$

II  $\text{Div } H = 0.$

This is identically satisfied.

III  $\text{Curl } E = -j\omega\mu\mu_0 H$

$$\frac{1}{\cos \alpha} \frac{\partial E}{\partial u} = -j\omega\mu\mu_0 H. \quad (2)$$

$$\text{IV} \quad \text{Curl } H = j\omega\epsilon\epsilon_0 E,$$

$$-\frac{1}{\sin \alpha} \left[ \frac{\partial H}{\partial v} + \frac{H}{u+v} \right] = 0. \quad (3)$$

$$-\frac{1}{\cos \alpha} \left[ \frac{\partial H}{\partial u} + \frac{H}{u+v} \right] = j\omega\epsilon\epsilon_0 H. \quad (4)$$

Equation (1) gives

$$E = \frac{1}{u+v} f_1(u, w). \quad (5)$$

Equation (2) gives

$$H = \frac{1}{u+v} f_2(u, w). \quad (6)$$

Inserting Equations (5) and (6) in (2), we obtain

$$\frac{\partial f_1(u, w)}{\partial u} - f_1(u, w) \frac{1}{u+v} = -j\omega\mu\mu_0 \cos \alpha f_2(u, w).$$

The right-hand member of this Equation is independent of  $v$ . Thus the left-hand member should be independent of  $v$ , which gives

$$f_1(u, w) = 0.$$

Thus there is no electric field of the assumed type which satisfies Maxwell's equations. For symmetry reasons, the waves must be TM waves.

#### APPENDIX II—COAXIAL-LINE TO CONICAL-LINE COUPLING

It will be shown that the mode transformation from the TEM mode in the coaxial line to the TM modes in the conical line introduces an effect similar to a shunt capacitance.

There is a longitudinal  $E$ -component in the conical line (Appendix I). To match the boundary conditions there must thus be a longitudinal  $E$ -component in the coaxial line. However, the wave impinging upon the boundary surface from the coaxial line is a TEM wave. The  $E$ -component must belong to reflected waves. The lowest TM mode in a coaxial line has a cutoff wavelength

$$\lambda_{c1} \approx 2(a-b)$$

where  $a$  and  $b$  are the outer and inner radii. The values of  $\lambda_{c1}$  for the lines shown in Figures 6 and 8a are

Figure 6:  $\lambda_c = 1.33$  cm.  $\lambda_{min} = 2.2$  cm.

Figure 8a small line:  $\lambda_c = .81$  cm.  $\lambda_{min} = 5$  cm.

Figure 8a big line:  $\lambda_c = 2.34$  cm.  $\lambda_{min} = 5$  cm.

$\lambda_{min}$  is the shortest measured wavelength. In all cases  $\lambda_{min} > \lambda_c$ . The TM modes will thus be nonpropagating and contain only reactive power. The field components of these modes in a cylindrical coordinate system are

$$E_z(r, z) = R(r) e^{-z \frac{2\pi}{\lambda_c}} \sqrt{1 - \left(\frac{f}{f_c}\right)^2}$$

$$E_r = -\sqrt{1 - \left(\frac{f}{f_c}\right)^2} \frac{\lambda_c}{2\pi} \frac{\partial E_z}{\partial r}$$

$$H_\phi = -\frac{j f \lambda_c}{\eta f_c} \frac{\partial E_z}{\partial r}.$$

Where  $\eta$  is the intrinsic impedance of the dielectric in the line. The ratio between the stored electric and magnetic power for the lowest TM mode is

$$\frac{W_E}{W_M} = \frac{\epsilon \epsilon_0 \int (E_r^2 + E_z^2)^2 dv}{\mu \mu_0 \int H_\phi^2 dv} = \left(\frac{f_c}{f}\right)^2 - 1 + \frac{\int R^2(r) dv}{\int \left(\frac{\partial R(r)}{\partial r}\right)^2 dv \left(\frac{f}{f_c}\right)^2 \cdot \left(\frac{\lambda_0}{2\pi}\right)^2}$$

If  $\left(\frac{f_c}{f}\right)^2 > 2, \quad W_E > W_M.$

The expressions for  $\lambda_c$  and  $\lambda_{min}$  show that in our case,  $(f_c/f)^2 > 2$ . The stored electrical energy is then bigger than the stored magnetic energy for the lowest TM mode. For higher modes,  $W_E/W_M$  will be still bigger. Thus the TM modes introduce a capacitive effect. It is more appropriate to represent this effect with a shunt capacitance than with a series capacitance, because the discontinuity effect has a finite value when the frequency approaches zero.

APPENDIX III—FORMULAS FOR  $\phi_a$  AND  $\phi_b$  IN FIGURE 5

The impedances of the coaxial and the conical lines in Figure 5a are

$$Z_{cx} = \frac{60}{\sqrt{\epsilon_1}} \ln \frac{b}{a}$$

$$Z_{cn} = \frac{60}{\sqrt{\epsilon_2}} \ln \frac{\tan \frac{\phi_b}{2}}{\tan \frac{\phi_a}{2}}.$$

For  $Z_{cx} = Z_{cn}$ ,

$$\tan \frac{\phi_b}{2} = \tan \frac{\phi_a}{2} \left( \frac{b}{a} \right)^{\sqrt{\epsilon_2/\epsilon_1}} \quad (7)$$

When the dielectric constant of the material in the conical line is lower than that in the coaxial line, the boundary surface should be cut as is shown in Figure 5a. Then

$$a \cot \phi_a = b \cot \phi_b + (b - a) \sqrt{\frac{\epsilon_2}{\epsilon_1}}. \quad (8)$$

If Equation (7) is inserted in Equation (8),

$$\tan \frac{\phi_a}{2} = \frac{1 - p^{(1-m)}}{(p-1)(2m-1)},$$

$$\tan \frac{\phi_b}{2} = \frac{(p^{(m-1)} - 1)p}{(p-1)(2m-1)},$$

where  $p = b/a$ ,  $m = \sqrt{\frac{\epsilon_2}{\epsilon_1}}$ .

An example of how the boundary surface should look in case the dielectric constant in the conical line is lower than in the coaxial line is shown at the left end of the taper in Figure 13b. The same expressions for  $\tan (\phi_a/2)$  and  $\tan (\phi_b/2)$  are valid in this case, except that the sign of  $m$  in the denominator is changed.

# A MINIMUM NOISE FIGURE FOR THE TRAVELING-WAVE TUBE\*

BY

STANLEY BLOOM AND ROLF W. PETER

Research Department, RCA Laboratories,  
Princeton, N. J.

*Summary*—The transmission-line analog of a modulated electron beam is employed in the derivation of a general expression for the minimum obtainable noise figure of a traveling-wave tube, for arbitrary values of space charge and helix loss. The existence of this minimum noise figure is a consequence of the lack of correlation between the initial noise current and velocity fluctuations of the beam. This condition prevails in the limit of very high frequencies.

Practical design instructions are given for the realization of this optimum noise figure; they consist of formulas for the optimum radio-frequency beam impedance at the input of the given helix. The required impedance transformation from cathode to helix can be effected in many different ways. Impedance diagrams, or Smith charts, commonly used in the solution of transmission-line problems, can be adopted to simplify the design of an optimum impedance transformation along the beam in a low-noise gun.

## INTRODUCTION

THE propagation of noise space-charge waves along the electron beam of a traveling-wave tube, or any other beam-type amplifier, is most conveniently described in terms of the transmission-line analog of the modulated electron beam.<sup>1</sup> According to this analogy, any section of a single-velocity, laminar-flow beam behaves like a section of lossless transmission line, that is, like an impedance transformer. If the equivalent radio-frequency (r-f) noise current  $I_a$  and r-f noise voltage  $V_a$  are known at the plane of the virtual cathode, the output values at any subsequent plane can be computed from a knowledge of the transformer matrix elements. Thus the values of beam-noise current and voltage at the plane of the helix input can be found and used to calculate the noise power output of the amplifier and thence the noise figure.

In the early treatments of noise in beam-type amplifiers the electrons are assumed to leave the virtual cathode with zero d-c velocity, i.e., the Llewellyn and Peterson<sup>2</sup> space-charge factor,  $\zeta$ , is taken to be unity. Then the transformer matrix elements multiplying  $I_a$  are

\* Decimal Classification: R339.2.

<sup>1</sup> S. Bloom and R. W. Peter, "Transmission-Line Analog of a Modulated Electron Beam," *RCA Review*, Vol. 15, p. 95, March, 1954.

also zero, so that only  $V_a$  enters into the analysis. This is the model of Rack,<sup>3</sup> Llewellyn and Peterson, which was used by Pierce<sup>4</sup> and others to compute the noise figure of the traveling-wave tube.

If, more realistically, the d-c, or mean, velocity of the electrons at the virtual cathode is given its small but finite thermal value, then both the initial noise current  $I_a$  and noise voltage (velocity)  $V_a$  must be considered. This was first done by Watkins in an unpublished portion of his dissertation.<sup>5</sup> For  $I_a$  Watkins takes full shot noise and for  $V_a$ , as in the earlier treatments, the value corresponding to the Rack velocity. Furthermore, he assumes  $I_a$  and  $V_a$  to be *uncorrelated*. The noise figures due to each alone are then added to obtain the over-all noise figure. These separate noise figures vary oppositely with respect to certain parameters so that the over-all noise figure possesses a minimum value.

In this paper, the assumptions of full shot noise for the initial current ( $I_a$ ) and of the Rack value for the uncorrelated initial noise voltage ( $V_a$ ) will be adopted, without detailed justification. It can be shown, however, that this represents the limiting case, which holds under the condition of long transit angles in the diode region.

Watkins' treatment considers only the case of zero space charge and zero helix losses, and is limited to a very special kind of impedance transformer between the diode and the helix, namely, two drift spaces joined by an infinitely short d-c voltage jump.

In the present study a *generalized* treatment is employed, applicable to practical traveling-wave tubes having arbitrary space charge and arbitrary helix losses. Furthermore, the entire region extending from the virtual cathode to the helix drift space will be lumped into a single impedance transformer characterized simply by its matrix elements. Such an approach will not only yield a formula for the minimum noise figure obtainable under various given conditions of space charge and helix loss but will also furnish practical instructions for realizing this noise figure.\*

---

<sup>2</sup> F. B. Llewellyn and L. C. Peterson, "Vacuum-Tube Networks," *Proc. I.R.E.*, Vol. 32, p. 144, 1944.

<sup>3</sup> A. J. Rack, "Effect of Space Charge and Transit Time on Shot Noise in Diodes," *Bell Sys. Tech. Jour.*, Vol. 17, p. 592, 1938.

<sup>4</sup> J. R. Pierce, *Traveling-Wave Tubes*, D. Van Nostrand Company, Inc., New York, N.Y., 1950.

<sup>5</sup> D. A. Watkins, "Noise Reduction in Beam Type Amplifiers," dissertation, Stanford University, 1951.

\* In a recent article, F. N. H. Robinson ("Microwave Shot Noise in Electron Beams and the Minimum Noise Factor of Traveling-Wave Tubes and Klystrons," *Jour. Inst. Radio Eng. (Brit.)*, Vol. 14, p. 79, 1954) also treats the problem of minimum traveling-wave tube noise figure. His analysis, however, like Watkins', holds only for the idealized case of zero space charge and zero circuit loss and leads to the same result for minimum noise figure.

DERIVATION OF FORMULA FOR MINIMUM NOISE FIGURE

The system being considered is shown in Figure 1. The region from plane *a* (which will later be identified with the virtual cathode) to the beginning of the helix drift space, plane *c*, is depicted as a general impedance transformer. Actually, it represents the low-noise electron gun which is equivalent to a transmission line of variable characteristic impedance. The values of the r-f current and voltage at the trans-

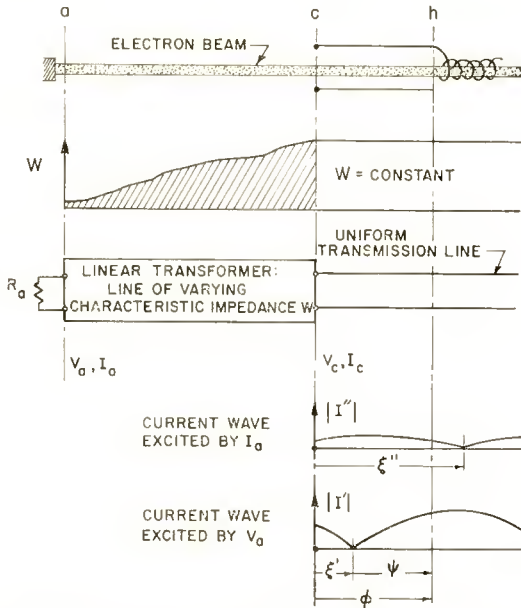


Fig. 1—The portion of the electron beam from virtual cathode (*a*) to beginning of helix drift space (*c*) is represented by a lossless transmission line of varying characteristic impedance. The subsequent portion of the beam with constant impedance is represented by a uniform transmission line. The current distribution of the two uncorrelated noise waves is shown along this line.

former output can be expressed in terms of the input values by the following matrix equation:

$$V_c = A V_a + j B I_a \tag{1}$$

$$I_c = j C V_a + D I_a$$

where the matrix elements are real and, by conservation of r-f power ( $V^* I + V I^*$ ), obey

$$AD + BC = 1. \tag{2}$$

Following the transformer is a drift space at helix potential where the beam has a constant characteristic impedance  $W$ , related to the total d-c current  $I_0$ , d-c voltage  $V_0$ , plasma frequency  $\omega_p$ , and signal frequency  $\omega$  by <sup>1</sup>

$$W = 2 \frac{V_0 \omega_p}{I_0 \omega}.$$

If the distance  $z$  from the transformer is measured in plasma-frequency radians,  $\phi = z\omega_p/v_0$ , where  $v_0$  is the d-c beam velocity, then  $V$  and  $I$  in the drift space are given by

$$\begin{aligned} V &= V_c \cos \phi + j W I_c \sin \phi \\ I &= j W^{-1} V_c \sin \phi + I_c \cos \phi \end{aligned}$$

which, with Equation (1), becomes

$$\begin{aligned} V &= (A \cos \phi - CW \sin \phi) V_a + j (B \cos \phi + DW \sin \phi) I_a \\ I &= j W^{-1} (A \sin \phi + CW \cos \phi) V_a \\ &\quad + W^{-1} (DW \cos \phi - B \sin \phi) I_a. \end{aligned} \tag{3}$$

Now, as stated earlier, the noise voltage  $V_a$  and noise current  $I_a$  at the virtual cathode will be assumed to be uncorrelated. Then, properly, in computing the noise figure of the tube, the space-charge waves due to  $V_a$  must be treated separately from those excited by  $I_a$ . Denoting the former by primes and the latter by double primes, the two pairs of space-charge waves in the helix drift space are

$$\begin{aligned} V' &= A V_a \frac{\cos(\phi - \zeta')}{\cos \zeta'} \\ I' &= j \frac{A V_a \sin(\phi - \zeta')}{W \cos \zeta'} \end{aligned} \tag{4a}$$

and

$$\begin{aligned} V'' &= j B I_a \frac{\cos(\phi - \zeta'')}{\cos \zeta''} \\ I'' &= - \frac{B I_a \sin(\phi - \zeta'')}{W \cos \zeta''} \end{aligned} \tag{4b}$$

where the phase angles are defined by

$$\tan \zeta' = -\frac{CW}{A}; \quad \tan \zeta'' = \frac{DW}{B}. \quad (5)$$

The over-all noise figure is the sum of the noise figure associated with the  $V_a$  waves and that associated with the  $I_a$  waves:

$$F = 1 + k |\alpha V' + j\beta W I'|^2 + k |\alpha V'' + j\beta W I''|^2,$$

where, for brevity, we call

$$\begin{aligned} \alpha &\equiv \delta_2 + \delta_3 \\ \beta &\equiv (\delta_2 \delta_3 - y^2)/y \\ k &\equiv y/2 KTW \Delta f \\ y &\equiv \sqrt{4QC} = \omega_p/\omega C = W I_0/2 V_0 C. \end{aligned}$$

Here  $QC$  is Pierce's space-charge factor and  $C$  his gain parameter. The  $\delta_2$  and  $\delta_3$  are Pierce's propagation constants for the two non-increasing forward waves; they are complex functions of  $QC$  and of the helix loss. The room temperature is  $T$  in Kelvin degrees,  $K$  is the Boltzmann constant and  $\Delta f$  the frequency bandwidth. The derivation of the basic formula for the noise figure of the traveling-wave tube is given by Pierce<sup>4</sup> and, for the case of non-zero  $QC$ , by Watkins.<sup>6</sup>

Inserting the values of r-f voltages and r-f currents given by Equations (4) we obtain for the noise figure

$$\begin{aligned} \frac{F-1}{k} &= |V_a|^2 \frac{A^2}{\cos^2 \zeta'} |\alpha \cos \psi - \beta \sin \psi|^2 \\ &+ |I_a|^2 \frac{B^2}{\cos^2 \zeta''} |\alpha \cos (\psi - \zeta'' + \zeta') - \beta \sin (\psi - \zeta'' + \zeta')|^2 \end{aligned}$$

where

$$\psi \equiv \phi - \zeta'$$

is the angle measured from the voltage-maximum (or current-zero) of the  $V_a$  wave in the helix drift space to the beginning of the helix.

This expression for the noise figure can be simplified, since, by Equations (2) and (5),

<sup>6</sup> D. A. Watkins, "Noise Reduction in Beam Type Amplifiers," *Proc. I.R.E.*, Vol. 40, p. 65, January, 1952.

$$\frac{W}{AB} = \frac{\sin (\xi'' - \xi')}{\cos \xi'' \cos \xi'}, \tag{6}$$

and therefore

$$\begin{aligned} \frac{F-1}{k} &= |V_a|^2 \left( \frac{W}{B} \right)^2 \frac{\cos^2 \xi''}{\sin^2 (\xi'' - \xi')} f(\psi) \\ &+ |I_a|^2 \frac{B^2}{\cos^2 \xi''} f(\psi - \xi'' + \xi'), \end{aligned} \tag{7}$$

where

$$f(\psi) \equiv |\alpha \cos \psi - \beta \sin \psi|^2. \tag{8}$$

Since the  $V_a$  noise figure predominates, the over-all noise figure is smallest when  $\sin^2 (\xi'' - \xi')$  is a maximum.\* Thus

$$\xi'' - \xi' = \pm \frac{\pi}{2}. \tag{9}$$

When this value for the phase difference is inserted into Equation (7) and a differentiation is made with respect to the quantity  $(W/B)^2 \cos^2 \xi''$ , it is seen that the noise figure has a lowest value of

$$\frac{F-1}{k} = 2W |I_a V_a| [f(\psi) f(\psi \mp \pi/2)]^{\frac{1}{2}} \tag{10}$$

when

$$\left( \frac{W}{B} \right)^2 \cos^2 \xi'' = \frac{|I_a|}{|V_a|} W \left[ \frac{f(\psi \mp \pi/2)}{f(\psi)} \right]^{\frac{1}{2}}. \tag{11}$$

Since the function defined by Equation (8) consists of a constant plus a sinusoid, it can be written in the form

$$2f(\psi) = (f_{\max} + f_{\min}) + (f_{\max} - f_{\min}) \cos (2\psi + \gamma) \tag{12}$$

where

---

\* Rigorously, differentiation of  $F$  with respect to  $\xi'' - \xi'$  shows that the minimizing value is that of Equation (9) when  $\psi$  has its minimizing value given by Equation (16).

$$\tan \gamma = \frac{\alpha\beta^* + \alpha^*\beta}{|\alpha|^2 - |\beta|^2} \tag{13}$$

and

$$\begin{aligned} 2f_{\max} &= |\alpha|^2 + |\beta|^2 + |\alpha^2 + \beta^2| \\ 2f_{\min} &= |\alpha|^2 + |\beta|^2 - |\alpha^2 + \beta^2|. \end{aligned} \tag{14}$$

These functions ( $f_{\max}$  and  $f_{\min}$ ) have been computed by Watkins<sup>6</sup> in terms of the space-charge factor  $QC$  and helix loss parameter  $d$  under

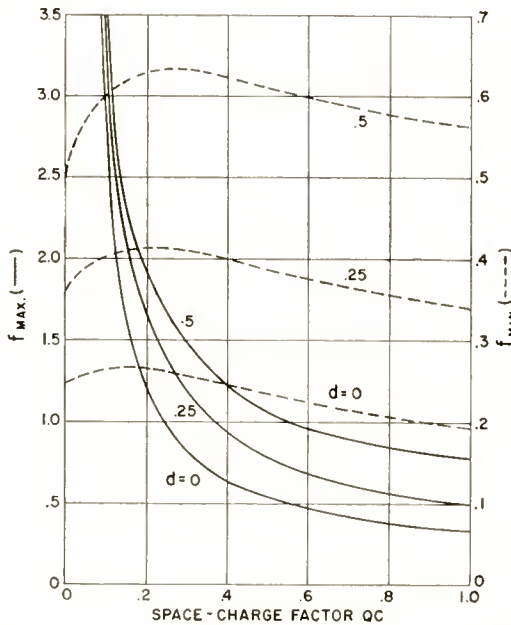


Fig. 2—The functions  $f_{\min}$  and  $f_{\max}$  versus the space charge factor  $QC$ , are shown for several values of the helix loss parameter  $d$  of a traveling-wave tube operating at maximum gain. (From D. A. Watkins.<sup>6</sup>)

the supposition that the tube is operating at maximum gain; Watkins' curves are reproduced in Figure 2.

In terms of the minimum and maximum of  $f(\psi)$ , Equation (10) becomes

$$\frac{F - 1}{k} = W |J_a V_a| [(f_{\max} + f_{\min})^2 - (f_{\max} - f_{\min})^2 \cos^2 (2\psi + \gamma)]^{\frac{1}{2}} \tag{15}$$

which is a minimum when the helix position is such that

$$2\psi + \gamma = \pi. \tag{16}$$

Thus, we find for the minimum noise figure of the traveling-wave tube, subject to the fundamental assumption that at plane  $a$  uncorrelated noise voltage and current excitations  $V_a$  and  $I_a$  exist and that beyond plane  $a$  single-velocity theory is valid,

$$F = 1 + \frac{|I_a V_a|}{K T \Delta f} \sqrt{4QC} \sqrt{f_{\min} f_{\max}}. \tag{17}$$

We now place plane  $a$  at the virtual cathode of a space-charge-limited diode and take for the entrant noise convection current full shot noise,

$$|I_a|^2 = 2e I_0 \Delta f. \tag{18}$$

The entrant r-f noise velocity, as evaluated by Rack, is the mean square value of the fluctuation of the average velocity of the anode-directed electrons at the plane of the virtual cathode;

$$\overline{|v_a|^2} = (4 - \pi) \frac{e K T_c \Delta f}{m I_0}.$$

Since the r-f voltage is related to the r-f velocity by<sup>1</sup>

$$V = \frac{v_0 v}{e/nl}$$

it follows that

$$|V_a|^2 = \frac{(4 - \pi) K T_c \Delta f}{e I_0 / m} \overline{v_{0a}^2} \tag{19}$$

or,

$$|V_a|^2 = 2 (4 - \pi) (K T_c)^2 \Delta f / e I_0 \tag{20}$$

since the mean square thermal velocity is  $\overline{v_{0a}^2} = 2 K T_c / m$ .

Thus, with

$$|V_a I_a| / 2 = \sqrt{4 - \pi} K T_c \Delta f,$$

we obtain for the minimum noise figure

$$F = 1 + 2 \sqrt{4 - \pi} \frac{T_c}{T} \sqrt{4QC} \sqrt{f_{\min} f_{\max}}, \quad (21)$$

the impedance transformer and the helix position being subject to the constraints of Equations (9), (11), and (16). It is seen that the value of the minimum noise figure is independent of the particular impedance transformation.

An important relation for the noise current in the drift space is obtainable quite easily from the transmission-line formalism. Since the entrant excitations  $V_a$  and  $I_a$  are uncorrelated, the total noise power must be the sum of the separate noise powers, e.g.,

$$|I|^2 = |I'|^2 + |I''|^2.$$

Thus in a drift region following *any* type of impedance transformer, it is seen by Equations (4), that

$$|I(\psi)|^2 = |V_a|^2 \left( \frac{A}{W} \right)^2 \frac{\sin^2 \psi}{\cos^2 \zeta'} + |I_a|^2 \left( \frac{B}{W} \right)^2 \frac{\sin^2 (\psi - \zeta'' + \zeta')}{\cos^2 \zeta''}. \quad (22)$$

If this is put into the form of a constant term plus a sinusoid, the minimum and maximum values are found to obey

$$|I_{\min} I_{\max}| = \frac{AB}{W^2} \frac{\sin (\zeta'' - \zeta')}{\cos \zeta'' \cos \zeta'} |V_a I_a|,$$

which, because of the general relation Equation (6), itself a consequence only of Equation (2), reduces to simply

$$W |I_{\min} I_{\max}| = |V_a I_a|. \quad (23)$$

According to Equation (23), *the product of noise-current minimum and maximum along a drifting beam, multiplied by the constant characteristic impedance, is invariant to arbitrary impedance transformations and is equal to the product of the initial amplitudes of uncorrelated noise current and voltage excitations.*\*

\* It was pointed out to the authors by D. A. Watkins that a formula similar to Equation (23) establishing the invariance of  $W |I_{\max} I_{\min}|$  has been derived by J. R. Pierce in a paper to be published.

In a formal way, a resistance value (real) can be attributed to the ratio of the initial current and voltage excitations,

$$R_a = \frac{V_a}{I_a} = \frac{|V_a|}{|I_a|}, \tag{24}$$

since this satisfies the requirement that the total noise power be the sum of the individual uncorrelated noise powers, i.e.,

$$|I|^2 = |I' + I''|^2 = |I'|^2 + |I''|^2. \tag{25}$$

Then Equation (23) takes the familiar form

$$R_a |I_a|^2 = W |I_{\max} I_{\min}|, \tag{26}$$

which is simply the expression for the conservation of real power  $R_a |I_a|^2$  traveling along a transmission-line of characteristic impedance  $W$ .

DISCUSSION OF FORMULAS

Let us now investigate the implications of the conditions which minimize the traveling-wave tube noise figure.

By virtue of Equations (12) and (16),

$$f(\psi \mp \pi/2) / f(\psi) = f_{\max} / f_{\min} \equiv \eta^2. \tag{27}$$

Thus Equation (11) becomes, after substituting the value of  $\zeta''$  from Equations (5),

$$\frac{W |V_a / I_a|}{B^2 + (DW)^2} = \eta. \tag{28}$$

Finally, Equation (9) together with Equations (5) gives

$$AB / CD = W^2. \tag{29}$$

Combining the power conservation relation, Equation (2), with Equations (27), (28), and (29), the optimum impedance-transformer matrix elements, in terms of the element  $D$ , are given by

$$A = DW \eta \left| \frac{I_a}{V_a} \right|, \text{ and}$$

$$B = \left[ \frac{W}{\eta} \left| \frac{V_a}{I_a} \right| - (DW)^2 \right]^{\frac{1}{2}} = \frac{W}{\eta} \left| \frac{V_a}{I_a} \right| C. \quad (30)$$

The noise current standing-wave ratio in the helix drift region when the impedance transformer is optimized for minimum noise figure can now be evaluated. Equation (22) becomes, because of Equations (5) and (9),

$$\left| \frac{I}{I_a} \right|^2 = \frac{1}{W} \left| \frac{V_a}{I_a} \right| \left( \eta \sin^2 \psi + \frac{1}{\eta} \cos^2 \psi \right). \quad (31)$$

Thus the noise current standing-wave ratio  $\eta$  under optimum conditions is given by

$$\frac{|I|_{\max}^2}{|I|_{\min}^2} = \eta^2 = \frac{f_{\max}}{f_{\min}}. \quad (32)$$

This ratio can be measured with a movable cavity probe which is responsive only to the fundamental radial mode of space-charge wave propagation. It is shown in Figure 3 as a function of the space-charge factor  $QC$  and the helix loss parameter  $d$ .

The quantity  $(F-1)T/T_c$  from Equation (21) versus  $QC$  for various values of  $d$  is given by Figure 4. From these curves the minimum noise figure is obtainable once the temperature ratio is known. In the limit of zero space charge and zero loss ( $QC=0=d$ )

$$2\sqrt{4QC} \sqrt{f_{\min} f_{\max}} \rightarrow 1$$

and Equation (21) reduces to essentially\* the result of Watkins.<sup>5</sup>

Suppose, now, that the impedance transformer is optimized for lowest noise figure but that the helix position is varied. The noise figure will then go through minima and maxima, spaced  $\pi/2$  plasma-frequency radians apart. From Equation (15), the noise figure standing-wave ratio is

$$\frac{F_{\max}}{F_{\min}} = \frac{1 + \sqrt{4 - \pi} \frac{T_c}{T} \sqrt{4QC} (f_{\min} + f_{\max})}{1 + 2\sqrt{4 - \pi} \frac{T_c}{T} \sqrt{4QC} \sqrt{f_{\min} f_{\max}}}. \quad (33)$$

\* For the initial d-c velocity at the potential minimum,  $v_{0a}$ , Watkins takes the mean value, whereas the r.m.s. value is used here, since to be consistent, r.m.s. values must be taken on both sides of Equation (19).

This ratio versus  $QC$ , for various values of  $d$  and for an assumed temperature ratio  $T_c/T = 1020/290 = 3.5$  is depicted in Figure 5. These curves show what the increase in noise figure will be if the helix is at its worst position, i.e., one-quarter plasma wavelength away from the optimum.

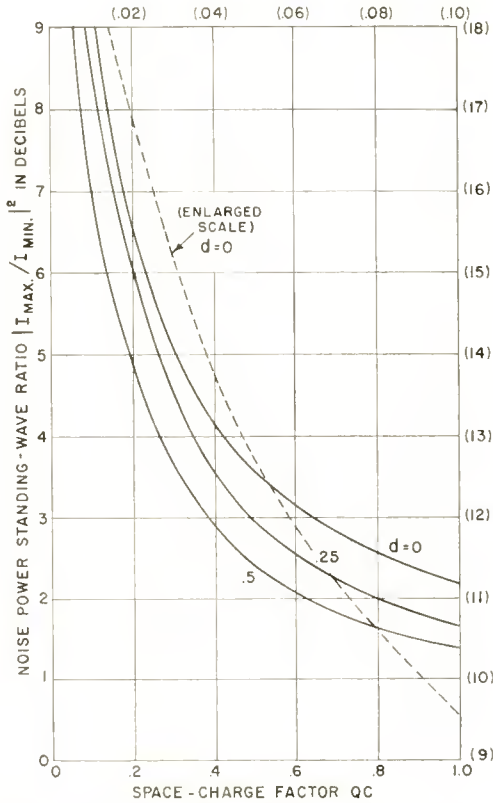


Fig. 3—When the impedance transformation from cathode to helix is optimized to yield a minimum noise figure, the noise power standing-wave ratio along the beam in the helix drift space is  $|I_{max}/I_{min}|^2$ . This ratio can be measured by a sliding cavity probe.

IMPEDANCE TRANSFORMATION FROM CATHODE TO HELIX

It will be noticed that it has not been necessary to specify the actual location of the beginning of the helix drift space, plane  $c$ . This is to be expected since the drift region was considered as part of the whole impedance transformer between cathode and helix. Fundamentally, the noise behavior of the traveling-wave tube is determined simply by the two uncorrelated noise waves in the beam at the helix-input plane. In a formal way, useful for gun design purposes, the relative amplitudes

and phases of these two waves can be expressed in the form of an r-f impedance on the beam. In this section this impedance is computed and its value at the helix input is found under optimum conditions.

The r-f beam impedance in the drift region is defined as

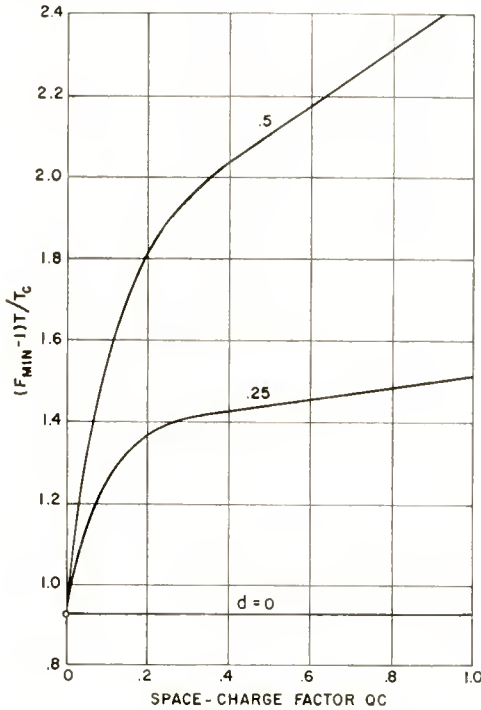


Fig. 4—The minimum noise figure,  $F_{\text{min}}$ , of the traveling-wave tube, as a function of space-charge factor  $QC$ , helix loss  $d$ , and ratio  $T/T_c$  of room to cathode temperatures. For zero loss, the minimum noise figure is  $1 + .925 T_c/T$  for all values of  $QC$ .

$$Z \equiv \frac{V}{I} = \frac{V' + V''}{I' + I''} \tag{34}$$

where the terms on the right are given by Equations (4). Introducing the optimizing condition Equation (9) and making use of Equation (24),

$$\frac{Z}{W} = \frac{CBW R_a - j [(CW R_a)^2 - B^2] \sin \psi \cos \psi}{B^2 \cos^2 \psi + (CW R_a)^2 \sin^2 \psi}$$

But because of Equation (30), the optimum matrix elements  $B$  and  $C$  obey

$$\frac{B}{C} = W R_a / \eta,$$

so that, on writing

$$Z/W = z = r + jx,$$

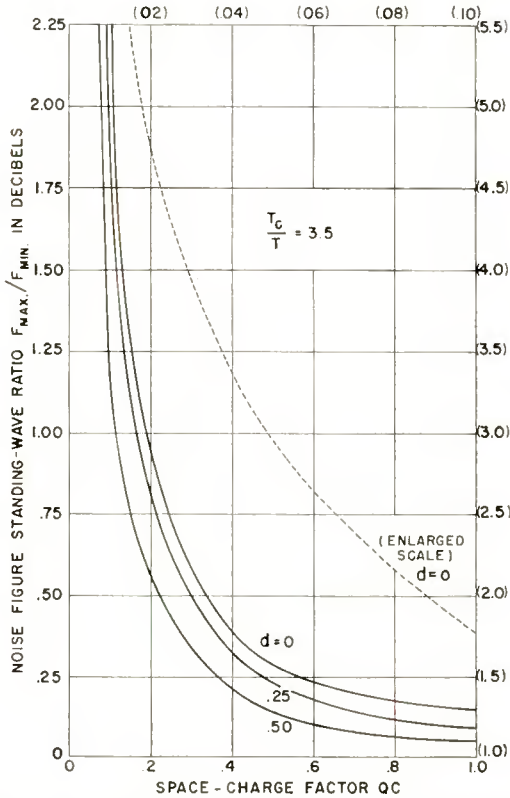


Fig. 5—When the impedance transformation is optimized for minimum noise figure, but the helix input is moved along the beam, the noise figure goes through successive minima and maxima spaced  $\pi/2$  radians apart. The noise figure standing-wave ratio  $F_{\max}/F_{\min}$  is shown for the temperature ratio  $T_c/T = 3.5$ .

the normalized r-f resistance and r-f reactance along the drift region are

$$r(\psi) = \left( \eta \sin^2 \psi + \frac{1}{\eta} \cos^2 \psi \right)^{-1}$$

$$x(\psi) = - \left( \eta - \frac{1}{\eta} \right) \sin \psi \cos \psi \left( \eta \sin^2 \psi + \frac{1}{\eta} \cos^2 \psi \right)^{-1} \tag{35}$$

Expressed in polar coordinates, the normalized r-f impedance along the drift space takes the simple form

$$z = \frac{1 + \kappa}{1 - \kappa}, \quad (35a)$$

where the complex reflection coefficient is

$$\kappa = \frac{\eta - 1}{\eta + 1} e^{-2j\psi}, \quad (36)$$

and the standing-wave ratio is

$$\eta = \frac{1 + |\kappa|}{1 - |\kappa|}. \quad (37)$$

Finally, with the optimum helix position specified by  $2\psi = \pi - \gamma$ , the optimum coefficient becomes

$$\kappa_{opt.} = \frac{1 - \eta}{1 + \eta} e^{j\gamma} \quad (38)$$

at the helix input. The normalized impedance there is

$$\begin{aligned} r_h &= 2 \left[ \eta + \frac{1}{\eta} + \left( \eta - \frac{1}{\eta} \right) \cos \gamma \right]^{-1} \\ x_h &= - \left( \eta - \frac{1}{\eta} \right) \sin \gamma \left[ \eta + \frac{1}{\eta} + \left( \eta - \frac{1}{\eta} \right) \cos \gamma \right]^{-1}. \end{aligned} \quad (38a)$$

The ratio  $\eta$  and the angle  $\gamma$  can be computed from Figure 3 and Equation (13) once the values of the space-charge factor  $QC$ , helix loss  $d$  and complex propagation constants  $\delta_2$ ,  $\delta_3$  are known for a given helix and beam.

With Equations (38) or (38a) it is now possible to design a gun for optimum noise figure. The problem is reduced to finding a transducer which transforms  $R_a$  at the cathode into  $Z_h$  at the helix input.

The characteristic beam impedance at the cathode is  $W_a = 2 V_{0a} \omega_{pa} / \omega I_0$ , where the plasma frequency is defined as

$$\omega_p = \left[ \frac{e i_0}{m \epsilon_0 v_0} \right]^{1/2},$$

$\epsilon_0$  being the dielectric constant and  $i_0$  the d-c current density. Thus, since by Equations (18) and (20)

$$R_a = \sqrt{4 - \pi} K T_c / e I_0,$$

the normalized r-f resistance at the cathode is given by

$$\begin{aligned} r_a = R_a / W_a &= \sqrt{(4 - \pi) \epsilon_0 e / m} \frac{K T_c \omega}{e \sqrt{i_0}} / v_{0a}^3 \cdot 2 \\ &= 1.52 \times 10^{-9} f T_c^{1/4} / i_{0a}^{1/2} \text{ (MKS)} \end{aligned}$$

where  $f = \omega / 2\pi$ .

Thus the values of  $r_a$  and  $z_h$  can be computed and entered as points on an impedance diagram (e.g., on a Smith chart). Any curve connecting these two points and consisting of path segments which correspond to transmission-line sections of arbitrary characteristic impedance, represents, then, a possible impedance transformation leading to minimum traveling-wave-tube noise figure.

# RCA TECHNICAL PAPERS†

First Quarter, 1954

Any request for copies of papers listed herein should be addressed to the publication to which credited.\*

"Accuracy and Speed on Shortwave Teleprinter Services," J. B. Moore, <i>Proceedings of the National Electronic Conference</i> (February) .....	1954
"Audio Oscillator Uses New R-C Design," J. H. Owens, <i>Electronics</i> (March) .....	1954
"Calculation of the Energy Band Structures of the Diamond and Germanium Crystals by the Method of Orthogonalized Plane Waves," F. Herman, <i>Phys. Rev.</i> (March 15) .....	1954
"Camera Adapter for TV Receivers," L. E. Flory, W. S. Pike, and G. W. Gray, <i>Electronics</i> (January) .....	1954
"Ceramic-Metal Seals of the Tungsten-Iron Type," D. G. Burnside, <i>RCA Review</i> (March) .....	1954
"Color Television—What it Means to the Broadcaster," J. H. Roe, <i>Broadcast News</i> (January-February) .....	1954
"Converted Limousine Aids TV Pickup," L. Weiland, <i>Electronics</i> (January) .....	1954
"A Demountable Vacuum System for Electron-Tube Development," T. M. Shrader, <i>RCA Review</i> (March) .....	1954
"Design Monographs for Electroplating Fine Wire," J. Paull and M. E. Stangl, <i>Design News</i> (February 15 and March 15)....	1954
"Design Tables for Low- and High-Pass Filters for the Reduction of TVI," M. Seybold, <i>Ham Tips</i> (March-April) .....	1954
"The Electron-Voltaic Effect in p-n Junctions Induced by Beta-Particle Bombardment," P. Rappaport, <i>Phys. Rev.</i> (Letter to the Editor) (January 1) .....	1954
"Effect of Temperature on Iron Powder Cores," G. Katz, <i>Electrical Manufacturing</i> (February) .....	1954
"Experimental Study of Limits Imposed by Plural Scattering in Electron-Diffraction Studies," S. G. Ellis, <i>National Bureau of Standards Circular #527</i> .....	1954
"Ferrites and Their Properties at Radio Frequencies," R. L. Harvey, <i>Proceedings of the National Electronic Conference</i> (February) .....	1954
"Ferromagnetic Spinel with Rectangular Hysteresis Loops," I. J. Hegyi, <i>Jour. Appl. Phys.</i> (February) .....	1954
"Film-Pulled, Theater-Type, Magnetic Sound Reproducer for Use With Multitrack Films," J. D. Phyfe and C. E. Hittle, <i>Jour. S.M.P.T.E.</i> (March) .....	1954
"Filter Using Coaxial Transmission Line as Elements," H. B. Yin T. U. Foley, <i>RCA Review</i> (March) .....	1954

† Report all corrections or addition to RCA Review, RCA Laboratories, Princeton, N. J.  
\* RCA Industry Service Laboratory Bulletins are not published and are issued only as a service to licensees of the Radio Corporation of America.

- "Flame Photometric Determination of Sodium and Potassium in Phosphors," S. B. Deal, *Analytical Chemistry* (March) ..... 1954
- "High-Frequency Operation of P-Type Point-Contact Transistors," F. L. Hunter and B. N. Slade, *RCA Industry Service Laboratory Bulletin LB-940* (March 15) ..... 1954
- "High-Frequency Operation of P-Type Point-Contact Transistors," F. L. Hunter and B. N. Slade, *RCA Review* (March) ..... 1954
- "How to Plan for Color," L. E. Anderson, *Broadcast News* (January-February) ..... 1954
- "Investigation of Ultra-High Frequency Television Amplifier Tubes," W. Y. Pan, *RCA Review* (March) ..... 1954
- "Mass Spectrometric Study of the Molecular Sublimation of Graphite," R. E. Honig, *Jour. Chem. Phys.* (January) ..... 1954
- "Metal-to-Ceramic Seals for Magnetron Waveguides," N. E. Pryslak, *Electronics* (January) ..... 1954
- "The New TF-12BH High-Gain Antenna," I. T. Newton, Jr. and H. H. Westcott, *Broadcast News* (March-April) ..... 1954
- "Portable 16mm Arc Projector Adapted for 3-D Projection," J. J. Hoehn, A. J. Cardile, and R. A. Woods, *Jour. S.M.P.T.E.* (March) ..... 1954
- "Power Transistors for Audio Output Circuits," L. J. Giacoletto, *Electronics* (January) ..... 1954
- "Radiation from CdS Crystals Generated by DC Electric Fields," R. W. Smith, *Phys. Rev.* (Letter to the Editor) (January 15) 1954
- "RCA Color Camera, TK-40A," F. W. Millspaugh, *Broadcast News* (January-February) ..... 1954
- "RCA Color Film Camera, TK-25A," W. J. Poch, *Broadcast News* (January-February) ..... 1954
- "The RCA Colorplexer," J. H. Wentworth, *Broadcast News* (January-February) ..... 1954
- "RCA Color Slide Camera, TK-4A," W. E. Tucker and F. J. Janda, *Broadcast News* (January-February) ..... 1954
- "RCA Color Sync Generator Equipment," A. H. Lind, *Broadcast News* (January-February) ..... 1954
- "RCA Color TV Monitor, TM-10A," A. H. Lind, *Broadcast News* (January-February) ..... 1954
- "RCA Color Television System," J. H. Wentworth, *Broadcast News* (January-February) ..... 1954
- "RCA Develops New UHF Television Waveguide," O. E. Wagner, *Broadcast News* (March-April) ..... 1954
- "Recrystallization of Germanium from Indium Solution," J. I. Pankove, *RCA Review* (March) ..... 1954
- "Sensitivity of Microphones to Stray Magnetic Fields," L. J. Anderson, *Broadcast News* (March-April) ..... 1954
- "Simple 'Degaussing' Procedure Protects Magnetic Tracks," E. Stanko, *Inter. Project* (March) ..... 1954
- "Some Studies of the Contamination Induced by Electron Bombardment in Kinematic Vacuum Systems," S. G. Ellis, *National Bureau of Standards Circular #527* ..... 1954
- "Space-Charge-Wave Amplification Along an Electron Beam by Periodic Change of the Beam Impedance," R. W. Peter, S. Bloom, and J. A. Ruetz, *RCA Review* (March) ..... 1954
- "A Specimen Heater for Electron Diffraction," R. G. Picard and E. G. Dornfeld, *Rev. Sci. Instr.* (February) ..... 1954
- "Survey of Transistor Development," B. N. Slade, *Broadcast News* (March-April) ..... 1954
- "A Symmetrical Transistor Phase Detector for Horizontal Synchronization," B. Harris and A. Macovski, *RCA Review* (March) 1954

- "A System for Recording and Reproducing Television Signals by Means of Magnetic Tape," J. T. Fischer, J. G. Woodward, M. Artzt, J. A. Zenel, A. R. Morgan, W. D. Houghton, and H. F. Olson, *RCA Industry Service Laboratory Bulletin LB-937* (January 27) ..... 1954
- "A System for Recording and Reproducing Television Signals," H. F. Olson, W. D. Houghton, A. R. Morgan, J. Zenel, M. Artzt, J. G. Woodward, and J. T. Fischer, *RCA Review* (March) .... 1954
- "The Tacitron, A Low-Noise Thyratron Capable of Current Interruption by Grid Action," J. A. Olmstead, W. M. Webster, and E. O. Johnson, *RCA Industry Service Laboratory Bulletin LB-939* (March 12) ..... 1954
- "Television Lighting Routines," W. R. Ahern, *Jour. S.M.P.T.E.* (March) ..... 1954
- "Television Transmitter Operation with Color Signals," T. M. Gluyas and N. J. Oman, *Broadcast News* (January-February) ..... 1954
- "Test Equipment for Color Television," J. A. Bauer, *Broadcast News* (January-February) ..... 1954
- "Transmission-Line Analog of a Modulated Electron Beam," S. Bloom and R. W. Peter, *RCA Review* (March) ..... 1954
- "Use of Point-Contact Transistors in Switching Service," *RCA Application Note AN-160*, RCA Tube Division, Harrison, N. J. (March) ..... 1954
- "Video Amplifiers in Color Signal Transmission," A. H. Lind, *Broadcast News* (January-February) ..... 1954
- "Vidicon Film Cameras," H. N. Kozanowski, *Broadcast News* (March-April) ..... 1954
- "Vidicon Film-Reproduction Cameras," H. N. Kozanowski, *Jour. S.M.P.T.E.* (February) ..... 1954
- "Vidicon for Film Pickup," R. G. Neuhauser, *Jour. S.M.P.T.E.* (February) ..... 1954
- "X-Ray Noise Observation Using a Photoconductive Pickup Tube," A. D. Cope and A. Rose, *Jour. Appl. Phys.* (February) ..... 1954

## AUTHORS

S. Bloom—(See *RCA Review*, Volume XV, No. 1, March 1954, p. 137.)



Harrison, N. J.

T. S. CHEN received the B.S. degree from Tangshan Chiao-Tung University, China in 1933, and the M.S. degree from Purdue University in 1934. He attended the Massachusetts Institute of Technology and received the S.M. degree in 1935 and the Sc.D. degree in 1938 from the Department of Electrical Engineering. He was a Professor of Electrical Engineering at the National Central University, China, until 1947. He joined the Radio Corporation of America in 1951 and has been engaged in the development of microwave tubes in the Special Development Group of the Tube Division at

MURLAN S. CORRINGTON received the B.S. degree in Electrical Engineering in 1934 from the South Dakota School of Mines and Technology, and the M. Sc. degree in 1936 from Ohio State University. From 1935 to 1937, he was a graduate assistant in the Physics Department of Ohio State University. In 1937 he joined the Rochester Institute of Technology, where he taught mathematics, mechanics, and related subjects. Since 1942 he has been engaged in Mathematical Engineering in the Advanced Development Section of the Home Instruments Division, Radio Corporation of America, at Camden, N. J. He is Manager of Audio, Acoustics, and Antennas for the Section. Mr. Corrington is a member of Sigma Pi Sigma, the Acoustical Society of America, the Society for Industrial and Applied Mathematics, and a Fellow of the Institute of Radio Engineers.



BENGT A. DAHLMAN graduated from the Royal Institute of Technology in Stockholm, Sweden in 1951. During that year he served in the Swedish Navy. While in service he was engaged in radar work at the Research Institute of National Defense. This work continued until 1952 when he joined the RCA Laboratories at Princeton, N. J. for work on microwave circuits and transistors. Mr. Dahlman has recently returned to the Research Institute of National Defense in Sweden.

WALTER LYONS received the B.Sc. degree in Electrical Engineering in 1928 from McGill University in Montreal, Canada. During 1929-1930 he attended the Columbia University Graduate School and in 1932 received the M.Sc. degree from McGill University where he was also Demonstrator in Physics, 1930-1932. From 1924 to 1932, he was associated with various activities including Bell Telephone Laboratories, Inc., N. Y. Edison Co., Victor Talking Machine Co., Western Union Telegraph Co., Balkert Radio Co., and the Hazeltine Corp. In 1932 he joined Wells-Gardner, in 1933-34 Emerson Radio and Television Corp., in 1934-1937 Hazeltine Corp., in 1937-1938 Majestic Radio and Television Corp., and in 1938 RCA Victor Division. In 1945 he became Staff Engineer of RCA International Division and in 1946 Plant Design Engineer for RCA Communications, Inc. Mr. Lyons is a Member of Sigma Xi, the Institute of Radio Engineers, the Radio Club of America, and the Cold Iron Society.





LOUIS PENSACK received the B.S. degree from Long Island University in 1932 and spent the next year as a graduate assistant at the University of Pittsburgh. In 1936 he received the M.S. degree in Physics from New York University. He joined the cathode-ray tube development section of RCA in 1937 and in 1940 was transferred to the Research Department of RCA Victor Division. Since 1941, he has been with RCA Laboratories where he has worked on kinescopes and storage tubes and transistors. Mr. Pensak is a member of Sigma Xi and a Senior Member of the Institute of Radio Engineers.

R. W. Peter—(See *RCA Review*, Volume XV, No. 1, March 1954, p. 140.)

RICHARD W. SONNENFELDT received the B.S. degree in Electrical Engineering in 1949 at Johns Hopkins University. From 1941-1943 and from 1946-1949 he designed control circuits and systems for the Charles Electric Company of Baltimore. In 1949 he joined the RCA Victor Division and has been engaged in advanced development work on monochrome and color television receivers and circuits. Mr. Sonnenfeldt is a member of Tau Beta Pi, Omicron Delta Kappa, and a Senior Member of the Institute of Radio Engineers.



RICHARD C. WEBB received the B.S. degree in Electrical Engineering from the University of Denver in 1937, the M.S. degree in 1944 and the Ph.D. degree in 1951 from Purdue University. From 1937 to 1939 he was a student engineer with the Bell Telephone System and from 1939 to 1945 he was an instructor and research assistant at Purdue University. From 1945 to 1952 he was a member of the Research Department of the RCA Laboratories Division at Princeton, N. J., where he was concerned with the development of color television camera equipment, industrial television and instrumentation for television measurements. Since 1952 he has been with the Denver Research Institute of the University of Denver. Dr. Webb is a member of the Society of Motion Picture and Television Engineers, the Institute of Radio Engineers, Tau Beta Pi, Eta Kappa Nu and Sigma Xi.

